

CRANFIELD UNIVERSITY

ADRIAN CUBILLO

PHYSICS-BASED APPROACH TO DETECT METAL-METAL
CONTACT IN THE HYDRODYNAMIC BEARING OF A
PLANETARY TRANSMISSION

IVHM Centre
School of Aerospace, Transport and Manufacturing (SATM)
PhD in health condition monitoring

PhD
Academic Year: 2013 - 2016

Supervisor: Suresh Perinpanayagam
October 2016

CRANFIELD UNIVERSITY

IVHM Centre
School of Aerospace, Transport and Manufacturing (SATM)

PhD Thesis

Academic Year 2013 - 2016

ADRIAN CUBILLO

PHYSICS-BASED APPROACH TO DETECT METAL-METAL
CONTACT IN THE HYDRODYNAMIC BEARING OF A
PLANETARY TRANSMISSION

Supervisor: Suresh Perinpanayagam
October 2016

This thesis is submitted in partial fulfilment of the requirements for
the degree of PhD in Health Condition Monitoring

© Cranfield University 2016. All rights reserved. No part of this
publication may be reproduced without the written permission of the
copyright owner.

ABSTRACT

Health condition monitoring, commonly referred as Integrated Vehicle Health Management (IVHM) for fleets or vehicles, studies the current and future health state of a system. Health monitoring techniques based on data driven approaches have proven successful in several areas and are easily scalable; however they do not rely on the understating of the physics of failure; whereas Physics-based Model (PbM) approaches require expert knowledge of the failure modes and are based on the understanding of the component behaviour and degradation mechanisms. The development of IVHM is particularly challenging for legacy aircraft due to the restrictive regulations of the aerospace industry.

This thesis proposes a novel PbM technique to detect metal-metal contact in hydrodynamic bearings. The planetary transmission of an aircraft's Integrated Drive Generator (IDG) is used as a case study. Research on the detection of metal-metal contact in hydrodynamic bearings has focused on data driven approaches using vibration or acoustic emissions rather than on PbMs. The proposed technique estimates metal-metal contact by modelling the physical phenomena involved in the failure mechanism and only the speed, load and temperature are required as inputs, all of them available in the IDG and not requiring any additional sensors.

The study of metal-metal in hydrodynamic bearings in the field of tribology has focused on mixed lubrication models of the whole bearing, or computational models accounting for local effect under the hydrodynamic lubrication region. In addition to the IVHM technique, this thesis contributes to the field of tribology by proposing a computational mixed lubrication model capable of studying metal-metal contact locally along the lubricated surface of the bearing. Experimental results of a plain journal bearing have been used to validate the PbM and a replica of the transmission of the IDG has been tested to evaluate the effectiveness of the proposed technique at detecting metal-metal contact.

Keywords: IVHM, PHM, PbM, journal bearing, diagnostics, mixed lubrication, aerospace

ACKNOWLEDGEMENTS

I would like to acknowledge the essential help of all the people without whom I would not have been able to complete this thesis. This list includes my family, all my colleges in the IVHM centre during these three years, my old and new friends, and housemates that I will always consider friends as well. A special mention for the following:

Dr Surshkumar Perinpanayagam, my principal supervisor, for his help along these three years, providing all the necessary resources and having an always positive attitude.

Adrian Uriondo, my colleague and friend, not only for his essential help and advice on the technical aspects, but also for his moral support and good moments during all these years.

Dr Manuel Esperon-Miguez, my colleague and friend, for his support, guidance and advice at the beginning of the project and during the design of the test rig in particular.

My family, for their moral support from the beginning of this project; which has proven to be crucial.

Georgina Hamblin, for her moral support, help during the thesis write up and for translating my ideas so they can be understood by a normal “human bean”.

TABLE OF CONTENTS

ABSTRACT	i
ACKNOWLEDGEMENTS.....	iii
LIST OF FIGURES.....	vii
LIST OF TABLES	xi
LIST OF ABBREVIATIONS	xiii
1 Introduction.....	1
1.1 Background.....	2
1.1.1 IDG description	3
1.1.2 Failure mode	6
1.1.3 IVHM solution requirements	8
1.2 Proposed solution	9
1.3 List of publications	10
2 Literature Review	13
2.1 Health Condition Monitoring.....	14
2.1.1 Benefits and challenges	14
2.1.2 Diagnostics and prognostics techniques	16
2.1.3 Hydrodynamic bearings.....	18
2.1.4 Conclusions of health condition monitoring	21
2.2 Physics-based Modelling	23
2.2.1 Generic Approach	23
2.2.2 Relevant degradation models.....	25
2.2.3 Conclusions of Physics-based Modelling	34
2.3 Metal-metal contact modelling of hydrodynamic bearings	34
2.3.1 Friction in line contacts.....	35
2.3.2 Conclusions of metal-metal modelling of hydrodynamic bearings	37
2.4 Summary and gaps in the knowledge	38
2.4.1 Literature review discussion	38
2.4.2 Gaps in the knowledge.....	41
3 Research objectives and methodology.....	43
3.1 Research problem definition	44
3.2 Aims, hypotheses and objectives.....	46
3.3 Contributions.....	49
3.4 Methodology	50
4 Metal-metal contact Physics-based model	57
4.1 Model Description	59
4.1.1 Basic principles	60
4.1.2 PbM overview.....	64
4.1.3 Film thickness	66
4.1.4 Hydrodynamic model.....	67

4.1.5 Viscosity	70
4.1.6 EHL	71
4.1.7 Asperity contact component	72
4.1.8 Forces equilibrium and friction coefficient	75
4.2 Implementation	77
4.2.1 Hydrodynamic bearing of planetary transmission.....	78
4.2.2 Plain journal bearing.....	84
4.3 Summary	87
5 Health condition monitoring	89
5.1 IVHM tool	91
5.1.1 IVHM tool capabilities	91
5.1.2 IVHM tool description	93
5.1.3 Data management.....	98
5.2 Metal-metal contact under aircraft operational conditions.....	104
5.2.1 Description	105
5.2.2 Load and inlet lubricant temperature impact	106
5.3 Summary	111
6 Design of experiments.....	113
6.1 Plain journal bearing experimental set-up.....	115
6.2 IDG journal bearing experimental set-up	118
6.2.1 Test rig Design	119
6.2.2 Experiments	128
6.3 Summary	130
7 Experimental and PbM results.....	132
7.1 Results of plain journal bearing.....	133
7.1.1 Results	134
7.1.2 Conclusions of results of plain journal bearing	139
7.2 Results of the hydrodynamic bearings of the IDG's planetary transmission.....	140
7.2.1 Comparison between PbM and experiments.....	142
7.2.2 Additional results	146
7.2.3 Conclusions of results of hydrodynamic bearing of the IDG's planetary transmission	155
7.3 Summary	157
8 Discussion	161
8.1 Mixed lubrication Physics-based Model.....	162
8.2 Novel technique to predict metal-metal contact in the hydrodynamic bearing of the IDG	164
9 Conclusions and contributions.....	167
10 Future work	169
References	171
Appendices.....	187

LIST OF FIGURES

Figure 1 IDG - Source: www.megakeep.com	4
Figure 2 Open IDG showing the constant speed drive. The planetary transmission sits on the front with twin hydraulic units on each side and control cylinder in the middle.	4
Figure 3 Planetary transmission diagram	6
Figure 4 Example of damage of adjacent components (left: planetary gear $\varnothing=37\text{mm}$, centre: carrier shaft $\varnothing=94\text{mm}$ and bearing shaft $\varnothing=24\text{mm}$, left: carrier shaft 2 $\varnothing=94\text{mm}$).....	7
Figure 5 Architecture of an IVHM system	14
Figure 6 Percentage occurrence of types of hydrodynamic bearing damage [36]	20
Figure 7 Physics-based approach [41]	24
Figure 8 Qualitative Stribeck curve: friction (μ)-Sommerfeld number (N : speed, p : load, η : dynamic viscosity of the lubricant, R : radius of the bearing, c : clearance of the bearing)	31
Figure 9 Methodology process	51
Figure 10 Rolling bearing (left) and hydrodynamic plain bearing (right)	60
Figure 11 Hydrodynamic bearing parameters [112]	61
Figure 12 Qualitative Stribeck curve – ω : rotating speed, η : dynamic viscosity, Q radial load, R : radius, c : radial clearance.....	62
Figure 13 Metal-metal contact PbM flowchart	64
Figure 14 Axis reference (u : sliding contact velocity)	66
Figure 15 Contact between rough and flat smooth surfaces- h , d_a , mean plane of summits and surface mean plane respectively [126]	73
Figure 16 Mean square error of Gaussian fitting curve of $F32(x)$ –left. And Polynomial fitting curve of $F52(x)$ –right.....	74
Figure 17 Hydrodynamic bearing 3D model of the IDG – lubricant pressure boundary conditions	79
Figure 18 Hydrodynamic bearing 3D model of the IDG – lubricated (green) and fixed (blue) surfaces	80
Figure 19 Boundary conditions scheme	84
Figure 20 Initial GUI: Configuration of flight simulation and IVHM tool	93

Figure 21 IVHM tool GUI: 1- health indicators, 2- health assessment, 3- operational conditions, 4- Decision making in the aircraft.....	94
Figure 22 IVHM tool process and data flow diagram.....	98
Figure 23 3D linear interpolation notation – x_i : simulated operational conditions, p : actual operational conditions, $p_{r,c}$ lower dimension interpolations.	100
Figure 24 Estimated friction coefficient by the PbM in the hydrodynamic bearing of the IDG – Generator torque 40 Nm	107
Figure 25 Estimated percentage of load transmitted through the asperities by the PbM in the hydrodynamic bearing of the IDG – Generator torque 40 Nm	108
Figure 26 Estimated friction coefficient by the PbM in the hydrodynamic bearing of the IDG – Generator torque 80 Nm	108
Figure 27 Estimated percentage of load transmitted through the asperities by the PbM in the hydrodynamic bearing of the IDG – Generator torque 80 Nm	109
Figure 28 Estimated friction of load transmitted through the asperities by the PbM in the hydrodynamic bearing of the IDG – Generator torque 296 Nm.....	109
Figure 29 Estimated percentage of load transmitted through the asperities by the PbM in the hydrodynamic bearing of the IDG – Generator torque 296 Nm	110
Figure 30 Schematic of the friction apparatus (not in scale) 1 – Guiding poles; 2- load cell; 3 – base; 4 – linkage bar; 5 – housing; 6 – shaft; 7 ‘ lip seal; 8 – computer system; 9 – load applying device; 10 – lubrication system [82]	115
Figure 31 Redesigned replica of the planetary transmission of the IDG.....	120
Figure 32 3D Replica of the planetary transmission. 1 – Hydrodynamic bearing, 2 – Planetary gear, 3 and 4 – Carrier shaft (input), 5 – Crown gear (output)	121
Figure 33 Layout of replica of planetary transmission. 1 – Hydrodynamic bearing, 2 – Planetary gear, 3 and 4 – Carrier shaft (input), 5 – Crown gear (output), 6 – External gear, T1 – thermocouple close to bearing	122
Figure 34 Test rig housing.....	123
Figure 35 Test rig layout – Electrical set-up	124
Figure 36 Lubrication system layout.....	125
Figure 37 IDG rig Control and DAQ systems.....	126
Figure 38 PbM and experimental comparison of Stribeck curve for (a) 667 N and (b) 1112 N loads	134

Figure 39 Comparison of minimum film thickness considering the deformations of the bearing or the hydrodynamic phenomena only, for high and low loaded conditions	136
Figure 40 Comparison of maximum hydrodynamic pressure ($p_{h,max}$) and maximum asperity contact pressure ($p_{a,max}$) for high and low load in the plain journal bearing.....	137
Figure 41 Comparison of the percentage of contact area for high and low load in the plain journal bearing	138
Figure 42 PbM predicted Stribeck curve for a generator torque of 20 and 40 Nm	142
Figure 43 Planetary transmission experimental results of input torque for a constant generator torque of 20 Nm with lubricant at ambient temperature	143
Figure 44 Planetary transmission experimental results of input torque for a constant generator torque of 40 Nm with lubricant at ambient temperature	143
Figure 45 Lambda (λ) representing mixed lubrication at 250 rpm, 40 Nm, 20 °C (metal-metal contact if ($\lambda < 4$))	147
Figure 46 Lambda (λ) representing mixed lubrication at 132 rpm, 40 Nm, 20 °C (metal-metal contact if ($\lambda < 4$))	147
Figure 47 Lambda (λ) representing mixed lubrication at 10 rpm, 40 Nm, 20 °C (metal-metal contact if ($\lambda < 4$))	148
Figure 48 Experimental absolute outlet lubricant temperature T_1 for a generator torque of 20 Nm.....	149
Figure 49 Experimental absolute outlet lubricant temperature T_{1t} for a generator torque of 40 Nm.....	150
Figure 50 Experimental temperature gradient $\Delta T = T_1 - T_{RTD}$ for a generator torque of 20 Nm.....	151
Figure 51 Experimental temperature gradient $\Delta T = T_1 - T_{RTD}$ for a generator torque of 40 Nm.....	151
Figure 52 Experimental inlet pressure for a generator torque of 20 Nm.....	152
Figure 53 Experimental inlet pressure for a generator torque of 40 Nm.....	153
Figure 54 Experimental inlet flow for a generator torque of 20 Nm	154
Figure 55 Experimental inlet flow for a generator torque of 40 Nm	154

LIST OF TABLES

Table 1 Comparison of literature in DDM and PbMs for rotating machinery in diagnostics and prognostics based review papers from Jardin et al. [29] and Heng et al. [16]	18
Table 2 Major causes of premature hydrodynamic bearing failure across all industries [31]	19
Table 3 Applications of PbMs based on fatigue and wear for health condition monitoring.....	26
Table 4 Hydrodynamic journal bearing of the IDG - mesh properties, fluid and solid domains.....	81
Table 5 Geometrical properties of the hydrodynamic bearing of the IDG	81
Table 6 Lubricated surface properties of the hydrodynamic bearing of the IDG	81
Table 7 Mechanical properties of the hydrodynamic bearing of the IDG	82
Table 8 Properties of the lubricant Mobil Jet Oil II [132]	82
Table 9 Viscosity-temperature model parameters for Mobil Jet Oil II	83
Table 10 Plain journal bearing mesh properties, fluid and solid domains	85
Table 11 Geometrical properties of the plain journal bearing	85
Table 12 Lubricant surface properties of the plain journal bearing	86
Table 13 Mechanical properties of shaft and housing of plain journal bearing .	86
Table 14 Properties of the lubricant SAE 30	86
Table 15 Plain journal bearing properties [82]	116
Table 16 Plain journal bearing lubricant – SAE 30 oil properties.....	116
Table 17 Properties of the hydrodynamic bearing of the IDG replica	123
Table 18 Main characteristics of the lubrication system	125
Table 19 IDG and test rig sensors	127
Table 20 IDG experimental procedure – range of operational conditions.....	128
Table 21 Jet oil II properties [132]	129
Table 22: comparison of experimental and PbM on the detection of metal-metal contact	145

LIST OF ABBREVIATIONS

AE	Acoustic Emissions
ANN	Artificial Neural Network
CAMO	Continuous Airworthiness Management Organization
CBM	Condition Based Monitoring
CFD	Computational Fluid Dynamics
GUI	Graphical User Interface
DAQ	Data Acquisition
DDM	Data Driven Model
EHL	Elasto-hydrodynamic lubrication
FEA	Finite Element Analysis
HCF	High Cycle Fatigue
HUMS	Health and Usage Monitoring System
IDG	Integrated Drive Generator
IVHM	Integrated Vehicle Health Management
LCF	Low Cycle Fatigue
MRO	Maintenance, Repair and Overhaul
PbM	Physics-based Model
PHM	Prognostics Health Management
RUL	Remaining Useful Life
VSD	Variable Speed Drive

1 Introduction

The study of the health of a system, commonly referred as health condition monitoring, is a broad area of research where different disciplines are required. Specific engineering disciplines may be required to understand the behaviour of the system. Data analysis is also required to extract the health information from the data generated by the system. In addition, maintenance, logistics and cost analysis knowledge are required to obtain the maximum benefit of health condition monitoring and create a business case.

Additional challenges appear when the system is a vehicle or fleet of vehicles, commonly referred as Integrated Vehicle Health Management (IVHM). The sensors should be integrated in the vehicle. In the aerospace sector the integration of IVHM systems in legacy aircraft is an additional challenge. Significant modifications of the design require certification processes that may be slow and offset the benefit of using IVHM. Thus, minimizing changes in the design by avoiding the addition of new hardware or sensors is an important aspect to maximize the benefits of IVHM.

The health assessment can be divided in diagnostics and prognostics. Diagnostics consists in the detection, localization and isolation of a failure. Prognostics consist in the detection of the degradation of a system before total failure occurs and may include the estimation of the Remaining Useful Life (RUL).

The health assessment, diagnostics and prognostics, can be conducted through Data Driven Model (DDM) or Physics-based Model (PbM) approaches. DDMs apply algorithms that do not require an understanding of the physics of the system to assess its health state. The health assessment is obtained by looking at statistical parameters or applying more complex machine learning techniques into historical data. Whereas PbMs represent the system under healthy and faulty conditions through physical principles by modelling its behaviour and degradation mechanisms.

This project proposes a novel health condition monitoring technique based on PbMs to detect metal-metal contact in the hydrodynamic bearing of the planetary transmission of an aircraft system, the Integrated Drive Generator (IDG) without any additional sensor. In addition, the proposed PbM is contribution to the field of tribology. The PbM evaluates metal-metal contact effects locally along the lubricated surface instead of considering a whole bearing.

In the following sections of chapter 1 the background of the project is introduced along with a personal statement that includes the list of publications related to this thesis. Chapter 2 will introduce the relevant literature. Chapter 3 describes the research objectives based on the findings from the literature and defines the contributions of the project. Chapter 4 provides a comprehensive description of the PbM. Chapter 5 describes the application of the PbM, presented in chapter 4, for health condition monitoring of the IDG's planetary transmission hydrodynamic bearing. Chapter 6 describes the test rigs and experimental set-ups required to validate the predictions of metal-metal contact. Chapter 7 compares metal-metal contact between the experiments and the PbM along with additional experimental and PbM results. The results and relevance of each contribution are discussed in chapter 8 and the key conclusions are summarized in chapter 9. Finally, the next steps forward are proposed in chapter 10.

1.1 Background

The work presented in this thesis is part of an European project, RepAIR, which aims to reduce the maintenance cost of aerospace industry through the use of

IVHM and new repair technologies, in particular Additive Manufacturing for metals.

In order to explore novel IVHM techniques a real case study of an airplane is used. The case study consist in the hydrodynamic bearings of a planetary transmission, which is part of an Integrated Drive Generator (IDG).

This section presents the necessary background to define the research problem definition. First, the function of the transmission is described (see 1.1.1), secondly, the failures mode that requires a novel IVHM technique is presented (see 1.1.2) and finally the requirements of an alternative IVHM solution are provided (see 1.1.3).

1.1.1 IDG description

The IDG extracts mechanical power from the jet engine and transforms it into electricity to feed all the elements of the electrical system. The IDG produces electrical power that are distributed using a 3 phase A.C. circuit with a constant frequency.

To ensure the speed of the electric generator remains constant, IDGs rely in the use of a constant speed drive; which are a combination of a planetary transmission with a hydraulic pump unit that modifies the gear ratio of the transmission; thus, regulating the output speed that goes to the generator.

Some aircraft use two separate units: an independent constant speed drive, and a generator. However, most modern aircraft use IDGs for simplicity and weight saving (see Figure 1).



Figure 1 IDG - Source: www.megakeep.com

Several mechanical failures sustained by IDGs are caused by the constant speed drive, specifically, by their planetary transmissions (see Figure 2). In addition, it is common practise to consider the IDG as a line replaceable unit by the Maintenance, Repair and Overhaul (MRO) organization responsible of the maintenance of the aircraft. Thus, any failure leads to the replacement of the complete IDG.

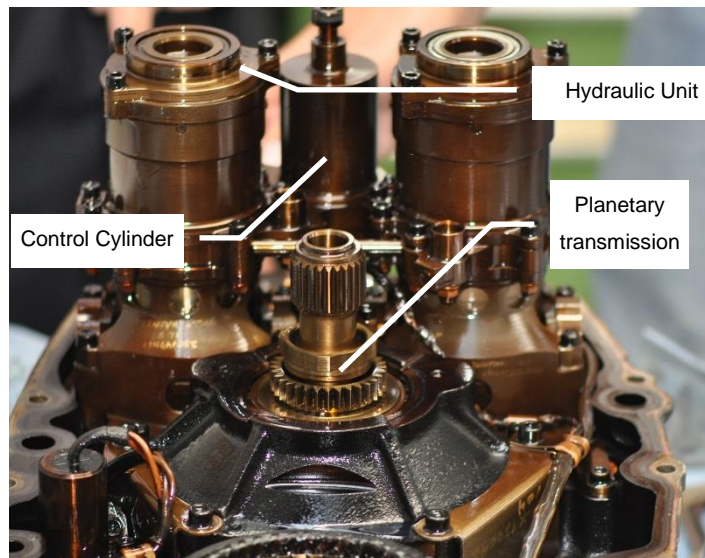


Figure 2 Open IDG showing the constant speed drive. The planetary transmission sits on the front with twin hydraulic units on each side and control cylinder in the middle.

A faulty line replaceable unit is replaced for a healthy one without disassembling its subcomponents when the aircraft is on the ground. The plane continues its missions and the availability of the aircraft is only affected by the time required to install a healthy line replaceable unit and replace the faulty one. The faulty line replaceable unit is sent to the specialized workshop where it will be tested, disassembled, repaired and tested again before it is installed in another airplane.

The transmissions controls the output speed through the hydraulic pump unit (see Figure 2) by modifying the gear ratio of the transmission. Typically a planetary transmissions consists in: carrier shaft, planetary gears and two crown gears. In order to transmit the power one of these elements must be fixed (zero speed); however, in the constant speed drive all these components are rotating. Instead, one of the crown gears is connected to the hydraulic pump unit; which imposes the crown gear rotating speed in one direction or the other (see Figure 3), and by doing so, the gear ratio can be regulated and power transmitted through the transmission even if none of its elements is at zero speed

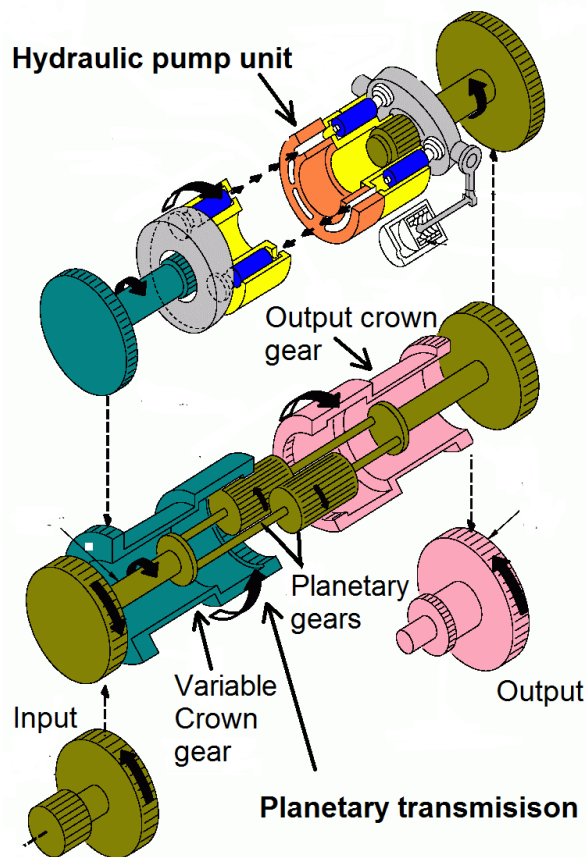


Figure 3 Planetary transmission diagram

1.1.2 Failure mode

Most critical failure modes of the IDG are due to electrical faults in the generator or due to mechanical degradation of the rotating components of the planetary transmission caused by fatigue, inadequate lubrication or excessive friction.

The input shaft that is attached to the turbine can be disconnected if total failure occurs in the IDG; thus, effectively disconnecting the IDG and not providing electrical power to the aircraft. The shaft can only be reconnected on the ground, and not during flight. However, typically there are redundant IDGs in the aircraft: one for each turbine and another one in the auxiliary power unit. The disconnection of one of the IDGs does not compromise the safety of the aircraft but it lead to the activation of the auxiliary power unit or the disconnection of non-critical electrical systems in the aircraft.

In order to avoid disruptions in the operation of the aircraft and the subsequent maintenance costs of replacing and inspecting non-faulty IDGs, minimizing the number of false alarms is critical. Having the capability to pinpoint the cause of the failure of an IDG can result in reduced time in the maintenance shop floor and savings in labour cost.

Fatigue related failures, e.g. pitting in the planetary gears, are caused by continuous degradation and most IDGs are replaced before a critical failure occurs. However, a critical failure, consisting in metal-metal contact in the hydrodynamic bearings of the planetary transmission, is not caused by constant degradation and IVHM capabilities could lead to increased availability of the aircraft and reduced maintenance costs.

In its current configuration this failure can only be detected through an increased oil temperature at the sump. However, the failure is only detected when total failure has occurred and the journal and planetary gear are stalled; thus causing severe damage in the adjacent components as well (see Figure 4).



Figure 4 Example of damage of adjacent components (left: planetary gear $\text{Ø}=37\text{mm}$, centre: carrier shaft $\text{Ø}=94\text{mm}$ and bearing shaft $\text{Ø}=24\text{mm}$, left: carrier shaft 2 $\text{Ø}=94\text{mm}$)

It should be noted that the same oil is used for the lubrication of the transmission and for powering the hydraulic pump unit that regulates the speed of the IDG. The hydraulic pump unit requires a significant amount of lubricant when activated; therefore, excessive friction in the transmission only increases the temperature of a small portion of lubricant; whereas the heat produced in the hydraulic pump

can significantly increase the temperature of the oil that will be used for lubrication.

1.1.3 IVHM solution requirements

The current system has proven ineffective in the detection of metal-metal contact in the hydrodynamic bearings of the IDG. The current system only relies on the lubricant temperature at the sump; however, this temperature is affected by the hydraulic unit and the failure is only detected after total failure has occurred with the subsequent damage of adjacent parts.

An alternative IVHM system must be able to detect or predict metal-metal contact in the early stages to avoid total failure and the subsequent damage of other components of the transmission. Thus, the IVHM tool would minimize the maintenance cost by reducing the testing and inspection times, and avoiding secondary damage to adjacent parts. In addition, the availability of the aircraft can be increased if total failure is avoided due to the IVHM system, e.g. if the pilot can actuate and avoid further damage. However, it should be noted that if the false alarms rate is too high, the additional cost may offset the benefits previously mentioned.

Certification costs can also offset any benefit if the design is modified and a certification process is required. Therefore, avoiding any modification of the IDG design is critical. If possible, the sensors and parameters already available in the IDG must be used, avoiding the installation of any additional sensor.

The IDG in the current configuration measures: sump temperature, rotating speed, oil pressure, and electrical parameters from the generator; thus, output torque can be obtained from the generator as well. It should be noted that information about input torque is not available, nor is vibration data.

1.2 Proposed solution

The proposed solution and main contributions of this thesis are described in detail in chapter 3, based on the gaps in the knowledge identified in chapter 2. This section only aims to provide a brief introduction of the content and contributions of the thesis.

In order to detect metal-metal contact in the hydrodynamic bearing of the IDG's planetary transmission a novel Physics-based Model approach that does not require additional sensors has been developed (chapters 4, 5). The model is compared to experimental results of a replica of the planetary transmission and a plain journal bearing (chapters 6, 7).

Metal-metal contact is estimated by a computational mixed lubrication model capable of representing the hydrodynamic, solid mechanics, and asperity contact phenomena locally along the lubricated surface; as opposed to previous mixed lubrication models that evaluate metal-metal contact globally in the whole hydrodynamic bearing.

1.3 List of publications

Journal papers

1. Cubillo, A., Uriondo, A., Perinpanayagaman, S. "Computational Mixed-TEHL model and Stribeck curve of a journal bearing", Tribology Transactions, Taylor & Francis, October 2016, DOI: 10.1080/10402004.2016.1245456.
2. Cubillo, A., Perinpanayagaman, S., Esperon-Miguez, M. "A review of physics-based models in prognostics: Application to gears and bearings of rotating machinery", Advances in Mechanical Engineering, SAGE publications, July 2016 vol. 8 (8), pp. 1-21, DOI: 10.1177/1687814016664660.

Conference papers

1. Cubillo, A, Perinpanayagam, S., Rodriguez, M., Collantes, I., Vermeulen, J. "Prognostics Health Management System based on Hybrid Model to Predict Failures of a Planetary Gear Transmission", Machine Learning and Cyber Physical Systems, Springer, 2015, Lemgo, pp. 33-44. DOI: 10.1007/978-3-662-48838-6_5.
2. Cubillo, A., Perinpanayagam, S., Rodriguez, M., Collantes, I., Vermeulen, J. "Physics-based IVHM Systems for Predicting the RUL of an Aircraft Planetary Gear Transmission", 2015, 5th EASN Conference, Manchester.
3. Cubillo, A., Perinpanayagam, S., Esperon-Miguez, M. "Multiphysics-based model for prognostics in a planetary transmission", 2014, PHM Texas conference.

Additional papers

1. Cubillo, A., Perinpanayagam S. “Challenges of redesigning a planetary transmission made by Additive Manufacturing”, Advances in Transdisciplinary Engineering, 14th International conference on Manufacturing Research, September 2016, Loughborough, pp. 81-86. DOI: 10.3233/978-1-61499-668-2-81.
2. Cubillo, A., Perinpanayagam, S., Esperon-Miguez, M. “Maintenance optimization of an aircraft fleet considering IVHM based on cost and availability considering the use of additive manufacturing”, Prognostics and Health Management Conference, Bilbao, July 2016.

To be submitted

1. Novel Physics-based technique to detect metal-metal contact in a hydrodynamic bearings of a planetary transmission of an aircraft system

2 Literature Review

The aim of this chapter is to put together all the relevant literature to develop a novel health condition monitoring technique to detect metal-metal contact in the hydrodynamic bearing of the planetary transmission. Thus, providing an understanding of the current state-of-the-art and a identifying the relevant gaps in the knowledge. Part of this literature review is based on the published review paper “*A review of physics-based models in prognostics: Application to gears and bearings of rotating machinery*” [1] included in the appendix A.

First, the concept of health condition monitoring and IVHM in particular are reviewed along with the research on hydrodynamic bearings’ diagnostics and prognostics (see 2.1).

Health condition monitoring can be based on DDM or PbM techniques. Whereas research in DDM approaches is extensive, PbMs applied to IVHM are more limited, as shown in subsection 2.1, this is particularly true for hydrodynamic bearings. Therefore, the state-of-the-art of PbMs for the diagnostics and prognostics of gears, rolling bearings, and hydrodynamic bearings is introduced in subsection 2.2. The research on IVHM for hydrodynamic bearings is limited compared to rolling bearings or gears, but their failure modes and degradation mechanisms have many aspects in common, which is the reason of extending the scope of the literature review.

Models capable of representing the hydrodynamic phenomena, under fully flooded and mixed lubrication, when metal-metal contact occurs, has been studied in the field of tribology. These models can potentially be used by health condition monitoring techniques to detect metal-metal contact. The state-of-the-art of PbMs capable of representing metal-metal contact in hydrodynamic bearings is reviewed in detail in subsection 2.3.

2.1 Health Condition Monitoring

The review of health condition monitoring introduces the main potential benefits and challenges normally encountered, the diagnostics and prognostics techniques and finally focuses on the research in hydrodynamic bearings.

2.1.1 Benefits and challenges

Prognostics and Health Management (PHM) refers to the capability to assess the current (diagnostics) and future (prognostics) health state of a system; which can be a machine, a process or a vehicle. As a result the maintenance plan can be optimized depending on the current health status of the system, called predictive maintenance or Condition-Based Maintenance (CBM), instead of relying on historical data and life estimation calculations (preventive maintenance) or reacting only when a failure occurs (reactive maintenance) [2].

IVHM refers to the capability to assess the current and future health state of a vehicle, integrating the whole picture in a framework that also takes into account the available resources and operational demand of the whole fleet [3]; therefore, the role of IVHM is to provide the required inputs to determine the optimal maintenance operations depending on the actual health status of the system. It should be noted that the term IVHM refers to vehicles and therefore the transmission of data between vehicle and ground or the implementation of sensors in the vehicle are also covered by IVHM. The IVHM architecture and data flow is illustrated in Figure 5.

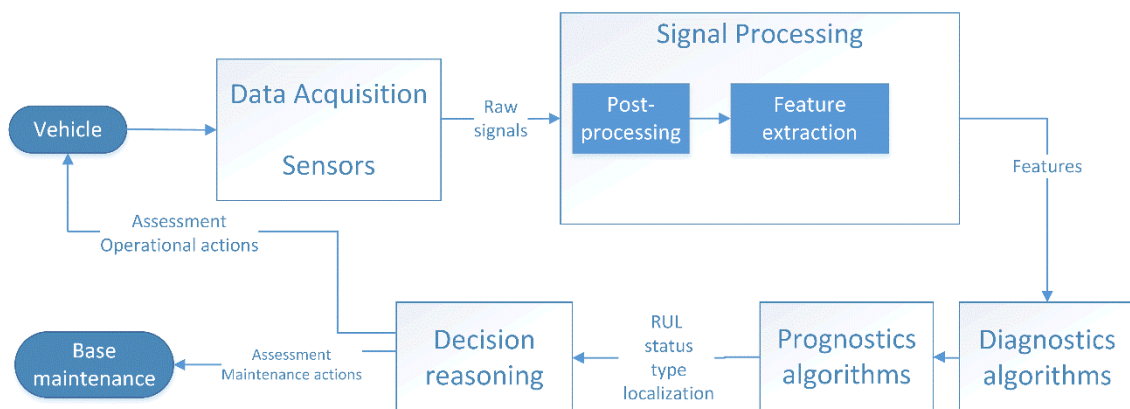


Figure 5 Architecture of an IVHM system

The examples of a vehicle that implements a complete IVHM system are limited. One of the best examples of IVHM in an aircraft is called Health and Usage Monitoring System (HUMS) that came into service in 1991, included in many helicopters nowadays. The functions and capabilities of HUMS are described by Land [4], showing that it is economically effective; however, a better understanding of how the aircraft will be used by the operator is needed along with full cooperation with the design authority.

The main benefits of a CBM strategy for diagnostics are the cost and time reduction due to fault localization and isolation capabilities as less testing and inspection are required. For prognostics, secondary damage can be avoided if the failure is detected in the early stages and a higher availability of the vehicle can be obtained if the failure is prevented due to the IVHM prediction. In addition, a planned maintenance operation can take place when the vehicle arrives with the subsequent benefits in terms of cost reduction and improved availability mentioned above if the RUL is estimated and the prognostics window is long enough to allow for a remedial action [3], [5].

Additional benefits include the reduced mean maintenance time due to fault localization, the reduced disruption and the increased safety due to the reduction of unexpected failures [6], [7]. However, these benefits must overcome the additional cost of the technology required to implement CBM.

All these benefits cannot be accomplished without overcoming the challenges of implementing the technology. The main challenges are related to the cultural change, the prediction of the health of the system and the management of the data. One of the most important threads to these new systems is the resistance to the necessary change of the organizational culture to address the barriers of IVHM [6], [8]. Baroth et al. [7] identify the cultural shift from conservative preventive and corrective maintenance strategies towards pro-active strategies based on the data provided by IVHM systems as the key aspect that provokes resistance in the organizations.

An additional problem is the extra cost due to false alarms, i.e. detecting non-existent failures. An increment of the value of the thresholds would reduce the false alarm rate but may also increase the number of undetected failures. Bechhoefer and Bernhard [9] have developed a methodology for minimizing false alarms affected by variations in the operational conditions and Dempsey et al. [10] have analysed the rate of false positives of an aircraft's gearbox and developed a methodology to define a threshold that minimizes the number of them while maintaining sensitivity to the failure. The optimization of the health indicator thresholds is out of the scope of this thesis.

The implementation of the sensors in the system or vehicle also has to be considered. The optimal selection of sensors is crucial to minimized extra weight and data stored and processed. Niculita et al. [11] showed how the optimal set is selected taking into account number of sensors, cost, weight, reliability and coverage from experimental data from multiple sensors using an unmanned aerial vehicle fuel rig as a case study.

If extra sensors are required, their implementation and their connection to a power supply in a vehicle can be problematic from an engineering point of view, but also due to regulations, which is especially evident in legacy aircrafts because the design cannot be modified without the certification authority approval, as shown by Esperon-Miguez[12].

2.1.2 Diagnostics and prognostics techniques

The information generated by a PHM system can be divided into diagnostics and prognostics: diagnostics includes anomaly detection, fault isolation, fault classification and its uncertainty [13]; while prognostics includes the estimation of the RUL, the uncertainty of the prediction and incipient fault detection. In addition, diagnostics and prognostics knowledge can be used for future improvements of the design [14], [15].

In order to evaluate the health of a system the various techniques are commonly categorized into Data-Driven Models (DDMs), Physics-based Models (PbMs) and hybrid models [16]–[18]. DDMs are based on statistical and machine learning techniques and do not rely on the knowledge of the physics that govern the system or its degradation mechanisms [17]: these techniques have proven successful for fault detection [19], classification [20] and RUL estimation [21]. PbMs consist in the use of mathematical models that describe the physics of the component to assess its current and future health, the performance of PbMs depends on the capability of the models to accurately represent the failure and degradation phenomena. Hybrid models refer to the integration of different models, either by using various approaches depending on the task, for instance a DDM for diagnostics and a PbM for prognostics [22]–[26]; or a combination of several models that represent the same phenomena to obtain a more robust health assessment, so called ensemble models [27], [28].

The main advantages of machine-learning techniques are their potential to be used in several systems as knowledge of the physics of the system is not required; thus, being easily scalable to different systems. However, machine-learning techniques have problems like risk of over fitting [24] and the necessity of large training data sets compared to PbM approaches [17]. Additionally, the synergies between PbMs and models used during the design phase make them particularly suitable when the health condition monitoring system is being developed during the design phase [18]. It should be noted that PbM approaches are system specific; thus, not easily scalable and it can be challenging to obtain measurable indicators directly related to the outputs of the PbM [13].

Reviews covering the state of the art of health condition monitoring for rotating machinery have already been published focusing on the methodologies and algorithms of PHM in rotating machinery [17], [29], and specific techniques like the empirical mode decomposition for fault diagnosis [30] or vibration analysis [31]. As shown in Table 1, research focuses on DDM techniques for condition health monitoring of rotating machinery rather than PbM. This is more significant due to the fact that PbMs are system and failure mode specific; thus, different PbM are required for each system or degradation mechanism.

Table 1 Comparison of literature in DDM and PbMs for rotating machinery in diagnostics and prognostics based review papers from Jardin et al. [29] and Heng et al. [16]

Diagnostics [29]		Prognostics [16]	
DDMs	PBMs	DDMs	PBMs
26	11	16	10

2.1.3 Hydrodynamic bearings

Most of the research in health condition monitoring of rotating machinery refers to gears and rolling bearings. In comparison, the literature in hydrodynamic bearings is limited. This section introduces the common failure modes of hydrodynamic bearings and the health condition monitoring techniques that can be applicable to them.

The main function of hydrodynamic bearings and rolling bearings is identical: to provide low friction in the sliding direction and to transmit the radial and axial loads, in addition, they can be used for heat dissipation. The main difference is the type of contact, hydrodynamic bearings consist in two surfaces that slide without any intermediate component, whereas rolling bearings include rotating elements in between. The most typical failure modes of hydrodynamic bearings are shown in Table 2 [32]; which is in accordance with the conclusions from Zeidan et al. [33].

Table 2 Major causes of premature hydrodynamic bearing failure across all industries [31]

Major causes of premature bearing failure	
Dirt	45.4%
Incorrect assembly	12.8%
Misalignment	12.6%
Insufficient lubrication	11.4%
Overloading	8.1%
Corrosion	3.7%
Improper journal finish	3.2%
Other	2.8%

Dirt, incorrect assembly and defects in the manufacturing process are particularly difficult to monitor. Thus, most of the research has been focused on detecting insufficient lubrication, which is related to metal-metal contact and leads to rapid degradation. The main failure mechanism related to insufficient lubrication is scuffing, consisting in a rougher surface due to particles or metal-metal contact, which eventually develops into seizure [34]. Even if a film of lubricant remains and there is not metal-metal contact, fatigue damage can occur due the cyclic stresses on the surface of the bearing as shown by Huang et al.[35], who studied fatigue wear in hydrodynamic bearings.

A variety of failure analysis of hydrodynamic bearings can be found in the literature. Venci et al. [36] studied the failures of over 180 engine bearings finding that abrasive wear is the predominant degradation mechanism followed by adhesive and fatigue wear as shown in Figure 6. However, research on health condition monitoring techniques is very limited.

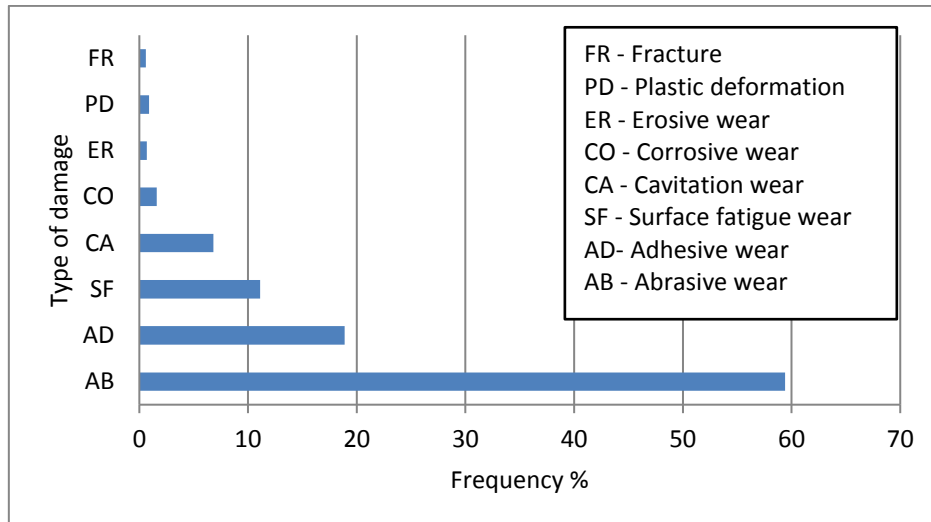


Figure 6 Percentage occurrence of types of hydrodynamic bearing damage [36]

A comparison between temperature measurements, electric resistance, vibration analysis and metallic particle measurements for detecting metal-metal contact have been conducted by Okamoto et al. [37], showing that:

- Vibration analysis at high frequencies can detect metal-metal contact.
- Temperature analysis yields good results but its sensitivity depends on the location of the sensor.
- Electrical resistance and debris analysis are effective in detecting metal-metal contact.

Moosavian et al.[38] used vibration analysis to detect oil starvation using Artificial Neural Networks (ANNs) while a less common technique, Acoustic Emissions (AEs), have also proven successful for detecting metal-metal contact [39]. It should be noted that research on wear and fatigue detection of sliding contacts, e.g. rolling bearings, can also be applied to hydrodynamic bearings considering line contact instead of point contact.

Regarding the use of PbMs in hydrodynamic bearings, many failure modes are not ideal for a PbM approach based on their degradation mechanism because the parameters of the degradation mechanism are unknown, e.g. dirt, incorrect assembly, misalignment, geometrical imperfections. However, the underlying degradation mechanisms of some important failure modes can be modelled and used for PHM.

Insufficient lubrication; which leads to scuffing is caused due to wear in the contact between the journal and the support. This failure mode can potentially be monitored with a degradation model capable of modelling the wear and increased friction in the contact. There are models capable of representing the friction and metal-metal contact phenomena in the literature (further details in section 2.3). However, these models have not been used for health condition monitoring of hydrodynamic bearings.

2.1.4 Conclusions of health condition monitoring

Health condition monitoring, and IVHM in particular, have the potential to provide benefits in terms of cost, availability and safety. The main benefits are the potential increased availability of a vehicle along with the reduction of the mean time to repair and the maintenance cost. However, the cultural resistance and the reliability of the IVHM system are critical factors. A particularly critical challenge is the restrictive regulation in legacy aircraft; which makes difficult the introduction of IVHM systems that require additional sensors.

The use of DDM or PbM approaches depend on the system as each approach have advantages and disadvantages. DDM approaches are easily scalable and can be easily implemented if sufficient data is available. However, if the data available is limited a PbM approach may be advisable. In addition, a PbM provides an understanding of the physics of failure that can lead to additional advantages; e.g. the failure may be avoided by re-designing the component or the operational conditions can be modified to avoid degradation.

Literature in DDMs techniques is more extensive than in techniques based on PbMs. In addition, DDMs are scalable to other systems; whereas PbMs are system and failure mode specific; thus, the state-of-the-art of PbMs is not as extensive.

The literature on health condition monitoring techniques for hydrodynamic bearings is limited, consisting in DDM techniques based on vibration or AEs. However, the research is focused on stand-alone hydrodynamic bearings with a fixed housing. Which means that the bearings are isolated from other adjacent components and the sensors can be located close to the bearing. These approaches may have limitations if the bearing is part of a planetary transmission where the housing and the journal are both in motion.

PbMs to detect metal-metal contact have not been used in hydrodynamic bearings. However, the physics of failure are well understood and it has the potential of being monitored through a PbM capable of predicting metal-metal contact.

2.2 Physics-based Modelling

The previous section introduced the concept of health condition monitoring, differentiating between DDMs and PbM techniques. Both approaches are valid; however, for the detection of metal-metal contact in hydrodynamic bearings DDMs normally rely on vibration and AEs. Whereas there are not PbMs to detect metal-metal contact even if the physics of failure are well understood. Therefore, a PbM approach is preferred in this project.

This section introduces the concept of physics-based modelling and provides a comprehensive review of its state-of-the-art for health condition monitoring in hydrodynamic bearings. A more extensive review of PbMs for PHM can be found in the review article published by the author of this thesis: “*A review of physics-based models in prognostics: Application to gears and bearings of rotating machinery*” [1] included in the appendices.

The state-of-the-art of PbM approaches for health condition monitoring of rotating machinery has not been reviewed in depth. Review papers normally include a section mentioning significant PbM approaches [17], [29]; but the description of the principles behind those models is limited.

2.2.1 Generic Approach

PbM approaches, also referred to as Model-based approaches, assess the health of the system by solving a set of equations derived from engineering and science knowledge [13], either for diagnostics or prognostics. However, the main advantage of PbMs consists in using degradation models to predict long term behaviour [40]. Luo et al. [41] proposes a generic process to develop prognostics based on PbMs by considering a set of equations that define the dynamics and the degradation of the system as shown in Figure 7. The process consists in a model of the system and its degradation, where random scenarios are simulated and compared to measurable data to identify the appropriate scenario (feature estimation) and, if possible, estimate the RUL.

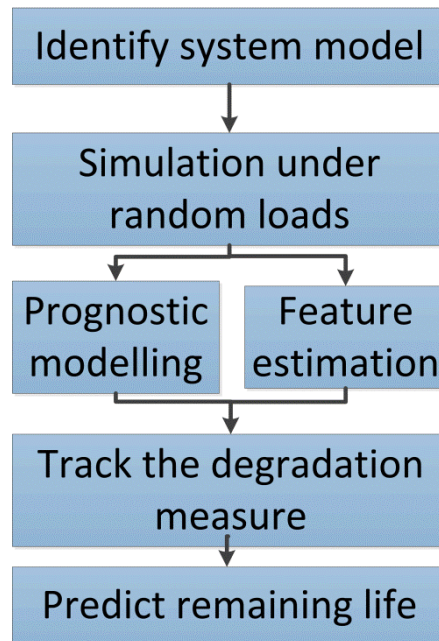


Figure 7 Physics-based approach [41]

Normally for diagnostics a fault is detected by comparison between the outputs of the physics-based model and the measurements from the real system. An example of diagnostics using PbMs is the classification of bearing defects by measuring the natural frequencies of the components of the bearing, obtained from knowledge of the physics of the system, and deviations from normal values are used as health indicators as shown by Li et al.[42].

It should be noted that prior knowledge of the current health status of the system (diagnostics) is required to develop prognostics capabilities. For prognostics based on PbMs, degradation models are used to represent the degradation mechanisms of the system and the RUL can be estimated as an output of these models. For instance, degradation models based on Paris law [43] to represent crack growth have been used by several authors to estimate the RUL of systems subject to fatigue by predicting crack growth [22], [44]–[49].

For RUL estimation, regardless of the approach (PbM, DDM or hybrid), the health condition monitoring algorithm provides an assessment of the current health of the system, normally by measuring a health indicator, and a prediction of the future health of the system. The prediction of the current health state should be as accurate as possible to allow for reliable future health estimations.

However, there are errors between the predicted value of a health indicator and the measured one. These errors are particularly critical for RUL estimation. Thus, it is advisable to have the capability to adjust the model in order to minimize these differences based on the previous errors between the predicted health indicator and the measured ones. This can be done by combining PbMs with parameter estimators to minimize these errors [3].

A unified formulation has been proposed by Jaw and Wang [50] to implement parameter estimators into PbMs given a generic set of system equations. However, this approach requires feedback about the current health state; which means that a PbM that estimates RUL can only be integrated with a parameter estimator if there is an alternative method of assessing the current health of the system (diagnosis) in real-time. It should be noted that the proposed PbM presented in this thesis aims to detect metal-metal contact in the early stages of the failure, but the estimation of the RUL is out of the scope of this thesis.

2.2.2 Relevant degradation models

The importance of representing accurately the physics of the system has been mentioned in previous sections. This subsection reviews the models of the most relevant degradation mechanisms related to hydrodynamic bearings: the degradation mechanisms fatigue and wear, summarized in Table 3.

Table 3 Applications of PbMs based on fatigue and wear for health condition monitoring

Fatigue	Wear
General fatigue models [56], [59]	General wear [119]
Cracks [14], [28]–[32], [107], [108]	Fretting [120]–[123]
Spalling [35], [37], [109]–[113]	Metal-metal contact [46], [124], [125]

Fatigue

Fatigue occurs in systems subject to cyclic loading, due to thermal and mechanical stresses. The degradation mechanism differs between High Cycle Fatigue (HCF) and Low Cycle Fatigue (LCF). In HCF stresses are below the yield stresses and $\Delta\sigma$ (stress range) is the factor that controls the degradation mechanism. However, for LCF the stress level is above the yield stress limit and there is plastic deformation. Thus, $\Delta\varepsilon$ (strain range) is the magnitude that controls the degradation [51].

For HCF, Wöhler [52] demonstrated that the cyclic stress range is the driven factor of fatigue degradation based on experimental fatigue data of railroad axles; thus, it should be represented using S-N curves that correlate the number of cycles and a characteristic stress level. The use of experimental S-N curves can be used for life prediction of metallic structures subject to fatigue. Analytical equations for the appropriate metallic structure can be found in well accepted standards like the British Standard 7608:2014 [53], which also provides the standard deviation as shown in Eq. [1], where N_f is the number of cycles, σ_a the stress amplitude, SD the allowed standard deviation and C_0 , d and m parameters dependent on the geometry.

$$\log(N_f) = \log(C_0) - d * SD - m * \log(\sigma_a) \quad [1]$$

Basquin law [54] proposed a stress based analytical equation based on the experimental work of Wöhler [52], shown in Eq. [2], where N_f also refers to the number of cycles, σ_a to the stress amplitude, σ'_f is the fatigue strength coefficient and b the fatigue strength exponent.

$$\sigma_a = \frac{\Delta\sigma}{2} = \sigma'_f (2N_f)^b \quad [2]$$

For LCF, plastic deformation is the main factor that controls the failure mechanism, Manson-Coffin law is commonly used to represent this degradation mechanism [55], [56]. This method considers that cyclic life depends on the deformation using a power law as shown in Eq. [3], where $\Delta\varepsilon_p$ is the plastic strain range and c and ε_f experimental constants. A more accurate model, the Manson and Halford model considers the elastic and plastic component of the strain; thus, being able to represent LCF and HCF degradation mechanisms, as shown in Eq. [4], where D represents the ductility, σ_u the ultimate tensile strength and E the Young Module [57].

$$\Delta\varepsilon_a = \frac{\Delta\varepsilon_p}{2} = \varepsilon_f (2N_f)^c \quad [3]$$

$$\Delta\varepsilon = D^{0.6} * N_f^{-0.6} + \left(\frac{3.5 * \sigma_u}{E} \right) * N_f^{-0.12} \quad [4]$$

Kacprzyński et al. [58] evaluated the plastic strain of a helicopter gear tooth using a Finite Element Analysis (FEA) model and later applies Manson-Coffin law to evaluate the number of cycles until crack initiation occurs.

A cumulative damage rule is required to take into account variable loading conditions. The simplest and a well-accepted approach was proposed by Miner [59] as shown in Eq. [5], where D is the cumulative damage, n_i are the current number of cycles under the actual loading condition and N_i are the number of cycles until failure; which is estimated if D is above 1. It should be noted that this approach considers the RUL independent of the order of the loads. Similar equations can be used to represent different types of cumulative damage. For instance, Qiu et al. [60] proposed a similar cumulative rule that is a function of the stiffness of the system instead of the number of cycles.

$$D = \sum_{i=1}^{load\ p} \frac{n_i}{N_i} \quad [5]$$

Cracks are a common consequence of fatigue damage, and the degradation mechanism that ultimately leads to failure due to fracture of the component. The previous models do not consider the physics that lead to the fracture and only rely on empirical results. An alternative approach is to predict the failure based on fracture mechanics. Crack growth is divided into three regions [51]:

- First region: slow crack growth and the crack length is not considered significant
- Second region: the crack growth rate becomes significant and constant
- Third region: the crack becomes unstable and the propagation rate increases until fracture occurs.

The initial length and the propagation rate of the crack can be estimated and used as an indicator of the RUL of a system subject to fatigue. The most widely accepted model for crack growth, the Paris law, was proposed based on experiments that proved the correlation between crack length and number of cycles by Paris et al. [43] as shown in Eq. [6], where a is the crack length, N the number of cycles, m and b are parameters of the material and K is an intensity coefficient that depends on the geometry and type of crack. A similar equation introduced by Hoeprich [61] can be used to represent spall area growth in bearings, shown in Eq. [7], where D is the defect area, C_0 and n material parameters, validated with experimental results by Li et al. [62] and further improved to consider thermal effects by Kotzalas and Harris [63]. It should be noted that specific degradation models can also be used for prognostics. For instance, the rolling contact fatigue model proposed by Sadeghi et al. [64] based on the crack propagation and crack initiation has the potential to be used for PHM.

$$\frac{da}{dN} = m\Delta K^b \quad [6]$$

$$\frac{dD}{dN} = C_0 D^n \quad [7]$$

Paris law represents the second region of crack growth but does not take into account the initial crack length and the instability of the crack. However, for PHM, being able to represent only the second region of the crack growth by using Paris law has proven sufficient to model the degradation of the system, as shown by Corbetta et al. [44], who estimated the crack growth on structures and the uncertainty of the prediction combining the PbM with particle filter for parameter estimation. Ray and Tangirala [45] also estimated the RUL based on Paris law but using a Kalman filter for parameter estimation. Orchard et al. [46] applied both, particle filter and an extended Kalman filter on a crack growth model based on Paris law to estimate crack length in the plate of the gearbox of a helicopter. Pais and Kim [65] developed a fatigue crack growth PbM for prognostics of aerospace panels by computing a FEA model and a fatigue crack growth model as a function of the usage history; a modified Paris law to consider variable amplitude loads was used.

Zio and Maio [22] combined Paris law with a support vector machine algorithm to select the appropriate degradation model to estimate crack length. Oppenheimer and Loparo [47] also calculated the RUL of rotor shafts due to cracks using Paris law, while Li and Lee [48] combined a dynamic model that estimates the stresses on a gear with Paris law to represent the degradation to estimate the RUL of the gear. A more sophisticated algorithm is proposed by Kacprzyński et al. [58], who estimated the RUL of helicopter gears by modelling the first region (crack initiation) using Manson-Coffin law presented above to estimate the number of cycles until a crack initiates and Paris law to estimate the crack growth afterwards. The spall degradation formula presented in Eq. [7] has been applied for RUL estimation of rolling bearings by several authors [66]–[68]; while Slack and Sadeghi [69] developed a more sophisticated explicit finite element spalling model that predicts the number of cycles until failure by modelling the crack initiation in the subsurface and its propagation. For diagnosis only, Fu and Gao [70] developed a PbM capable of estimating the natural frequency response of a crack in a fan blade assessing its size and location.

Wear

Wear is a degradation mechanism caused by friction between two sliding surfaces associated with loss of material, including damage due to direct contact between the surfaces and damage caused by the fluid between the surfaces [51]. Thus, wear is the main degradation mechanism of metal-metal contact in the hydrodynamic bearing.

However, the modelling of wear is particularly challenging due to the high influence of external factors that affects the contact such as the environment [71]. Wear can also be considered as a dissipation of energy mainly controlled by friction [72], and it is classified as: adhesive and abrasive (depending on the hardness of the materials in contact [73], corrosive, thermal and fatigue wear [74]. The phenomena differs between dry and lubricated contacts.

Regarding dry contacts, adhesive wear can be modelled using the Archard law, shown in Eq [8], where V_{wear} is the wear volume, H the material hardness, W the load, L the sliding distance and K the wear coefficient. Using this law more complex wear models can be obtained by modifying the value of the constant K , as shown by Watson et al.[74], who applied variants of Archard's law to represent adhesive, abrasive and corrosive wear.

$$V_{wear} = K \left(\frac{WL}{3H} \right) \quad [8]$$

Fatigue wear leads to cracks initiated below the surface that after a number of cycles leads to pitting or spalling with the subsequent removal of material. A degradation model for wear caused by sub-surface fatigue has been proposed by Ghosh et al. [75], who provided an experimental correlation between wear and crack propagation, which is a function of the shear stress on the surface as shown in Eq. [9], where N is the number of cycles to failure, a and b are empirical constants, and Q is the contact shear stress that depends on the friction coefficient and load applied.

$$\log(N) = a \cdot \log(Q) + b \quad [9]$$

However, wear is controlled by friction, as such; more accurate models should predict the friction between the sliding surfaces as well. The friction force is defined as the opposing force to the motion of a body to another, and depends on the normal force and the friction coefficient. For non-lubricated contacts Coulomb law [76] can be applied, considering the friction coefficient constant and independent of the speed and load as shown in Eq. [10], where F_T is the friction force, μ the friction coefficient and F_N the normal force, but for lubricated contact in motion hydrodynamic theory must be applied.

$$F_T = \mu F_N \quad [10]$$

For lubricated sliding contacts the friction is divided into 4 regions depending on the type of contact as shown in Figure 8: hydrodynamic lubrication, Elasto-Hydrodynamic Lubrication (EHL), mixed lubrication and boundary lubrication, where the friction coefficient is represented as a function of a lubrication parameter, the Somerfield number S , which includes the effect of speed, load and viscosity.

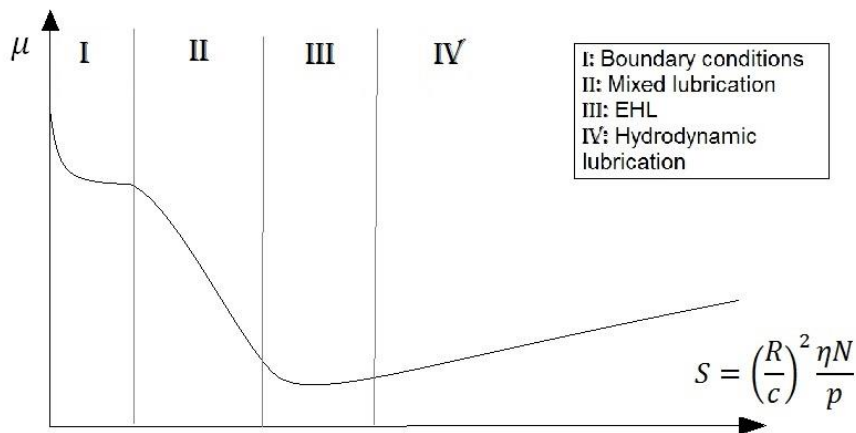


Figure 8 Qualitative Stribeck curve: friction (μ)-Somerfield number (N : speed, p : load, η : dynamic viscosity of the lubricant, R : radius of the bearing, c : clearance of the bearing)

Hydrodynamic contacts in rotating machinery, typically rolling and hydrodynamic bearings, are designed to operate on the hydrodynamic region, where the contact is fully lubricated and the friction forces are exclusively caused by the shear stresses of the lubricant. However, under high loads, low speed or low viscosity due to high temperatures they may operate in the mixed lubrication region, where partial metal-metal occurs.

The EHL regime applies under heavily-loaded conditions. The deformation of the bearings caused by the load significantly affects the film thickness and should be considered. Thus, a structural analysis is required to calculate the radial deformation along the bearing caused by the pressure field, and should be included in the calculation of the film thickness. EHL models have been used for estimating the minimum film thickness based on operational conditions, as shown by Choi et al. [77], who combined a multi-flexible dynamic model of the bearing with an EHL model that calculates the pressure distribution and film thickness.

An alternative approach is to use Computational Fluid Dynamics (CFD) for hydrodynamic lubrication and to combine it with computational structural analysis for EHL. Stefani and Reborá [78] developed a CFD model that takes into account the wall convection, the thermo-mechanical deformations and the mixing phenomena in the groove, while Jin and Zuo [79] also used a CFD model to study the effect of different groove depths in journal bearings.

Mixed lubrication refers to the region in which partial metal-metal contact occurs and part of the load is transmitted by asperities. In this situation surface parameters must be taken into account and the complexity and quantity of unknown parameters increases. Gelinck [80] have developed a mixed lubrication model for line contacts later improved and validated for point contacts by Liu [81] and in good agreement with experimental results as shown by Lu et al. [82]. Faraon [83] presented a similar approach for line contacts further improved for starved contacts by Faraon and Schipper [84].

For point contact Hua et al.[85] developed a mixed lubrication model that calculates the film thickness, pressure and temperature along the contact considering conductive thermal effects and stated the potential of the mixed lubrication model for scuffing prediction. A similar approach was used to detect scuffing in gears using a mixed lubrication model by Castro and Seabra [86]. Wang et al.[87], developed a mixed lubrication model that evaluates the influence of misalignment in hydrodynamic bearings under severe conditions that was validated using temperature data and stresses the influence of surface parameters when the film thickness is of the same order of magnitude as the roughness of the surface. In addition, wear models have been used by Zhang et al. [88] to detect failures in piston bearings as a function of temperature, friction and roughness as well.

Under boundary conditions the lubricant does not transmit any of the load and Coulomb and dry contact models are more suitable. Stribeck curve modes can be applied to any lubricated contact, point contact models are normally used for ball rolling bearings, whereas line contact models are used for hydrodynamic and roller bearings.

Li and Kahraman [89], [90] proposed a PbM to calculate the fatigue life of point contacts due to micro-pitting caused by metal-metal contact that was validated with experimental results by assuming crack propagation negligible compared to crack initiation. However, thermal effects were not considered. Li et al. [91] experimentally validated a similar model that predicted wear of point contacts, by integrating the calculation of the friction coefficient and a heat transfer model that estimated the friction coefficient and the temperature. Marble and Morton [92] validated a degradation model for wear caused by spalling in rolling bearings as a function of the area of the defect, the load and material constants. Watson et al. [74] developed an algorithm capable of predicting the RUL of clutches by combining a dynamic model of the system and wear degradation models based on Archard's law presented above taking into account corrosive, adhesive and abrasive wear. However, none of these approaches have been applied to hydrodynamic bearings.

2.2.3 Conclusions of Physics-based Modelling

This section has provided an overview of the PbM approaches for health condition monitoring. In order to develop a PbM for health condition monitoring the system under healthy and faulty conditions should be understood and there should be models capable of assessing the health of the system.

In addition, the inputs of those models should be known or measurable, otherwise the model cannot be executed. If RUL is estimated, a second measure of the current health condition is advisable as it allows for model correction by using a parameter estimator.

Common failure modes of hydrodynamic bearings were presented in section 2.1. An overview of typical PbMs and health condition monitoring techniques based on fatigue and wear has been given. It was shown that most techniques model the degradation through exponential laws, e.g. Paris law to represent crack growth or in combination with FEA models.

The main degradation mechanism of metal-metal contact is wear. PbMs applied to health condition monitoring of wear are limited. However, the techniques to model wear presented above have the potential to be applied to PHM. The most relevant approach for this thesis is the work of Castro and Seabra [86]; where metal-metal contact is modelled and proposed as a useful technique to detect scuffing in gears; however, no further investigation was done hydrodynamic bearings.

2.3 Metal-metal contact modelling of hydrodynamic bearings

The phenomena involved in metal-metal contact was briefly reviewed in the previous section. The potential of detecting metal-metal contact by the use of a PbM based on the friction under hydrodynamic and mixed lubrication was shown. However, a more comprehensive literature review on tribology and hydrodynamic and mixed lubrication contacts is required. The aim of this section is to provide the necessary background to model the friction in a hydrodynamic bearing under hydrodynamic and mixed lubrication.

2.3.1 Friction in line contacts

The first attempts to model the friction were conducted by Avitzur [93], [94], who showed that, for two sliding surfaces under low pressure, friction decreases as speed increases in a region called “mixed lubrication”, while friction rises at a slower rate in a region called “hydrodynamic lubrication”. A regime called “elastohydrodynamic lubrication” (EHL) was later introduced because the cavitation phenomena and solid deformations cannot be neglected under high loaded conditions, as shown by Meldahl [95]. Additionally, the viscosity-pressure effects have to be considered under EHL as shown by Grubin et al. [96].

In order to represent not only the journal bearing phenomena in the designed operational conditions, but also under inadequate lubrication, a model should be capable of representing mixed lubrication and EHL regimens. Liu [81] developed and validated with experiments an analytical model that includes both regions for point and line contacts. Faraon and Schipper [84] proposed a similar model valid only for line contact that includes mixed and hydrodynamic lubrication. The same modelling approach was compared with experimental results for the mixed lubrication regimen by Lu et al. [82] for a plain journal bearing showing a good agreement between the model and the experiments. However, these techniques are applied to the whole bearing assuming a plain bearing and integrating over all the lubricated surface.

There are alternative mixed lubrication models. Jiang et al. [97] used a robust approach for point contacts to model mixed lubrication by analysing the micro and macro scale asperity contacts. Chang and Jeng [98] developed a mixed lubrication model for rolling contact-sliding contacts only valid for low asperity-load ratios, confirming that surface roughness, hardness, load and speed are important parameters that significantly affect the severity of mixed lubrication [99].

An alternative approach is proposed by Xiong et al. [100], who compute the journal bearing mixed lubrication conditions by reducing the Reynolds equation when mixed lubrication occurs instead of dividing the lubricant and asperity contact phenomena. However, the most extended approach to model mixed

lubrication by modifying the Reynolds equation consists in the addition of flow and shear factors to take into account the asperity effects, this approach was first proposed by Patir and Cheng [101]; however, only Gaussian surface roughness distributions can be used. Alternative models have been proposed to avoid limitations in the surface roughness distribution as shown by Fatu et al. [102].

The effect of roughness effects have been discussed by several authors, Mihailidis et al. [103] showed that decreasing the number of surface irregularities reduces the friction coefficient; whereas Zhu [104] showed that maximum pressure, contact-load ratio and friction increase as the roughness increases under mixed lubrication.

The EHL regime is modelled using the Reynolds equations [105], where solid deformations are estimated and pressure-viscosity effects are taken into account. This can be done combining EHL and multi-flexible dynamics, as shown by Choi et al. [77]. An alternative approach to model the EHL regimen is based on computational fluid dynamics (CFD) along with computational structural analysis as shown by Shenoy et al. [106].

Journal bearings, under extreme operating conditions, increase their temperature due to the shearing of the lubricant and eventually, if there is contact between asperities, by friction, reaching several tens of Celsius (Bonneau et al. [107]). The thermo-elasto-hydrodynamic lubrication problem consists in solving two additional equations: the energy equation of the fluid and the thermal equation in the surrounding solids (shaft and housing). Zhang et al. [108] calculated the temperature profile of a plain journal bearing using a thermal model coupled with the hydrodynamic phenomena to study different boundary conditions and Laukiavich et al. [109] also considered thermal effects to study its influence in the bearing clearance; however, metal-metal contact was not considered.

2.3.2 Conclusions of metal-metal modelling of hydrodynamic bearings

The different approaches to model the Stribeck curve, i.e. the friction in the hydrodynamic bearing, have been reviewed. There are models available for hydrodynamic and mixed lubrication; thus, they can be used to represent healthy conditions (hydrodynamic lubrication) and faulty conditions (mixed lubrication).

Models can be divided in analytical and FEA/CFD models. Analytical models provide information about the whole bearing assuming a plain journal bearing. Whereas FEA/CFD models provide information along the bearing surface as well.

Hydrodynamic and EHL lubrication have been studied using analytical and FEA/CFD models. However, the well accepted mixed lubrication model based on the asperity distributions has been used in analytical models only.

The disadvantage of using analytical models that assume a plain bearing is that unique features of non-plain bearing may not be taken into account, e.g. slots to distribute the lubricant or hollow journals. Whereas FEA/CFD models may overcome this problem.

In order to represent the healthy and faulty conditions of a non-plain hydrodynamic bearing a FEA/CFD model capable of computing mixed and hydrodynamic lubrication regimes is needed. Thus, asperity models based that represent the mixed lubrication phenomena should be integrated in FEA/CFD models.

2.4 Summary and gaps in the knowledge

The literature reviewed covered health condition monitoring from a high level perspective and focused on the detection of failures in hydrodynamic bearings. Concluding that the potential of PbMs has not been investigated as much as DDMs techniques.

The PbM approach for health condition monitoring is further reviewed focusing on the most relevant degradation mechanisms for hydrodynamic bearings: fatigue and wear. It is concluded that PbMs capable of estimating the friction under hydrodynamic and mixed lubrication can effectively be applied for the detection of metal-metal contact in hydrodynamic bearings.

Finally, the state-of-the-art of the mixed and hydrodynamic lubrication models is reviewed in order to identify the most appropriate PbM approach to detect metal-metal contact. This section summarizes all the conclusions from the literature review and identify the relevant gaps in the knowledge.

2.4.1 Literature review discussion

There are multiple benefits from the use of health condition monitoring and IVHM in particular. Diagnostics IVHM systems that allow for fault detection, localization and isolation can help to reduce the mean time to repair because testing and fault localization tasks can be avoided. In addition to these benefits, an IVHM system that includes short-term prognostics capabilities can further reduce mean time to repair and overall maintenance cost by avoiding total failure and secondary damage to adjacent parts. Finally, if long-term prognostics capabilities are available, the RUL can be estimated; thus, allowing for planned maintenance and the subsequent reduction of maintenance cost and time. Moreover, in addition to the maintenance cost and time benefits, prognostics systems capable of avoiding unexpected failures can improve the availability of the vehicle or system.

For legacy aircraft, a critical factor is the restrictive regulation, which can complicate the introduction of IVHM. This is particularly critical if the introduction of IVHM requires additional sensors and hardware.

The technique proposed in this thesis falls into the short-term prognostics category. Being able to detect the incipient failure, localize it, and avoid further damage to adjacent parts. By detecting the early stages of the failure further damage may be avoided with the subsequent benefit in terms of availability of the vehicle. However, RUL is not estimated. An important characteristic of the proposed technique is that no additional sensors are required for its implementation, simplifying its introduction into legacy aircraft.

The decision between using PbMs or DDMs is not trivial as both have advantages and disadvantages. DDMs are easily scalable and can find trends in complex data. However, if the data available is limited PbM approaches may be preferable as data is only needed for validation. In addition, a PbM provides an understanding of the physics of failure, which can be used in the design to avoid or minimize the failure mode. Not all the failure modes can be monitored using PbM approaches, the degradation mechanisms must be well understood and there should be models capable of representing the degradation. The main input parameters of these models should be known, or monitored.

It should be noted that each DDM technique can be applied in several systems of complete different nature, e.g. an artificial neural network can be used for detecting failures in batteries and in gears. Whereas PbMs are specific for each system and failure mode. However, the literature in DDMs is more extensive than in PbMs for health condition monitoring of rotating machinery. This is even more relevant in hydrodynamic bearings. PbMs have not been used to detect metal-metal contact in hydrodynamic bearings. Even if the physics of failure are well understood and there are tribology models available in the literature.

In addition, techniques based on vibration and AE have been applied to journal bearings isolated from other components and with the sensors close to the journal because the housing is fixed. This is not the case of hydrodynamic bearings of planetary transmissions, where both parts of the bearing are moving and several gears are between the bearing and the closest fix element where a sensor can be installed.

It has been shown that developing a PbM technique to detect metal-metal contact in the hydrodynamic bearing of a planetary transmission would fulfil an important gap in the knowledge. In addition, this technique is preferred to DDMs because there are not large data sets available no accelerometers, microphones or debris sensors are installed in the transmission. In addition, all the elements of the transmission and bearings are rotating; thus, the installation of a sensor near the source of the damage is complicated and would require the approval from the corresponding certification agency. In the following the potential PbMs are discussed into detail.

In order to use a PbM as a health condition monitoring technique, the model must be capable of representing the behaviour of the system under healthy and faulty conditions, and the inputs of the model should be known or measurable.

Most PbM approaches for rotating machinery represent the degradation through exponential laws, e.g. Paris law for crack growth, or by FEA models that can represent the faulty behaviour of the system, but most of these failures are due to fatigue degradation. The main degradation mechanism of metal-metal contact is wear, for which the application of PbMs is limited. Castro and Seabra [86] provide the most relevant approach, where a mixed lubrication model is applied to the detection of scuffing in gears. However, a similar approach has not been used on hydrodynamic bearings.

In order to detect metal-metal contact a model should be capable of representing hydrodynamic and mixed lubrication phenomena. In tribology there are models available, either by modifying the Reynolds equation, or by including an asperity contact component that divides the problem in dry contact and fully lubricated contact. The last approach is well accepted, but has only being applied to the whole bearing instead of integrating it into a CFD/FEA model where metal-metal contact is evaluated locally along the lubricated surface.

The potential advantages of integrating the asperity contact in the CFD/FEA model are the addition of unique features, e.g. slots that distribute the lubricant, the ability to study the local effects on the lubricated surface, and the effect of the actual bearing deformations along the lubricated surface.

2.4.2 Gaps in the knowledge

From the literature review the following relevant gaps in the knowledge have been identified:

1. Physics-based Models have not been used for the detection of metal-metal contact in hydrodynamic bearings.
2. Mixed lubrication models based on asperity contact dividing the phenomena in dry and fully lubricated contact have not been applied locally along the lubricated surface in hydrodynamic bearings.

In order to fulfil these gaps in the knowledge this thesis proposes a novel technique to detect metal-metal contact in hydrodynamic bearings based on PbM by calculating the friction under hydrodynamic and mixed lubrication conditions. The novel CFD/FEA PbM proposed in this thesis allows for the evaluation of metal-metal contact along the lubricated surface of the bearing as opposed to previous mixed lubricated models based on the asperity contact approach.

3 Research objectives and methodology

The previous chapters introduced the necessary background to understand the background of the thesis, in chapter 1, and a review of literature in chapter 2 from a high level perspective of IVHM to the particularities of the hydrodynamic bearings focusing on PbMs and their potential to detect metal-metal contact and two main gaps in the knowledge were identified:

The research problem can be defined based on the background presented in chapter 1 and the relevant gaps in the knowledge; thus providing a clear definition of the scope, aims, contributions, and methodology of this thesis.

The research problem and scope of the thesis are presented in section 3.1. The aims, objectives and hypotheses are provided in section 3.2. The contributions are shown in section 3.3. Finally the methodology to achieve these objectives is described in section 3.4.

3.1 Research problem definition

As shown in the literature review (chapter 2). The use of IVHM has multiple benefits in terms of maintenance cost and mean time to repair and it can lead to higher availability of the vehicle. Health condition monitoring techniques can include diagnostics, short-term prognostics, or long-term prognostics capabilities.

The technique presented in this thesis falls into the short-term prognostics category, consisting in the detection of a failure in its early stages before total failure occurs but without enough time to plan the maintenance. Short-term prognostics can lead to maintenance cost savings. The reduced inspection time and cost because the failure is localised in advance. Secondary damage to adjacent parts is minimize as total failure is avoided. In addition, the availability of the vehicle can be increased if a potential failure is totally avoided. However, in the strictly regulated aerospace sector, the integration of additional sensors would lead to expensive certification processes that can offset the benefits previously mentioned.

As shown in the background section 1.1, metal-metal contact in the hydrodynamic bearings of the IDG's planetary transmission currently is only detected when total failure has occurred. Thus, there are not short-term prognostics capabilities. However, the secondary damage provoked by metal-metal contact is severe and multiple gears and adjacent bearings are damaged as well. The development of a novel technique to detect the failure in advance and avoid secondary damage would lead to significant cost reduction. However, to be effective no additional sensors should be added to the system. In addition, further damage can be avoided with the subsequent higher availability of the vehicle.

Short-term prognostics could be developed based on DDMs, PbMs or a combination of those. Historic data is limited and there are not debris sensors, accelerometers or microphones available in the IDG. Thus, techniques to detect metal-metal contact based on DDMs using debris analysis, vibration or AEs cannot be applied without adding additional sensors.

Instead, a PbM approach based on the estimation of the friction in the hydrodynamic bearing under normal and metal-metal contact conditions could potentially be applied without adding any additional sensor. Moreover, PbMs have never been applied to detect metal-metal contact in hydrodynamic bearings, being a significant gap in the knowledge that could be addressed with this case study.

PbMs capable of representing mixed lubrication phenomena using an asperity contact approach are well known. However, they are applied to the whole bearing and cannot take into account particularities like grooves or hollow shafts. The hydrodynamic bearings of the planetary gears are an example of these particularities. Therefore, a CFD/FEA approach to model metal-metal contact using the asperity contact approach, in which metal-metal contact is evaluated locally along the lubricated surface, would be preferred. The implementation of the asperity contact locally in mixed lubrication models is an additional gap in the knowledge in the field of tribology. Both gaps in the knowledge can be addressed by developing a PbM model capable of representing mixed lubrication locally and applying it to the detection of metal-metal contact as a health condition monitoring technique.

The novel PbM is compared to experimental friction coefficient measurements of a plain journal bearing from the literature under mixed and hydrodynamic lubrication regimens for high and low loading conditions. The PbM is also implemented for the planetary transmission of the IDG and the results are compared to the mechanical losses of a replica of the transmission mounted on a test rig to replicate the metal-metal contact phenomena.

The experimental results aim to provoke metal-metal contact without stalling the bearing completely; thus avoiding total damage. Therefore, experiments are conducted at relatively low speed, torque and oil temperature. In the IDG load and oil temperature can be higher; thus, metal-metal contact can occur at higher speeds than in the experiments presented in this thesis.

3.2 Aims, hypotheses and objectives

The first aim of the thesis is to develop a condition health monitoring tool capable of detecting metal-metal contact due in the hydrodynamic bearings of the planetary transmission of an aircraft's IDG with limited sensor capabilities using a physics-based modelling approach. Covering the first relevant gap in the knowledge.

The second aim of the thesis is to develop a mixed lubrication model for line contacts capable of evaluating the asperity contact phenomena locally along the lubricated surface. Thus, covering the second relevant gap in the knowledge.

Hypotheses

In the literature review (chapter 2) common failures of hydrodynamic bearings were shown along with the limited techniques to detect metal-metal contact in hydrodynamic bearings. It was shown that mixed lubrication models can potentially be used to detect metal-metal contact, similar techniques have been proposed in other rotating machinery components, e.g. gears [86].

The potential of using mixed lubrication models to detect metal-metal contact in hydrodynamic bearings is due to the following hypotheses:

- Metal-metal contact occurs due to contact between both sliding surfaces of the bearing with the subsequent increased friction coefficient.
- Lower speeds, higher loads and higher temperatures lead to a smaller minimum film thickness in the hydrodynamic bearing; and partial metal-metal contact can occur.
- Increased friction coefficient will lead to higher mechanical losses; which can be partially dissipated through heat transmitted to the lubricant.

The main objectives of the project can be divided in the model development, test rig construction, and experiments and validation.

PbM development

The development of the PbM and its application to health condition monitoring is the second core objective of the project. A comprehensive description of the PbM is provided in chapter 4 and its implementation for health condition monitoring is described in chapter 5. The process to successfully develop the PbM is divided in:

- Model hydrodynamic phenomena
- Model Elasto-hydrodynamic phenomena
- Model Metal-metal contact phenomena
- Integration into the PbM
- Application to health condition monitoring

Test rig construction

In order to test and validate the novel health condition monitoring technique experimental data is required. A test rig capable of replicating the conditions of mixed lubrication and detect metal-metal is needed. Additional experimental results of the actual transmission of the IDG are advisable in addition to the validation of the PbM using experimental results of a plain journal bearing. A comprehensive description of the test rig designs can be found in chapter 6. The process to obtain the experimental results of the planetary transmission can be divided in the following objectives:

- Test rig requirements definition
- Test rig design: lubrication, mechanical, electrical systems
- Re-design of the planetary transmission
- Definition and implementation of sensors, Data Acquisition (DAQ) systems and control.
- Construction and integration

Experiments and validation

In order to provide evidence of the effectiveness of the novel PbM and metal-metal contact detection technique the results of the PbM must be compared to experimental results. The experimental set-ups are covered in chapter 6, whereas the results and comparison with the PbM are shown in chapter 7.

3.3 Contributions

The main novelties of the thesis, shown below, cover both gaps in the knowledge identified in chapter 2:

First novelty

The development of a PbM able to represent mixed lubrication through an asperity contact approach locally along the lubricated surface of the bearing using a CFD/FEA novel approach.

Second novelty

The development of a novel technique to detect metal-metal contact in the hydrodynamic bearing of a planetary transmission of an aircraft's IDG using a PbM approach without installing additional sensors in the aircraft.

In order to achieve the main novelties of the thesis, the contributions of the thesis can be divided as follows:

- The development of a novel technique to detect metal-metal contact in hydrodynamic bearings based on PbMs, see chapter 4 and 5.
- The development of a novel PbM able to represent mixed lubrication through an asperity contact approach implemented locally along the lubricated surface, see chapter 4.
- The validation of the PbM with experimental results (chapter 7) provides the necessary data for a critical analysis of different potential health indicators of metal-metal contact.
- Proof of concept of an IVHM system capable of detecting metal-metal contact in the hydrodynamic bearings of the IDG without additional sensors, see chapter 4 and 5.

3.4 Methodology

This section describes the process to accomplish the aim and objectives previously stated. The development of an IVHM system varies depending on whether the monitored system is already installed in the vehicle or the IVHM and monitored system are designed in parallel. The latter scenario allows for modifications of the design to adapt the IVHM system, one example is the successful implementation of HUMS in new helicopters as shown by Land [4]. The former has limitations in terms of space, data transmission, sensors resolution or standardization as stated by Keller et al. [110] and Esperon-Miguez et al. [12], which makes retrofitting less cost effective [7]

The IVHM development process, illustrated in Figure 9, consists of: choosing the appropriate component, understanding the behaviour and failure modes of the system and identify the instrumentation and tests that are required to validate the IVHM tool. This process normally require the design and construction of a test rig if historical data is not available, the development of the necessary models for diagnostics or prognostics, and the validation and critical analysis of the experimental and model results; which corresponds with the objectives previously defined.

In the following, each aspect of the IVHM development process as shown in Figure 9 will be presented.

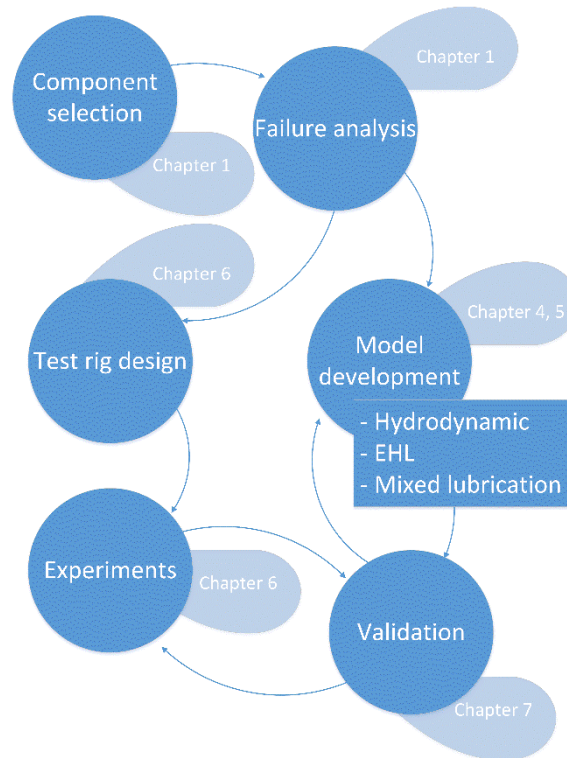


Figure 9 Methodology process

Component selection

A vehicle, and an aircraft in particular, has several components and systems but the resources to implement IVHM are limited. In order to select an optimal component and failure mode the following factors should be considered.

1. Type of failure mode
2. Testing and validation resources required
3. Business case

The nature of the failure mode should always be considered. Failures caused by gradual degradation can potentially be monitored, providing long-term prognoses. Failures caused by human or geometrical errors can prove to be difficult to monitor, it is important to select a failure mode that can potentially be monitored with the technology available.

The first stage of testing and validation normally requires a test rig. If test rig facilities are not available its cost may be considerable. The experiments should be representative of the real behaviour of the system and replicating the actual conditions may be out of budget; e.g. high temperatures and high speeds to replicate turbine conditions.

But the most important aspect to consider during the component selection phase is the viability of the business case. The potential benefits in terms of maintenance cost and time reduction along with higher availability of the vehicle should be balanced against the drawbacks like certification costs, false alarms, and implementation costs.

The failure of metal-metal contact in the planetary transmission of the IDG was selected based on these factors. The failure mode of metal-metal contact is understood and can potentially be monitored. The facilities required to test and validate a proof of concept are within budget. There is a business case because the proposed technique does not require additional sensors; thus, avoiding certification costs, and the inspection and secondary damage costs derived from the failure of the IDG are significant.

Failure Analysis

A correct understanding of the failure modes and degradation mechanisms that induce the failure along with the root causes must be understood to successfully develop IVHM capabilities based on PbMs. This knowledge is also advisable for DDMs approaches but not essential. The failure analysis of the failure studied in this thesis has been presented in chapter 1. The analysis is based on interviews with specialised personnel.

Test rig design

If historical data from all the required sensors are not available a test rig is required to generate the necessary data for validation, proof of concept and better understanding of the system. The development of the IVHM system and the construction of the test rig and experiments can be conducted in parallel. A detailed description of the test rigs is provided in chapter 6.

Experiments

In order to validate the algorithm experimental data are required. If historical data of all sensors are available and sufficient faulty data have been recorded a test rig may not be necessary. However, in most cases historical data are insufficient or unavailable.

In order to validate the algorithm experiments under healthy and faulty conditions should be conducted. Experimental faulty conditions are typically produced by the following type of tests:

- Seeded fault tests
- Accelerated degradation tests
- Provoked failures under controlled conditions

Seeded faults are artificially provoked in the system to evaluate its behaviour under faulty conditions without requiring to wait until the failure mode develops naturally; e.g. pitting is commonly seeded in gears to obtain faulty data and develop health condition monitoring algorithms.

Accelerated degradation tests are ideal for failure modes provoked by constant degradation; e.g. fatigue, creep, corrosion; where the degradation mechanism can be accelerated to avoid long tests by conducting the tests under more severe conditions.

For failures that occur in a short period of time but only under certain conditions; e.g. inadequate lubrication, the cause of the failure can be forced to obtain faulty data. However, several faulty tests at different conditions may be required and this approach can lead to the total failure of the component; with the subsequent cost and time due to the replacement of the component or system along with the potential human errors in the process.

In order to test metal-metal contact the latter option is preferred. A total failure and the subsequent replacement of the component after each experiment are not acceptable due to the cost of completely replacing, assembling and disassembling the planetary transmission. Therefore, it is essential that metal-metal contact is provoked without stalling the bearing or provoking major damage.

To avoid major damage during metal-metal contact in the experiments the tests are not conducted at nominal operational conditions. Instead, oil temperatures are below 40 °C and loads are lower than in the real system in order to provoke metal-metal contact at low rotating speeds with lower risk of damaging the transmission. The design of experiments is covered in chapter 6.

Model development

The development of the algorithm can be done in parallel with the design of the test rig and the experiments. However, if preliminary models are developed in advance, their outputs can be useful for the design of the test rig and for selecting the most appropriate sensors.

The methodology of the development of a DDMs and PbMs differ. PbMs do not normally required data for their development, the experimental data is used later for validation and by the IVHM tool. A DDM requires data to create or train the model and for validation as well. In the following the PbM development is considered only.

A PbM requires a functional and a degradation model. The functional model relates the monitored variables, called external loads, to the internal loads, that effectively contribute to the degradation of the system. For example, in the planetary transmission the radial load of the hydrodynamic bearing is an internal load required by the degradation model but only the output torque of the transmission is monitored, the relation between these two variables defines the functional model. The degradation model provides an estimation of the health of the system. It represents the physics of failure and describes the degradation of the system based on the values of the internal loads.

The PbM presented in this thesis computes the friction of the hydrodynamic bearing based on its speed, load and inlet oil temperature. This model can be divided in hydrodynamic, EHL and mixed lubrication regions. A comprehensive description of the PbM is provided in chapter 4 and the application of the PbM into the IVHM system installed in the aircraft is described in chapter 5.

Validation

The IVHM technique must be compared to experimental results representative of the real system, either by using historical data or by using a test rig. For DDM data must be divided in training and validation data. For PbM approaches the operational conditions tested in the experiments are simulated using the PbM and the results can be compared.

Metal-metal contact is calculated as a function of the friction coefficient in the model. The evidence of metal-metal contact is obtained, in the case of the plain journal bearing, by directly measuring the friction coefficient, and in the planetary transmission, by measuring the mechanical losses in the system. The effectiveness of the proposed PbM is obtained by comparing the model to these experiments. The results of the comparison between PbM and experimental results is provided in chapter 7.

4 Metal-metal contact Physics-based model

The novel health condition monitoring technique to detect metal-metal contact is based on a PbM. The description of the PbM is the core of the algorithm and it is presented in this chapter. The implementation of the PbM in the IVHM tool is presented in the following chapter 5.

The PbM presented in this chapter, a mixed lubrication model, is also a contribution to the field of tribology in addition to its application as a health condition monitoring technique. The PbM is able to represent mixed lubrication through an asperity contact approach implemented locally along the lubricated surface. The presented PbM and its contribution to the field of tribology has been published in Tribology transactions (Taylor and Francis) along with the comparison with experimental results of a plain journal bearing [111], see appendix B for further details.

This chapter provides a comprehensive description of the PbM and its implementation in a plain journal bearing and in the hydrodynamic bearing of the planetary transmission of the aircraft's IDG. It is a contribution to the health condition monitoring technique to detect metal-metal contact, later described in chapter 5, and to the field of tribology, as a models capable of representing mixed and hydrodynamic phenomena in line contacts locally along the lubricated surface. A comprehensive description of the PbM and all its assumptions and limitations is provided in section 4.1.

The PbM can be applied to different hydrodynamic bearings by modifying the boundary conditions and the parameters of the model. This thesis implements the PbM for the hydrodynamic bearing of the IDG and for a plain journal bearing in order to compare well recognized experimental results from the literature and provide additional evidence of its effectiveness in the planetary transmission. The implementation of the PbM into both, a plain journal bearing and the hydrodynamic bearing of the IDG's planetary transmission, are provided in section 4.2.

4.1 Model Description

The PbM proposed in this section aims to estimate the friction along a hydrodynamic bearing under mixed and hydrodynamic lubrication. As shown in the literature review, the friction under hydrodynamic and Elastohydrodynamic lubrication (EHL) has been studied not only using analytical models that consider the hydrodynamic bearing as a whole; but also using Finite Element Analysis (FEA) and Computational Fluid Dynamics (CFD) models to study the phenomena locally in all the lubricated surface of the bearing. However, for mixed lubrication conditions the most accepted approaches, based on modelling of the asperity contact phenomena by dividing the problem in dry and fully lubricated contact, estimate the friction coefficient of the whole bearing without considering local effects.

The main contribution of the model proposed in this section from a tribology point of view is the novelty of including mixed lubrication in a FEA/CFD model that evaluates the friction locally along the lubricated surface.

The model presented in this section includes EHL and mixed lubrication. The deformation of the solids and its effect on the film thickness is calculated by using FEA. The hydrodynamic phenomena are calculated using CFD. The asperity contact is modelled using the approach proposed by Gelinck and Schipper [80]; however, it is evaluated locally along the lubricated surface of the bearing.

The model has been developed using COMSOL Multiphysics by developing subroutines for the asperity contact and friction phenomena and structural, CFD and Heat transfer modules. For a given hydrodynamic bearing and lubricant the friction can be calculated as a function of the bearing rotating speed, the load and the inlet oil temperature, which are available information in the IDG of the aircraft. Thus, not requiring any additional sensors in the aircraft.

4.1.1 Basic principles

The main function of a bearing is supporting the rotating component; thus, transmitting the axial and radial loads while minimizing the friction to transmit all the load without significant mechanical losses.

Rolling bearings consist in an inner and an outer race fixed to the rotating and support components respectively with balls or rollers in between. Hydrodynamic bearings do not have any additional element between the rotating component and the support, the differences can be shown in Figure 10. It should be noted that this thesis focuses on the detection and modelling of metal-metal contact in hydrodynamic bearings only.

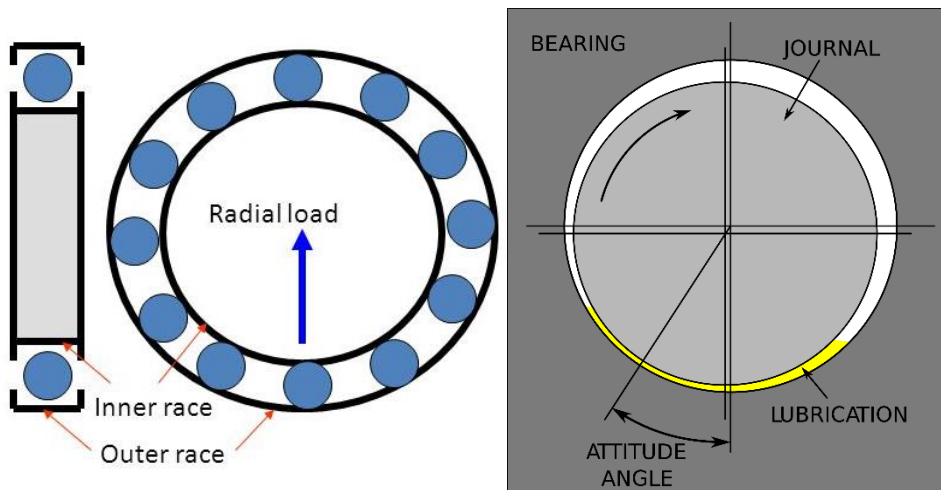


Figure 10 Rolling bearing (left) and hydrodynamic plain bearing (right)

Most bearings are oil or grease lubricated, the lubricant has two functions. Under normal operation the lubricant prevents metal-metal contact and separates the support and rotating component due to the lubricant film produced by the relative motion between them. In addition, the lubricant can also be used to dissipate heat. In the hydrodynamic bearing of the IDG there is not any external heat source near the hydrodynamic bearing of the IDG; thus, avoiding metal-metal contact is the main function of the hydrodynamic bearing.

A hydrodynamic bearing consists of two cylinders, as shown in Figure 11, with a clearance c that is filled with lubricant. The radial clearance c is defined as the total distance that the rotating component can be moved relatively to the support in the radial direction, as shown in Eq. [11], being R_s and R_j the support and journal radius respectively.

$$c = R_s - R_j \quad [11]$$

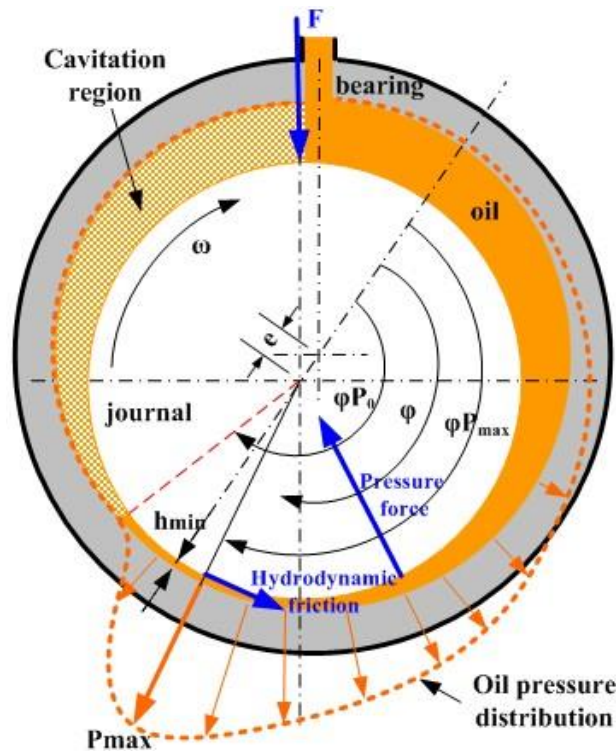


Figure 11 Hydrodynamic bearing parameters [112]

The lubricant film is generated due to the relative motion between the support and journal. The oil is compressed by the load and a hydrodynamic pressure capable of compensating the load for a given eccentricity e is generated. The eccentricity is defined as the distance between the centre of the journal and support.

The friction coefficient, an indicator of metal-metal contact, is commonly represented by the Stribeck curve; where the friction coefficient is represented as a function of different parameters; e.g. rotating speed, load or lubricant viscosity. A generic Stribeck curve is shown in Figure 12; where the friction coefficient is represented as a function of the Sommerfeld number: a lubrication parameter that includes the rotating speed ω , the viscosity η , and the load Q .

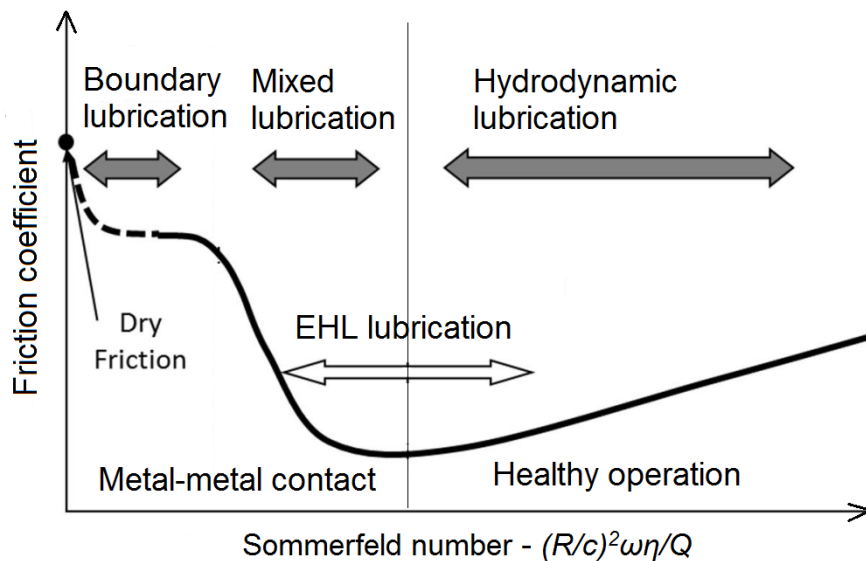


Figure 12 Qualitative Stribeck curve – ω : rotating speed, η : dynamic viscosity, Q radial load, R : radius, c : radial clearance

As shown in Figure 12, the fully lubricated condition occurs in the hydrodynamic region; where no metal-metal contact occurs and solid deformations are not critical. For heavy loaded conditions the deformation of the bearing significantly affects the film thickness and the hydrodynamic pressure, this region is called EHL. If the conditions are more severe partial metal-metal contact occurs, the region is referred as mixed lubrication. Under lower speeds the lubricant is not transmitting any load, all the load is carried by the asperities and the region is called boundary lubrication.

The main variables that define the Stribeck curve are the rotating speed ω , the viscosity η and the radial load Q as shown in Figure 12. Increasing the speed would increase the film thickness; thus, reduce the eccentricity and therefore the risk of metal-metal contact would be minimized. However, it should be noted that excessive speed would lead to an unnecessarily thick lubricant film and the friction coefficient would increase under fully lubricated.

Increasing the radial load Q will have the opposite effect, it would reduce the film thickness because a higher pressure distribution is required to support Q . Metal-metal contact is more critical under heavily loaded conditions.

Finally, a high lubricant viscosity would help to support the load and therefore, if viscosity is increased metal-metal contact is less critical as well. It should be noted that the viscosity is function of temperature. Oil lubricated contacts have significantly lower viscosity as temperature increases; therefore, in order to reduce the risk of metal-metal contact the lubricant temperature should be low.

4.1.2 PbM overview

In the following subsections the PbM subcomponents will be presented. The aim of this subsection is to provide an overview of the PbM and the relation between the different subcomponents of the model, as shown in Figure 13. The model requires an iterative process due to the coupled effects between the three main physical phenomena: hydrodynamic, solid mechanics and asperity contact.

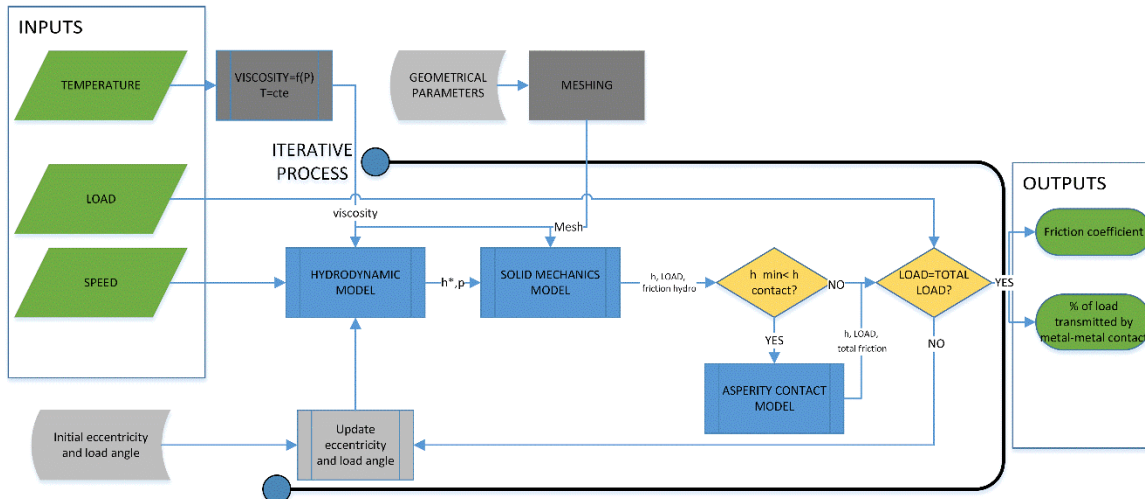


Figure 13 Metal-metal contact PbM flowchart

The hydrodynamic phenomena is solved by computing the Reynolds equation for a given eccentricity and load angle; obtaining the pressure distribution and film thickness h^* ; the load can be obtained by integrating the pressure distribution. However the deformation of the hydrodynamic bearing affects the film thickness and therefore the pressure distribution and both phenomena cannot be solved independently.

The load, an input of the overall PbM, is an output obtained from the pressure distribution, but cannot be used as an input in the Reynold equations. Therefore, an arbitrary eccentricity and load angle must be used as inputs of the Reynolds equation and modified in an iterative process until the resulting pressure distribution corresponds to the input load, as shown in Figure 13.

Metal-metal contact, occurring in the mixed lubrication region, means that part of the load is transmitted through the asperities. The total load, consisting in the load transmitted through the lubricant due to the lubricant pressure distribution, plus the load transmitted through the asperities, has to be considered as a whole. Therefore, the asperity contact component cannot be solved independently either because the total load is not equal to the hydrodynamic load under mixed lubrication.

The following subsections describes the following:

- The hydrodynamic model, which requires the calculation of the film thickness and the viscosity of the lubricant.
- The EHL component, which takes into account the deformation of the solid.
- The asperity contact component, computed locally along the lubricated surface and responsible of evaluating the percentage of load transmitted through metal-metal contact.
- The forces equilibrium and friction coefficient calculation that evaluates the total load and provides the output required by the PbM, that is, the percentage of load transmitted by metal-metal contact and the friction coefficient estimation.

The meshing of the CFD/FEA model depends on each particular case and will be discussed in the following section for both, the plain journal bearing and the hydrodynamic bearing of the IDG.

4.1.3 Film thickness

The film thickness is a critical parameter of the evaluation of metal-metal contact. Contact will occur if the film thickness is on the same order of magnitude as the roughness of the surfaces. The film thickness is required for the calculation of the hydrodynamic phenomena, that is, for solving the Reynolds equation.

If only hydrodynamic phenomena were taken into account, the film thickness would be defined by the eccentricity e and the clearance c as a function of the angular position θ . However, in EHL the deformation of the bearing is significant and the subsequent effect on the film thickness should be considered by adding the equivalent deformation δ of the shaft and shell, as shown in Eq. [12] where z is the axial coordinate of the bearing, as shown in Figure 14.

$$h(\theta, z) = c + e \cos(\theta) + \delta(\theta, z) \quad [12]$$

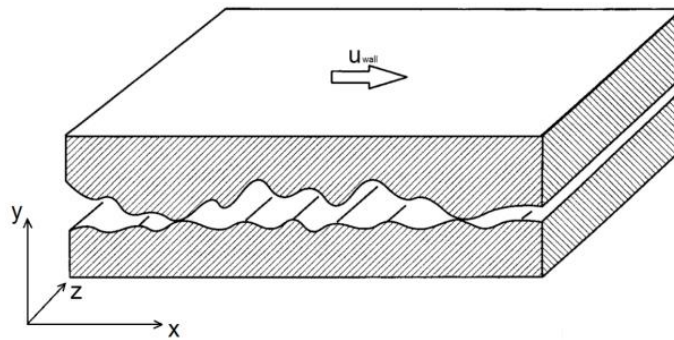


Figure 14 Axis reference (u: sliding contact velocity)

As mentioned in the previously in this chapter, the Reynolds equation requires the film thickness, which depends on the eccentricity e , as an input. However, the model input is the load and the film thickness is unknown. Therefore, an initial eccentricity e_0 must be assumed and modified in an iterative process until the required load is obtained.

4.1.4 Hydrodynamic model

The fluid dynamic phenomena of the bearing can be modelled using the following equations:

- The film thickness equation.
- The Reynolds equation.
- Cavitation equation.
- The force equilibrium equation.
- Internal energy equation.

The lubricant phenomena are modelled using the generalized Reynolds equation, deduced from Navier-Stokes equations. The following assumptions have to be considered [105], [113]: thin film fluid domain ($L_y \ll L_x, L_z$), Newtonian fluid, negligible lubricant body and tension forces, dominant viscous forces, and no slip; as shown in Eq. [13], where ρ is the density of the fluid and \vec{u}_{ave} the average speed field of the fluid. \vec{u}_{ave} is obtained as a function of the journal tangential velocity $\vec{u}_{j,t}$, shell tangential velocity $\vec{u}_{s,t}$, and the fluid pressure field p_h (see Eq. [14]), where η is the dynamic viscosity of the oil.

$$\nabla_t(\rho h \vec{u}_{ave}) = 0 \quad [13]$$

$$\vec{u}_{ave} = \frac{1}{2} (\vec{u}_{j,t} + \vec{u}_{s,t}) - \frac{h^2}{12 \eta} \nabla_t(p_h) \quad [14]$$

Additionally, in journal bearings, the cavitation effects have to be taken into account in the fluid region, as shown by Laukiavich et al. [109] and Lorenz et al. [114]. Several cavitation models have been developed [115], [116]. The well accepted Elrod-Adams cavitation model [116], [117] has been implemented in this model by reformulating the Reynolds equation in terms of a new variable α , and a relation between the fluid pressure and the density (see Eqs. [15, 16]).

$$\alpha \frac{\partial p_h}{\partial \alpha} = \frac{g}{\beta} \text{ where } \alpha = \frac{\rho}{\rho_{cav}} \quad \begin{cases} g = 0 & \text{if } \alpha < 1 \\ g = 1 & \text{if } \alpha \geq 1 \end{cases} \quad [15]$$

$$\nabla_t \left[\alpha h \left(\frac{1}{2} (\vec{u}_{j,t} + \vec{u}_{s,t}) - \frac{h^2}{12\eta} \frac{g}{\alpha\beta} \nabla_t(\alpha) \right) \right] = 0 \quad \begin{cases} g = 0 & \text{if } \alpha < 1 \\ g = 1 & \text{if } \alpha \geq 1 \end{cases} \quad [16]$$

Where ρ_{cav} represents the density at cavitation pressure and β the lubricant compressibility coefficient. The term α has different interpretations in the full film and cavitation region. In the full film region ($\alpha > 1$) it represents the fluid density changes due to the lubricant compression. However, in the cavitation region ($\alpha < 1$) it represents the proportion of liquid filling the gap assuming that the gas density is very low compared to the liquid density ($\rho_g/\rho_l \approx 10^{-3}$).

The switch function g changes the character of Eq. [16] from elliptic (full film region) to parabolic (cavitation region) and avoids computationally expensive calculations of the cavitation boundary. This function must satisfy the physical boundary condition at the cavitation interface:

- Flow continuity in the leading edge of the cavitation region.
- Liquid density remains constant equal to the cavitation density ρ_{cav} in the cavitation region.
- Flow leaving the cavitation region must balance the flow entering the full film zone in the reformation edge.

One of Elrod-Adams cavitation model drawbacks is that the pressure prediction is very sensitive to β , which has been considered constant through the fluid domain. To increase accuracy and avoid slow convergence problems artificial β values 10 or 100 times higher than the real physical value are applied.

If the local film thickness is close to the characteristic roughness length, the flaws hamper the lubricant flow and contact zones are created, affecting the Reynolds equation. Patir and Cheng [101], [118] devised a model that takes into account those aspects by modifying the Reynolds equation using a set of corrective factors with the assumption of isotropic surfaces following a Gaussian height distribution with standard deviation σ that is unaffected by hydrodynamic and contact pressures, as shown in Eqs. [17, 18].

$$\phi = 1 - 0.9e^{-0.56\frac{h}{\sigma}} \quad \text{if } \frac{h}{\sigma} > 0.5 \quad [17]$$

$$\nabla_t \left[\alpha \left(\frac{h}{2} (\vec{u}_{j,t} + \vec{u}_{s,t}) - \frac{h^3}{12\eta} \frac{g}{\alpha\beta} \phi \nabla_t(\alpha) \right) \right] = 0 \quad \begin{cases} g = 0 & \text{if } \alpha < 1 \\ g = 1 & \text{if } \alpha \geq 1 \end{cases} \quad [18]$$

Eq. [18] need to be solved with the appropriate boundary conditions, that is, inlet pressure, lubricant temperature, rotating speed. The boundary condition for the hydrodynamic bearing of the IDG and the plain journal bearing are described in the following section 4.2.

4.1.5 Viscosity

The viscosity of the lubricant, required for the hydrodynamic model, depends on the lubricant temperature and pressure. As previously mentioned, the function of the hydrodynamic bearing can be to reduce the friction and heat dissipation. However, in the hydrodynamic bearing of the planetary transmission or in the plain journal bearing used as case studies there are not adjacent heat sources. Thus, the lubricant temperature does not significantly varies inside the bearing and it is assumed constant and equal to the inlet lubricant temperature.

However, under high pressures, the influence of the pressure in the viscosity of the lubricant cannot be neglected, as shown by Grubin et al. [96]. The model accounts for this effect and solves the Reynolds equation considering the dynamic viscosity as a function of pressure along the lubricated surface. The most simplified model is the Barus law [119]; however, it can only be applied at low pressures. Whereas the Roelands model [120] is a better approximation for higher pressures.

The proposed model computes the viscosity as a function of the pressure using the Roeland equation as shown in Eq. [19], where η_0 is the dynamic viscosity at atmospheric pressure, c_p^* is the pressure coefficient equal to $1.962 \cdot 10^8 \text{ Pa}$ and the viscosity-pressure index Z is equal to 0.7.

$$\eta(p_h) = \eta_0 \cdot e^{[\ln(\eta_0)+9.671] \cdot [-1+(1+p_h/c_p^*)^Z]} \quad [19]$$

The dynamic viscosity at atmospheric pressure η_0 is considered at the inlet oil temperature T_{inlet} . The effect of temperature in the viscosity of the lubricant is commonly defined as a decreasing exponential law [121] as shown by Seeton [122] in Eq. [20]. Where β and $\eta_{0,T0}$ can be obtained from experimental data. It should be noted that the pressure and temperature effects in the viscosity are considered independent. More complex models can be used to account for the dependency between pressure and temperature in the lubricant viscosity, as shown by Larsson et al. [123]. However, for most lubricants there is not enough information available to determine all the experimental coefficients required by these type of models.

$$\eta_0(T_{inlet}) = \eta_{0,T0} e^{-\beta(T_{inlet}-T0)} \quad [20]$$

4.1.6 EHL

Under highly loaded conditions the assumption of a film thickness function of only geometrical and kinetic parameters is no longer acceptable and the deformation of both solids (shell and journal) must be take into consideration (see Eq. [12]). This reciprocal dependency between the film thickness and the solids wall constrains constitutes the classical EHL problem. Due to the order of magnitude of the loads on a journal bearing and the mechanical properties of both solids, it can be assumed the hypothesis of linear elasticity (linear relation between strains and displacements, and linear relation between strain and stresses). Thus, Eqs. [21-23] need to be solved in both solids with its respective boundary conditions.

$$\nabla \cdot \bar{\sigma}_{sol} = 0 \quad [21]$$

$$\bar{\sigma}_{sol} = \frac{E_{sol}}{1 + \nu_{sol}} \bar{\epsilon}_{el} + \frac{E_{sol} \nu_{sol}}{(1 + \nu_{sol})(1 - 2\nu_{sol})} \bar{I} \cdot trace(\bar{\epsilon}_{el}) \quad [22]$$

$$\bar{\epsilon}_{el} = \frac{1}{2} (\nabla \vec{u}_{sol} + \nabla \vec{u}_{sol}^T) \quad [23]$$

4.1.7 Asperity contact component

The asperity contact components aims to calculate the proportion of load carried by the asperities and by the lubricant under mixed lubrication. The approach has been applied and validated for line and point contacts by Liu [81] and Faraon and Schipper [84]. Analytical equations were used for the fluid dynamics and solid deformations. The asperity contact component presented in this thesis follows the same principles but it is implemented locally using CFD and FEA along the lubricated surface.

The total load carried by the hydrodynamic bearing is divided in load transmitted through the asperities and load transmitted through the lubricant. The contact model that represents the contact between the asperities was proposed by Greenwood and Williamson [124], which considers one of the surfaces completely smooth and the other with a density of asperities n , where the summit heights follow a Gaussian distribution ψ_s with standard deviation σ and an average radius of asperities β_a . Assuming an Hertzian contact in each asperity the load per asperity Q_i can be obtained as shown in Eq.[24], where E' is the combined elasticity modulus of both surfaces (see Eq. [25]) and w_d is the deformation of the summits. Thus, the pressure transmitted through the asperities p_a can be obtained as shown in Eq. [26].

$$Q_i = \frac{2}{3} E' \beta_a^{1/2} w_d^{3/2} \quad [24]$$

$$\frac{1}{2E'} = \frac{1 - \nu_1^2}{E_1} + \frac{1 - \nu_2^2}{E_2} \quad [25]$$

$$p_a = n \int_{h-d_a}^{\infty} Q_i \psi_s(z) dz = \frac{2}{3} n \beta_a^{1/2} E' \int_{h-d_a}^{\infty} w_d^{3/2} \psi_s(z) dz \quad [26]$$

Figure 15 represents the contact between the rough and the flat smooth surface; where two planes have been defined: the mean plane of the summits and the surface mean plane. The distance between these two mean planes is given by d_d . The surface mean plane is the reference plane for the hydrodynamic component; thus, d_d has to be subtracted from h in the inferior limit of Eq. [26] as shown by Lu et al. and [82], [81]. According to Whitehouse and Archard [125] d_d can be approximated by 1.15σ .

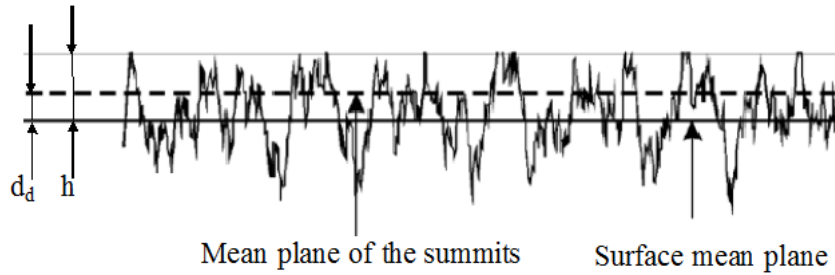


Figure 15 Contact between rough and flat smooth surfaces- h , d_d , mean plane of summits and surface mean plane respectively [126]

It is common practise to transform the integral shown in Eq. [26] into the identity $F_{3/2}$ (see Eqs. [27, 28]).

$$p_a = \frac{2}{3} n \beta_a^{1/2} E' \sigma^{3/2} F_{3/2} \left(\frac{h - d_d}{\sigma} \right) \quad [27]$$

$$F_k(\lambda) = \int_{\lambda}^{\infty} (s - \lambda)^k \psi^*(s) ds \quad [28]$$

The function $F_{3/2}$ is required for line contacts due to the use of the Greenwood and Williamson model [124], which applies to hydrodynamic bearings and roller bearings. As opposed to the Greenwood-Tripp contact model for point contacts [127], which uses the function $F_{5/2}$ and applies to ball bearings.

$F_{3/2}$ can be approximated to improve the model computational efficiency, as it is done with the identity $F_{5/2}$ for point contact using a polynomial function by several authors [77], [128]–[131]. However, because the asperity contact model assumes a Gaussian distribution of asperities a fitting curve based on a Gaussian expression is more adequate.

In this thesis the function $F_{3/2}$ is approximated by the Gaussian expression shown in Eq. [29]. In Figure 16 it is shown that a Gaussian fitting curve is more appropriate than the polynomial fitting curve typically used to estimate $F_{5/2}$ presented in Eq. [30] and used by several authors [77], [128]–[131].

$$\begin{cases} F_{\frac{3}{2}}(\lambda) = 1.989 e^{-\left(\frac{\lambda+2.169}{1.752}\right)^2} & \text{if } \lambda < 4 \\ F_{\frac{3}{2}} = 0 & \text{if } \lambda > 4 \end{cases} \quad [29]$$

$$\begin{cases} F_{\frac{5}{2}}(\lambda) = 4.4086 \cdot 10^{-5} (4 - \lambda)^2 & \text{if } \lambda < 4 \\ F_{\frac{5}{2}} = 0 & \text{if } \lambda > 4 \end{cases} \quad [30]$$

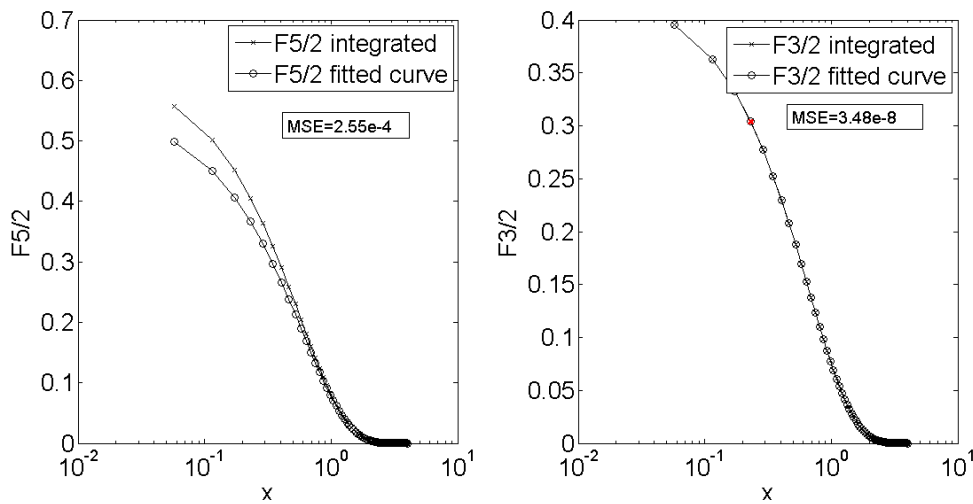


Figure 16 Mean square error of Gaussian fitting curve of $F_{\frac{3}{2}}(x)$ –left. And Polynomial fitting curve of $F_{\frac{5}{2}}(x)$ –right

4.1.8 Forces equilibrium and friction coefficient

The previous subsections provided, first the film thickness, used later by the hydrodynamic model to calculate the hydrodynamic pressure distribution using the Reynolds equation. The estimation of the film thickness took into account the deformation of the solid as shown in the EHL subsection. Finally, based on the film thickness, the asperity contact pressure distribution could also be estimated.

Once the asperity contact component and the Reynolds equation is solved considering solid deformations all the loads actuating the hydrodynamic bearing are known. The loads transmitted through the lubricant and through metal-metal contact are known and the total load can be obtained. If the resulting total load is equal to the input load predefined by the model a solution is reached. Otherwise the eccentricity e and load angle θ will be modified in accordance until a solution is reached.

The equilibrium of forces in the journal (see Eq. [31]) should include the loads transmitted through the lubricant due to hydrodynamic phenomena and the forces transmitted through the asperities. \vec{Q} is the total load, \vec{Q}_n is the normal load transmitted due to both, hydrodynamic and contact pressure (see Eq. [32]), and \vec{Q}_t is the load transmitted due to friction caused by the lubricant and metal-metal contact (see Eq. [33]), where $\vec{\tau}_j$ is the shear stress of the lubricant on the journal surface, μ_a the dry contact friction coefficient, \vec{n} the external unitary normal vector of the surface and \vec{u}_j and \vec{u}_s the journal and shell velocities respectively.

$$\vec{Q} = \vec{Q}_n + \vec{Q}_t \quad [31]$$

$$\vec{Q}_n = - \iint_A p_h \vec{n} dA - \iint_A p_a \vec{n} dA \quad [32]$$

$$\vec{Q}_t = \iint_A \vec{\tau}_j dA + \mu_a \iint_A p_a \frac{-(\vec{u}_{j,t} - \vec{u}_{s,t})}{\|\vec{u}_{j,t} - \vec{u}_{s,t}\|} dA \quad [33]$$

The cavitation and the roughness effects on the lubrication film also affect the shear stress and have to be taken into account as shown by Patir and Cheng [101], [118] in Eqs. [34, 35, 36] assuming isotropic roughness and Gaussian

distribution heights. A very small ε is introduced by Patir and Cheng [101], [118] to avoid numerical problems.

$$\vec{\tau}_j = -\frac{hg\phi_{fp}}{2\beta\alpha}\nabla_t(\alpha) + \frac{\eta\alpha}{h}(\vec{u}_{s,t} - \vec{u}_{j,t})\phi_f \quad [34]$$

$$\phi_{fp} = 1 - 1.4e^{-0.66\frac{h}{\sigma}} \quad [35]$$

$$\phi_f = \frac{h}{\sigma\sqrt{2\pi}} \int_{-h+\varepsilon}^{\infty} \frac{e^{-\frac{1}{2}\left(\frac{x}{\sigma}\right)^2}}{h+x} dx \quad [36]$$

Finally, the friction coefficient μ can be obtained by taking into account the load due to shear stress provoked by the lubricant film τ and the friction coefficient of the asperities μ_a as shown in Eq. [37].

$$\mu = \frac{\|\vec{Q}_t\|}{\|\vec{Q}_n\|} \quad [37]$$

4.2 Implementation

A comprehensive description of the PbM was provided in the previous section 4.1. The model can be applied to different hydrodynamic bearings, taking into account the geometry, materials and lubrication parameters. However, the boundary conditions and model parameters have to be defined for each case study.

The aim of this section is to provide a description of the implementation of the PbM for the hydrodynamic bearing of the planetary transmission of the IDG and for the plain journal bearing used for the validation of the PbM.

The plain journal bearing is implemented in order to compare the PbM results with experimental data available in the literature. The results of the PbM for a plain journal bearing will be compared to a well-accepted dataset of metal-metal contact experiments from the literature provided by Lu et al. [82] in chapter 7.

The planetary transmission of the IDG is implemented in order to provide additional evidence of the potential of the PbM approach to detect metal-metal contact by comparing the PbM results with experimental data from a replica of the planetary transmission of the IDG.

All the parameters of the PbM particular for these two case studies are provided in this chapter. A more detailed description of the planetary transmission and the plain journal bearing test rig set-ups experimental conditions is given in chapter 6.

4.2.1 Hydrodynamic bearing of planetary transmission

The PbM presented in the previous section 4.1 has to be implemented for the planetary transmission of the aircraft's IDG taking into account all the features that may affect the metal-metal contact phenomena. The journal geometry and bearing supports influence the deformations and therefore the film thickness is affected. A long groove affects the pressure distribution and cavitation phenomena. Thus, the actual lubricated surface and bearing geometry with the corresponding boundary conditions have to be implemented to take these effects into account.

The hydrodynamic bearing and planetary gear of the planetary transmission installed in the IDG are made of steel BS 080M40. Both bearing surfaces are manufactured in a lathe machine. The replica of the planetary transmission tested in the rig uses the same lubricant as the IDG, Mobil Jet Oil II [132].

The relative inlet lubricant pressure is assumed to be 1.3 bar; whereas the outlet pressure is considered atmospheric. Both boundary conditions are represented in the PbM as shown in Figure 17. The groove is a critical feature of the hydrodynamic bearing, it is assumed that the inlet oil pressure is constant along the groove and equal to the inlet lubricant pressure. It should be noted that, as opposed to common hydrodynamic bearings, in a planetary transmission the lubricant is supplied from the journal.

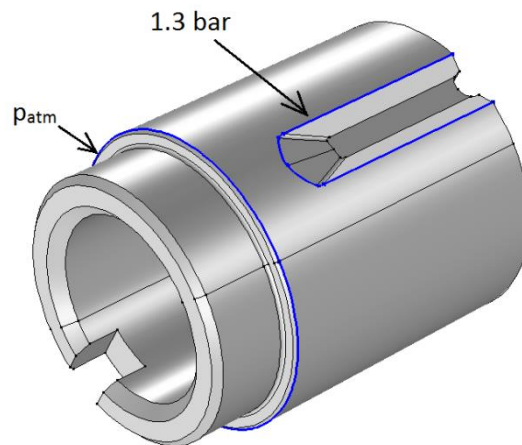


Figure 17 Hydrodynamic bearing 3D model of the IDG – lubricant pressure boundary conditions

The inlet lubricant temperature is considered an input that can be modified, as previously mentioned, the lubricant temperature along the lubricated surface is assumed equal to the inlet lubricant temperature.

The bearing consists in a hollow shaft, as shown in Figure 17, rather than a solid shaft as commonly occurs in a hydrodynamic bearing. Therefore, the deformations will differ from those of a solid shaft and the deformations of the lubricated surface are obtained based on a FEA model of the solid instead of calculating the deformation analytically. The deformation of the hydrodynamic bearing is also affected by how the hydrodynamic bearing is fixed to the support. The exterior surface, as shown in Figure 18 is tightly fixed to the carrier shaft and can zero displacement is assumed by the PbM. The lubricated surface where the Reynolds equation is computed is also shown in Figure 18.

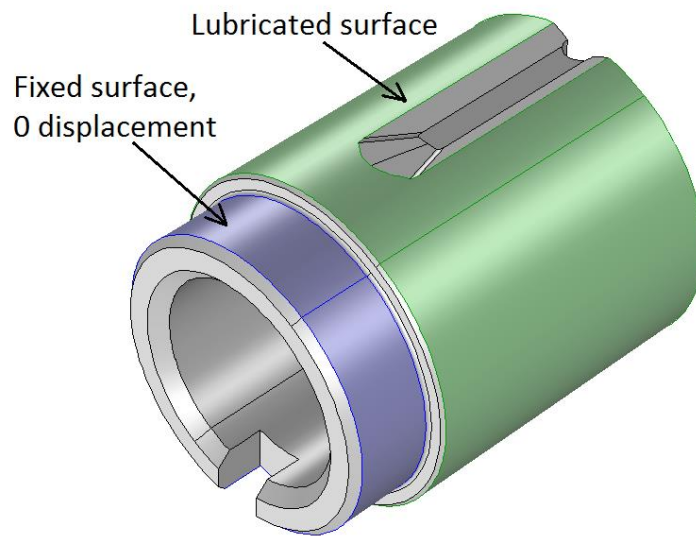


Figure 18 Hydrodynamic bearing 3D model of the IDG – lubricated (green) and fixed (blue) surfaces

The mesh should be optimized, only half of the bearing is meshed due to its symmetry. The fluid dynamics phenomena are more critical than the solid deformations and a finer mesh is required in the lubricated surface. A triangular mesh is used in the lubricant surface, optimized to obtain an even finer mesh near the boundaries and in the high pressure region. The solid domain consist in a regular tetrahedral mesh. The mesh discretization is fixed for every simulation. The main parameters of the mesh are shown in Table 4.

Table 4 Hydrodynamic journal bearing of the IDG - mesh properties, fluid and solid domains

Mesh parameter	Solid domain	Fluid domain
Number of elements	55148	12119
Minimum element quality	0.006592	0.3366
Average element quality	0.6354	0.9791
Maximum growth rate	5.248	5.808
Average growth rate	2.04	1.152

The main dimensions of the hydrodynamic bearing are given in Table 5. The surface properties, required for the asperity component, are shown in Table 6. And the mechanical properties of the materials are shown in Table 7 as well.

Table 5 Geometrical properties of the hydrodynamic bearing of the IDG

Parameters	Value
Length (mm)	48.34
Diameter (mm)	24.22
Clearance (mm)	0.1018

Table 6 Lubricated surface properties of the hydrodynamic bearing of the IDG

Parameters	Value
Density of asperities n (m⁻²)	10^{11}
Average asperity radius β_a (m)	$10 \cdot 10^{-6}$
Standard height deviation σ_s (m)	$0.2 \cdot 10^{-6}$

Table 7 Mechanical properties of the hydrodynamic bearing of the IDG

Parameters	Value
Young's module (GPa)	209
Shaft Poisson's ratio	0.33
Dry friction coefficient	0.2

The lubricant, Mobil Jet Oil II [132], is commonly used in aviation. And it is used in the aircraft and in the test rig as well. The main lubricant properties are shown in Table 8.

Table 8 Properties of the lubricant Mobil Jet Oil II [132]

Parameters	Value
Kinematic viscosity (cSt) at 40°C	27.6
Kinematic viscosity (cSt) at 100°C	5.1
Oil density (kg/m³)	1003,5

A critical aspect that affect the hydrodynamic phenomena is the lubricant viscosity. As shown in the previous section, the viscosity is a function of pressure and temperature. The PbM proposed in this thesis uses Eq. [19] to calculate the dynamic viscosity as a function of the pressure. And the temperture effect is considered decoupled, as shown in Eq. [20].

As previously mentioned, the pressure significantly varies along the lubricated surface; thus, the viscosity is calculated along the surface as a function of the hydrodynamic pressure (see subsection 4.1.5 for more details). However, the lubricant temperature along the lubricated surface is assumed equal to the inlet lubricant temperature.

The relation temperature effect on the dynamic viscosity for the hydrodynamic bearing of the planetary transmission is shown in Eq. [38]. The parameters $\eta_{0,IDG,T0}$, and β_{IDG} have to be obtained based on experimental results. As shown in Table 8, the viscosity of the Mobil Jet Oil II at 40 and 100 °C is known. Thus, both parameters can be obtained, as shown Table 9. Where the dynamic viscosity $\eta_{0,IDG}$ is obtained in Pa.s as a function of T_{inlet} , which is introduced in Kelvin.

$$\eta_{0,IDG} (T_{inlet}) = \eta_{0,IDG,T0} e^{-\beta_{IDG} T_{inlet}} \quad [38]$$

Table 9 Viscosity-temperature model parameters for Mobil Jet Oil II

Parameter	Value	Units
$\eta_{0,IDG,T0}$	189.5224	1/K
β_{IDG}	0.0282	Pa.s

4.2.2 Plain journal bearing

A plain journal bearing, previously studied by Lu et al. [82], is used to compare the PbM results with the experimental data. The reason for an additional case study apart from the planetary transmission of the IDG is that the experiments of a plain journal bearing can measure the friction coefficient as opposed to experiments of the planetary transmission that measure the mechanical losses in the system. The additional case study based on well accepted experimental results provides additional evidence of the validity of the PbM presented in this thesis.

The plain journal bearing consists in a journal and a support or housing. The journal is a plain shaft made of AISI 1020 steel and the housing is made of SAE 660 bronze alloy. The lubricant temperature is assumed 40 °C and no overpressure is considered.

Regarding the boundary conditions of the system, the external loads due to the interaction fluid-solids, and the interaction between both solids have been considered (asperity contact component). It is assumed that there are only elastic deformations and displacement is not allowed on the base of the support and the shaft edges as shown in Figure 19.

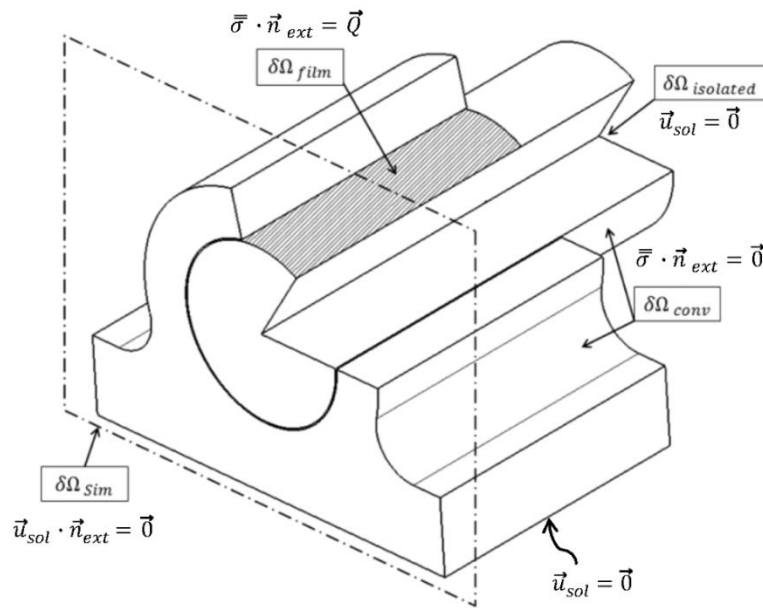


Figure 19 Boundary conditions scheme

The PbM is computationally expensive and the mesh should be optimized. Only half of the bearing is meshed due to the symmetry of the bearing. The fluid dynamics phenomena are more critical than the solid mechanics of the bearing and a finer triangular mesh is used for the lubricant domain, which is optimized following a geometrical distribution to obtain a finer mesh over the area of higher pressures, the mesh discretization is fixed and does not change as a function of the speed. The rest of the bearing consists in a thicker tetrahedral mesh. The main parameters are shown in Table 10.

Table 10 Plain journal bearing mesh properties, fluid and solid domains

Mesh parameter	Solid domain	Fluid domain
Number of elements	71811	2628
Minimum element quality	0.06401	0.6499
Average element quality	0.7548	0.9731
Maximum growth rate	3.968	2.091
Average growth rate	1.666	1.167

The dimensions of the bearing are shown in Table 11, whereas the surface properties required by the asperity contact component are shown in Table 12. In addition, the mechanical properties of the shaft and housing are shown in Table 13.

Table 11 Geometrical properties of the plain journal bearing

Parameters	Value
Length (mm)	25.4
Diameter (mm)	24.54
Clearance (mm)	0.085

Table 12 Lubricant surface properties of the plain journal bearing

Parameters	Value
Density of asperities n (m⁻²)	$2.5 \cdot 10^{10}$
Average asperity radius β_a (m)	$10 \cdot 10^{-6}$
Standard height deviation σ_s (m)	$0.2 \cdot 10^{-6}$

Table 13 Mechanical properties of shaft and housing of plain journal bearing

Parameters	Value
Shaft Young's module (GPa)	209
Housing Young's module (GPa)	100
Shaft Poisson's ratio	0.29
Housing Poisson's ratio	0.33
Dry friction coefficient	0.2

The lubricant consist in a SAE 30 oil. The properties of the lubricant required by the PbM are shown in Table 14. All the experiments of the plain journal bearing presented in the thesis are conducted at 40 °C; thus, the exponential law that relates lubricant viscosity and temperature is not required as opposed to the hydrodynamic bearing of the planetary transmission of the IDG.

Table 14 Properties of the lubricant SAE 30

Parameters	Value
Kinematic viscosity (cSt) at 40°C	93
Kinematic viscosity (cSt) at 100°C	10.8
Oil density (kg/m³)	869.3

4.3 Summary

This chapter covers the description of the PbM, which is the core of this thesis. The PbM is a novel mixed lubrication model in the field of tribology capable of computing metal-metal contact locally along the lubricated surface. The PbM also represents the main contribution of the condition health monitoring technique to detect metal-metal contact in a hydrodynamic bearing. Thus it is an essential part of both novelties of the thesis.

The main contributions of the novel PbM presented in this chapter, independently of its application to health condition monitoring, are the combination of mixed lubrication and EHL phenomena locally along the lubricated surface by using CFD/FEA as opposed to the previous mixed lubrication models based on an asperity contact component. The mixed lubrication model is described and compared to experimental results in the published journal paper “Computational Mixed-TEHL model and Stribeck curve of a journal bearing” [111] in Tribology transactions.

The novel technique to detect metal-metal contact in hydrodynamic bearings is further developed in chapter 5, but the PbM presented in this chapter is the main contribution of the health condition monitoring technique. As opposed to DDM techniques; which normally rely on the complex health assessment of statistical health indicators that are relatively easy to obtain, this thesis presents a technique based on a complex PbM that provides the friction coefficient and the percentage of metal-metal contact, which are direct indications of the damage due to metal-metal contact. The advantage of obtaining a health indicator that is a direct indication of the damage is that the health assessment can be as simple as a threshold. Therefore, the contribution of the technique to detect metal-metal contact is due to the novel PbM presented in this chapter, rather than its application or health assessment, shown in the following chapter 5.

The PbM is used in two different hydrodynamic bearings in this thesis, the hydrodynamic bearing of the planetary transmission and a plain journal bearing. The implementation of the PbM to both hydrodynamic bearings was detailed in this chapter, providing a detailed description of the boundary condition and parameters that should be defined in order to implement the model in any other hydrodynamic bearing.

5 Health condition monitoring

The application of a PbM approach to detect a failure mode requires the computation of the model in real-time to assess the health of the system. For models that are based on analytical equations the model may be executed in the vehicle or system directly. However, for more complex models, it is not feasible to execute the model in the vehicle due to computational and software limitations in the vehicle. Even if a complex model could be executed in the vehicle it may prove challenging to provide real-time health assessments; e.g. if the execution of the model requires 3 hours the health monitoring system would only provide results every 3 hours or more.

An alternative option consists in dividing the IVHM system in: PbM simulations, executed offline for a wide range of operational conditions, and an IVHM tool, installed in the aircraft, responsible of assessing the health of the system in real-time by comparing the conditions with a database previously generated.

The PbM developed in this thesis is based on a FEA/CFD model that requires significant computational power and specific software. The PbM cannot be computed in real-time in the aircraft. Therefore, the latter solution is preferred, consisting in the PbM executed offline and the IVHM tool accessing the model results from a database in real-time in the aircraft.

The core of the IVHM system, the PbM which is executed offline, is covered in chapter 4. The IVHM tool installed in the aircraft accesses the PbM results from a database and evaluates the health of the IDG in real-time. In addition, the IVHM tool provides recommendation to the pilot to avoid further damage, allows the disconnection of the IDG if the safety of the airplane is not affected, and can be used to trigger the required maintenance actions. The IVHM tool required to detect metal-metal contact and actuate in accordance in the aircraft is described in the following section 5.1.

The PbM requires 3 input parameters: speed, generator torque, and inlet lubricant temperature. All of them available in the aircraft and test rig. However, as previously mentioned, the experiments of the transmission in the test rig are conducted at low loads and ambient lubricant temperature to avoid total failure and allow multiple experiments of metal-metal contact. Thus, provoking metal-metal contact at low speeds. It should be noted that the input torque, used for validation in the test rig, is not required by the health condition monitoring technique.

The aircraft can operate under significantly higher loads lubricant temperatures; thus, metal-metal contact can occur at higher speeds, within the range of operation of the IDG. These conditions cannot be evaluated in the test rig; however, its impact can be analysed with the results of the PbM. The temperature, load and combination of both effects are analysed based on the results of the PbM in section 5.2. It should be noted that the PbM has not been compared to experimental data under such conditions.

This analysis is particularly relevant due to the particularities of the IDG. The lubricant temperature can be a critical factor because, as shown in the background section 1.1, the same oil is used for lubrication and for the hydraulic unit that regulates the speed. The hydrodynamic bearing does not significantly increase the lubricant temperature; however, the hydraulic pump can increase the lubricant temperature and lead to metal-metal contact in the planetary transmission at higher speeds.

The load in the hydrodynamic bearings, determined by the generator torque, can also lead to higher speeds at which metal-metal contact occurs. If the electrical demand by the systems of the aircraft increases the hydrodynamic bearing load will be higher and metal-metal contact may occur. This can be particularly critical if occurs in combination with higher lubricant temperature.

5.1 IVHM tool

The computational power and memory of an aircraft system is limited and the tasks carried out by the IVHM tool should be minimized. The PbM presented in this thesis requires significant computational power and resources and cannot be executed in the aircraft. Therefore, the FEA/CFD model is computed previously on the ground, and the results for all the range of operational conditions are stored in a database accessible by the IVHM tool in the aircraft.

The PbM is the first stage of the IVHM system, which is the core of the proposed health condition monitoring technique. The PbM was presented in chapter 4 and it is compared to experimental results in chapter 7. This section presents the second stage of the IVHM system, the application of the PbM for in the aircraft; which includes a description of the user-interface and its capabilities, the data processing to obtain the health of the system, and the actions and recommendations provided by the tool to minimize the damage without compromising the safety of the aircraft.

5.1.1 IVHM tool capabilities

The IVHM tool is a proof of concept of the integration of the PbM technique to detect metal-metal contact in the aircraft. At this stage the IVHM tool is represented by a Graphical User Interface (GUI) that represents the interaction between the pilot and the algorithm during a simulated flight where the operational conditions and the status of the redundant IDGs can be modified.

The IVHM tool has access to the database with the PbM results for the range of operational conditions of the IDG and monitors the speed, generator torque and inlet lubricant temperature in real-time. By estimated proportion of metal-metal contact the health of the system can be assessed. This information is provided to the pilot for the operation of the aircraft and can be used by the Continuous Airworthiness Management Organization (CAMO) responsible of triggering the necessary maintenance actions.

Therefore, the following requirements are required by the IVHM tool:

No additional sensors

An IVHM tool for legacy aircraft is particularly challenging when extra sensors have to be incorporated to the initial design due to certification constraints. The IVHM tool does not require any additional sensor, the health of the system is assessed based on speed, load and inlet oil temperature; which are available in the original design.

No major design modifications

The calculations of the IVHM tool should be feasible by the current system installed in the aircraft without additional hardware. The IVHM tool consists in analytical and logical clauses that do not require specific software or significant computational power.

Real-time

The metal-metal contact failure mode does not consist in continuous degradation. Degradation only occurs under certain operational conditions. The IVHM system should identify these critical conditions as soon as possible to react before total failure occurs. Therefore, the sampling rate of the IVHM tool should be relatively high. The calculations conducted by the IVHM tool are minimal, consisting in logical clauses and analytical equations.

Aircraft decision making

In order to maximise the potential of a prognostics IVHM tool, the health assessment can provide additional benefits if used during the operation of the vehicle, and not only for maintenance. The IVHM tool not only assesses the health of the system. It also provides recommendations to the pilot to avoid further damage and allows the disconnection of the IDG only if the other IDGs are operative.

5.1.2 IVHM tool description

The IVHM tool has been developed in order to represent the capabilities of the IVHM system and its implementation in the aircraft. This subsection describes the IVHM tool that can be executed in real-time replicating the aircraft conditions. A detailed description of the data management by the IVHM tool is provided in the following section 5.1.3.

The IVHM tool is developed in Matlab. An initial GUI is required to define the simulation parameters (see Figure 20). The sample rate, flight hours, IDG hours, or part ID are selected. The operational conditions during the flight are modified in real-time by the user.

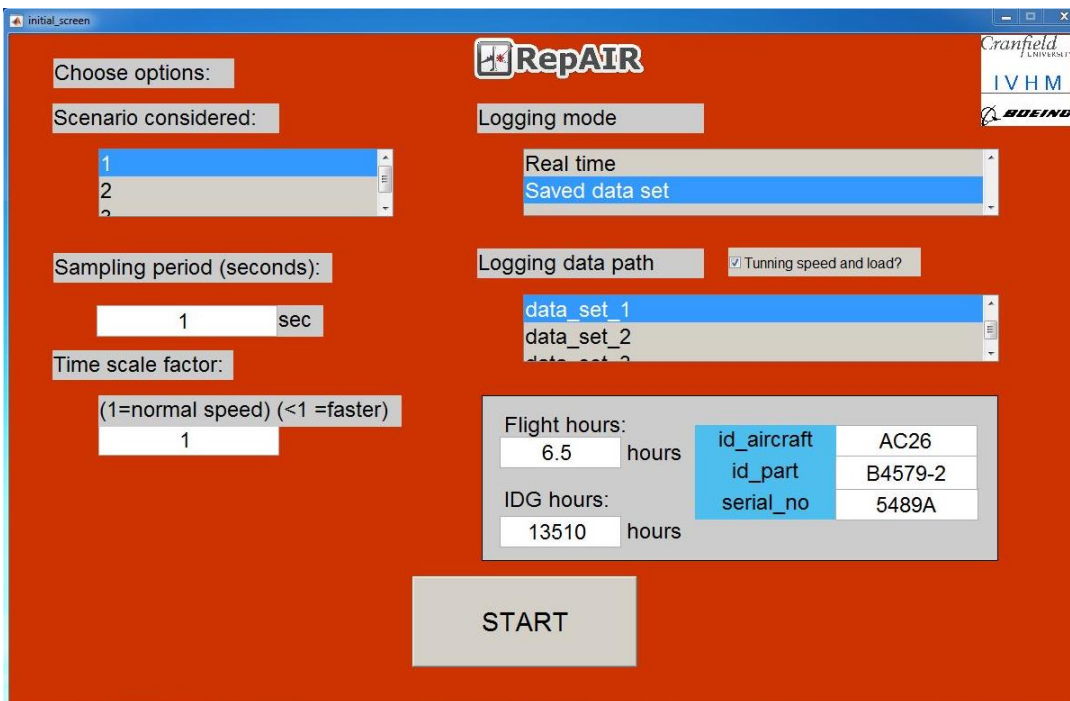


Figure 20 Initial GUI: Configuration of flight simulation and IVHM tool

The IVHM tool can be executed once the parameters defined in Figure 20, required to simulate the flight are defined. The IVHM tool GUI evaluates the health of the IDG due to metal-metal contact in real time, as shown in Figure 21, simulating the conditions during flight. This tool provides the health indicators over time, health assessment and the status of the redundant IDGs. The speed, generator torque, and lubricant temperature can be modified during the simulated flight.

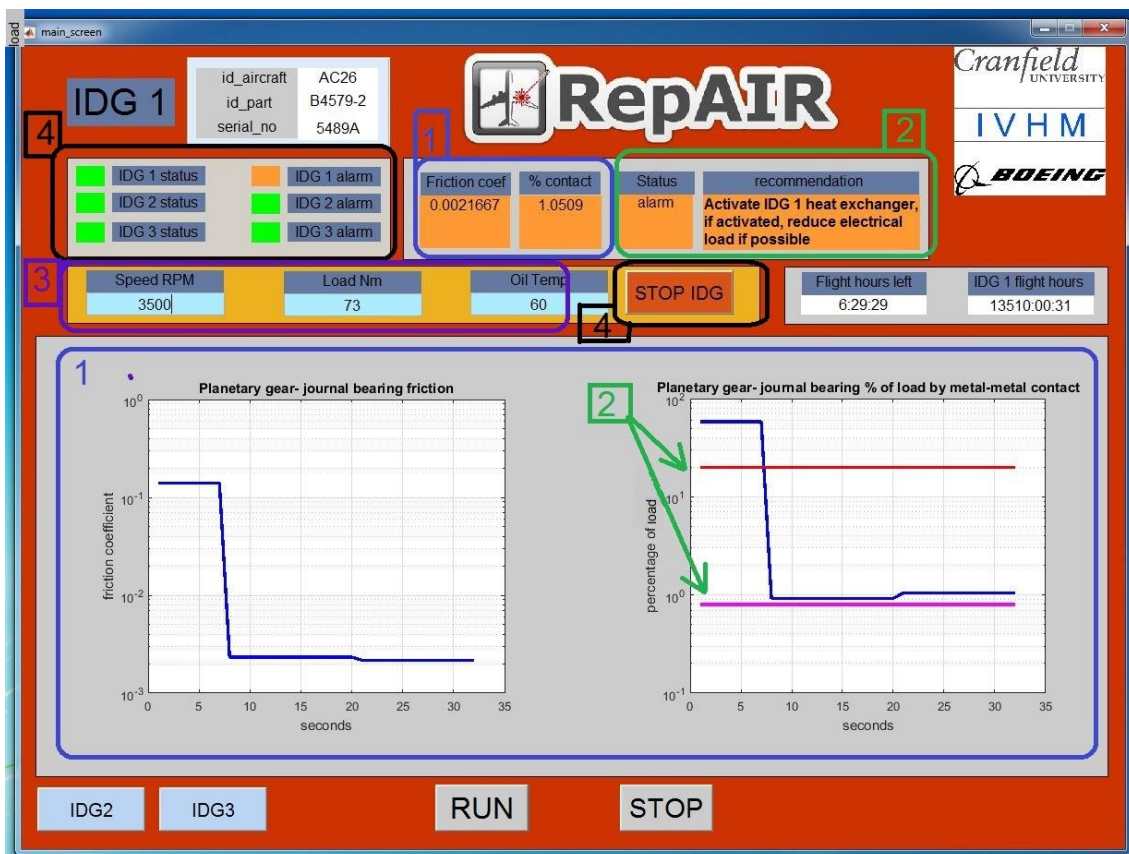


Figure 21 IVHM tool GUI: 1- health indicators, 2- health assessment, 3- operational conditions, 4- Decision making in the aircraft

The functionalities of the IVHM tool can be divided, as shown in Figure 21, as follows:

Health indicators

The health indicators proposed in this thesis, both directly provided by the PbM, are the friction coefficient (health indicator 1) and the percentage of load transmitted through metal-metal contact (health indicator 2). Their value along time can be tracked as shown in Figure 21-1.

Under metal-metal contact the friction coefficient increases significantly, a threshold on the friction coefficient could be used to detect metal-metal contact. However, in the hydrodynamic region the friction coefficient also increases as speed increases due to the higher film thickness and viscous forces. Thus, thresholds of the friction coefficient at the first stages of metal-metal contact could lead to false alarms.

The health indicator 2, the percentage of load transmitted through metal-metal contact is more robust because it is directly related to the failure mode and it only increases if metal-metal occurs. This indicator is not being affected by excessive friction due to higher film thickness and viscous forces.

Health assessment

The health assessment is based on the health indicator 2, the percentage of load transmitted through metal-metal contact. Two thresholds are defined to differentiate between healthy, alarm, and failure status as shown in Figure 21-2.

Under hydrodynamic regime all the load is transmitted through the lubricant and the status is considered “healthy”. The “alarm” status is triggered when partial metal-metal contact occurs but the contact is not severe. Under this situation metal-metal contact does not lead to a total failure. If the percentage of load transmitted through the asperities becomes significant and the second threshold is exceeded a “failure” status is triggered and total failure may occur.

It should be noted that this thesis aims to validate a novel technique based on a PbM to detect metal-metal contact, but the definition of the limits from which a failure is considered are not in the scope of this thesis. Thus, the thesis does not aim to define the optimal thresholds' values. The thresholds should be adjusted by the MRO organization to minimize the cost without compromising the availability of the aircraft. However, for qualitative purposes the alarm threshold is set at 0.8% of load transmitted through the asperities, and the "faulty" condition is considered for values above 20%.

The speed depends on the turbine thrust and cannot be modified to avoid the failure for safety reasons. However, the damage can be avoided if the load is reduced, which can be done by disconnecting non-essential electrical systems in the aircraft; or by reducing the oil temperature by using the heat exchanger installed in the IDG. These recommendations are provided by the IVHM tool to the pilot under "alarm" conditions. If metal-metal contact is more severe and total failure may occur the IVHM tool advises the pilot to disconnect the IDG.

The benefit of this additional functionality is that a potential failure can not only be mitigated, but it can be completely avoided by modifying the load or oil temperature with minor impact in the operation and safety of the aircraft. Therefore, a higher availability of the aircraft can be achievable, in addition to the maintenance cost and time reduction due to the reduction of inspection times and the reduction of secondary damage. If more severe metal-metal contact occurs the IDG can be disconnected before stalling occurs reducing secondary damage and inspection times.

Operational conditions

The operational conditions of the IDG can be monitored; in particular, the rotating speed, generator torque and inlet lubricant temperature are used as inputs by the IVHM tool. In order to test the proof of concept proposed in this thesis these operational conditions can be modified in the GUI as shown in Figure 21-3. Allowing to test variable operational conditions during the flight as it would occur in the real system.

Decision making in the aircraft

If there is a “failure” status the IDG can potentially be disconnected, as shown in Figure 21-4. However, if it is disconnected it cannot be reconnected during the rest of the flight. For safety reasons the IDG can only be disconnected if the other 2 IDGs are operative, the status of the redundant IDGs is accessible by the IVMH tool and the disconnection of the IDG is only allowed if this condition is met.

5.1.3 Data management

The capabilities and functionalities of the IVHM tool were described in the previous subsections. However, a comprehensive description of the data flow and process of the IVHM tool is required.

The process and data flow of the IVHM tool are shown in Figure 22. The processes and flow of information are divided between tasks executed on the ground and aircraft. The aircraft is divided in IVHM tool in IDG 1 and the redundant IDGs 2 and 3. The main processes and functionalities: FEA/CFD model, health indicators, health assessment and aircraft decision making will be described in sequential order. It should be noted that the IVHM tool does not include the process to launch a maintenance work order.

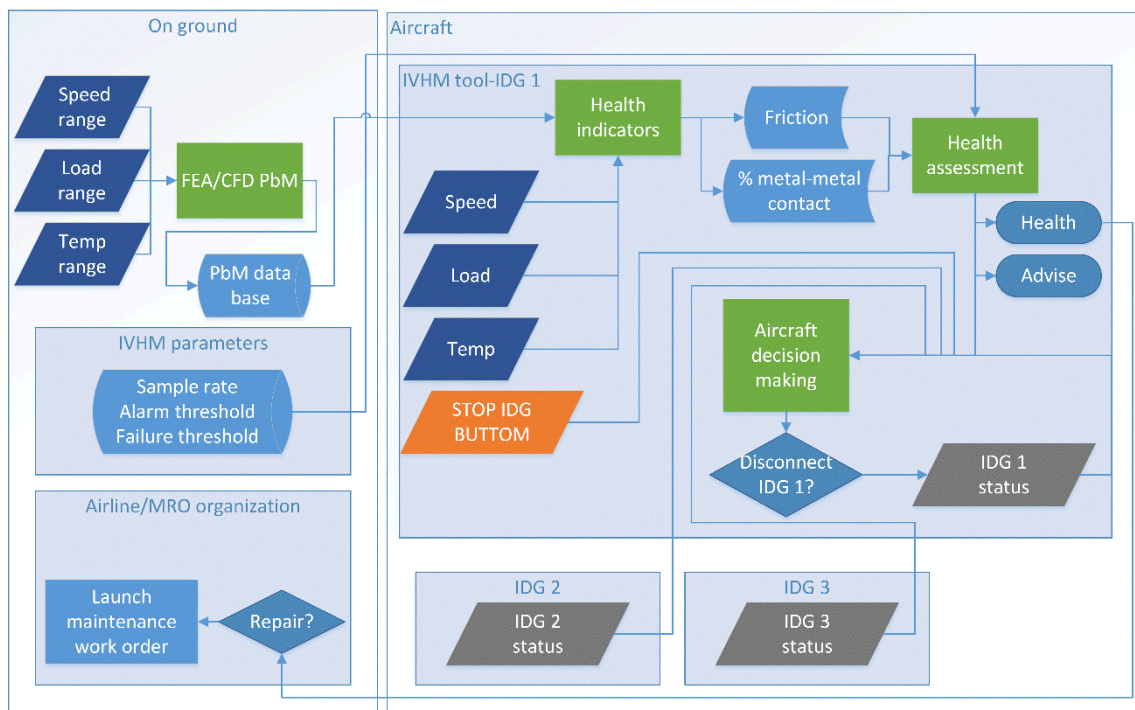


Figure 22 IVHM tool process and data flow diagram

FEA/CFD Physics-based Model

The first stage of the IVHM system consist in creating a database of PbM results for all the operational conditions. The database is used by the IVHM tool in the aircraft without executing the PbM in real-time. The databases store both health indicators, the total friction coefficient and percentage of load transmitted through metal-metal contact as a function of the operational conditions: carrier shaft speed, generator torque and inlet lubricant temperature.

Each simulation is executed for a specific load and inlet oil temperature and a wide range of speeds, from 10 to 6000 rpm; thus, providing the friction coefficient μ and percentage of load transmitted through asperities κ as a function of the speed.

This simulations should be executed for a wide range of loads and inlet oil temperatures. In this thesis the data base contains simulations for input IDG torques of 40, 80 and 296 Nm; and for inlet oil temperatures of 20, 40, 80, 100 and 140 °C. A detailed discussion of the results is included in the following section 5.2.

Health indicators

The potential health indicators, calculated by the IVHM tool, are the friction coefficient μ and the percentage of load transmitted through metal-metal contact κ . The PbM database stores these health indicators in 3D matrixes F and L , representing the μ and κ for all the simulated loads and temperatures as shown in Eq. [39, 40], where both health indicators are obtained for all the simulated operational conditions i,j,k ; corresponding to the rotating speed, generator load, and inlet lubricant temperature respectively.

$$F_{i,j,k} = \mu(s_i, l_j, T_k) \text{ where } s_i = \text{speed}, l_j = \text{load}, T_k = \text{oil temperature } \forall i, j, k \text{ in database} \quad [39]$$

$$L_{i,j,k} = \kappa(s_i, l_j, T_k) \text{ where } s_i = \text{speed}, l_j = \text{load}, T_k = \text{oil temperature } \forall i, j, k \text{ in database} \quad [40]$$

The monitored values of speed s^* , load l^* and oil temperature T^* , differ from those in the database and the estimated friction μ^* and percentage of metal-metal contact κ^* are obtained by trilinear interpolation. It should be noted that $\mu(s_i, l_j, T_k)$ and $\kappa(s_i, l_j, T_k)$ are not linear functions and several data points are required to minimize the interpolation errors.

In order to interpolate μ^* and κ^* at the actual operational conditions, represented by $p(s^*, l^*, T^*)$ in Figure 23, the closer data points x_{1-8} must be identified along with their corresponding μ and κ values, represented by V .

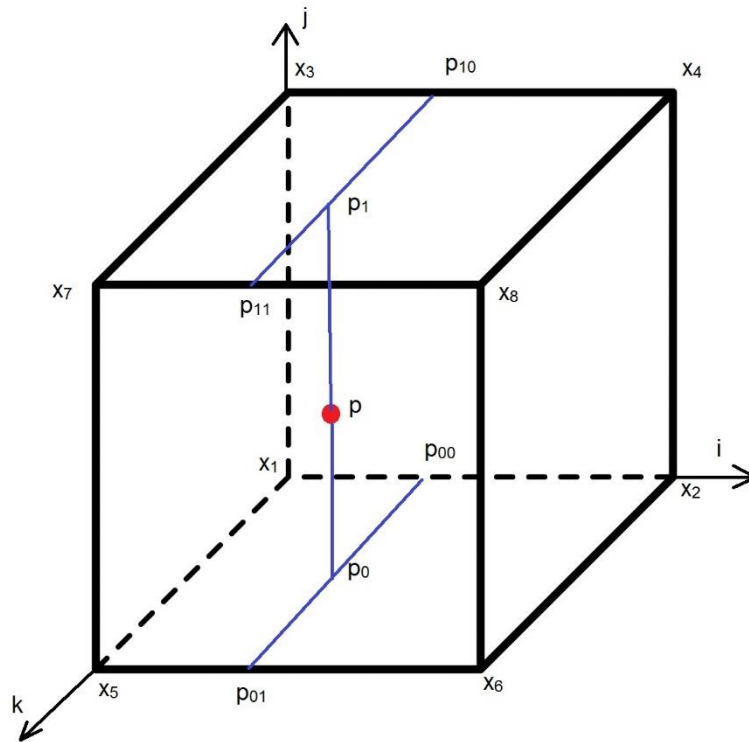


Figure 23 3D linear interpolation notation – x_i : simulated operational conditions, p : actual operational conditions, $p_{r,c}$ lower dimension interpolations.

The 1D interpolations of V for $p_{01}, p_{10}, p_{00}, p_{11}$ can be obtained by interpolating V between their corresponding $x_{i,i+1}$ points, as shown in Eq. [41]. $V(p_{r,c})$ can be used to interpolate $V(p_1)$ and $V(p_0)$ using the same approach by interpolating between $p_{01}, p_{10}, p_{00}, p_{11}$. Finally $V(p)$ is obtained repeating the same process by interpolating between p_1 and p_0 .

$$V(p_{r,c}) = V(x_i) + (V(x_{i+1}) - V(x_i)) \cdot \frac{p_{r,c} - x_i}{x_{i+1} - x_i} \text{ for } r, c = 1, 0 \quad [41]$$

As a result, the health indicators are obtained in real-time by interpolating μ^* and κ^* as a function of the actual operational conditions s^*, l^* and T^* using the data stored in F and L .

Health assessment

The complexity of the health assessment depends on how representative of the failure mode the health indicators are. DDMs techniques based on artificial intelligence evaluate multiple parameters as health indicators and find complex trends related to the failure. Thus, the contribution of such techniques normally relies on the health assessment rather than the calculation of representative health indicators.

The opposite occurs to PbM approaches, the degradation is modelled so the health indicators represent the physical phenomena of the failure mode. The challenge is to develop a reliable PbM capable estimates those health indicators. Under this circumstances the magnitude of the health indicator is directly related to the failure mode and the health assessment may consist in thresholds without the need for more complex health assessment techniques.

In this thesis the health indicators, friction μ and percentage of load transmitted through metal-metal contact κ , represent the physical phenomena of the failure mode and their magnitude can be used to define thresholds when degradation occurs.

The technique presented in this thesis has the potential to detect metal-metal contact in the early stages of the failure, when the load transmitted through the asperities is limited. Thus, it has short-term prognostics capabilities; however, it can also predict severe metal-metal contact and a potential total failure. Therefore, it has diagnostics capabilities as well. The IVHM tool requires two thresholds of the health indicator κ : an alarm threshold K_{alarm} for short-term prognostics, and a failure threshold for diagnostics $K_{failure}$ when a failure is expected to occur.

The friction coefficient μ is a valid health indicator; however, as it was previously mentioned, it increases not only due to metal-metal contact, but also due to excessive lubrication and could lead to false alarms.

The percentage of load transmitted through metal-metal contact κ is a more robust health indicator because its magnitude is directly related to the severity of the failure mode and it is unaffected by excessive lubrication.

The “health” state of the system can be “healthy”, “alarm” or “failure” depending on κ and the alarm and failure thresholds as shown in Eq. [42]. If the system is “healthy” no actions are required and no recommendation is given to the pilot. However, if there is an “alarm” state partial metal-metal contact may occur, a recommendation is provided to the pilot to return to a “healthy” state without compromising the operation of the aircraft.

$$health = \begin{cases} healthy & \text{if } \kappa < K_{alarm} \\ alarm & \text{if } K_{alarm} \leq \kappa < K_{failure} \\ failure & \text{if } \kappa > K_{failure} \end{cases} \quad [42]$$

To return to healthy conditions the rotary speed, load and inlet lubricant temperature can be modified. However, the speed is related to the turbine thrust and it should not be modified. Instead, it is recommended to use the oil heat exchanger to reduce the inlet oil temperature, and if it is already activated, reduce the load in the system by disconnecting non-essential electrical systems in the aircraft.

Aircraft decision making

The IDG can be physically disconnected from the turbine at any time during the flight if a critical failure occurs. However, it cannot be reconnected again until the plane is on the ground. Therefore, the decision of disconnecting the IDG should be taken only under a high risk of total failure in the IDG.

Some of the electrical systems in the aircraft are critical and the risk of having all the IDGs inoperative affects the safety of the aircraft. The IDG should only be disconnected if the other IDGs are operative; otherwise it should remain connected even if a failure occurs.

Because the IDG cannot be reconnected during flight, the IDG should not be disconnected under an “alarm” health status. However, if metal-metal contact is more severe and there is a “failure” health status, total failure is likely to occur and the IVHM tool recommends the pilot to disconnect the IDG. Regardless of the decision of the IVHM tool and the pilot, if any of the redundant IDGs is not operative the IVHM system does not disconnect the IDG, as shown in Eq. [43]. In the IVHM tool proposed in this thesis the disconnection of the IDG is advised to the pilot, who can decide to disconnect it. Alternatively, the IDG can be disconnected automatically by the IVHM tool.

$$\text{if } \left\{ \begin{array}{l} \text{IDG 1 = operative} \\ \text{stop IDG 1 = yes} \\ \text{IDG 1 health status = failure} \\ \text{IDG 2 = operative} \\ \text{IDG 2 = operative} \end{array} \right\} \text{ then IDG 1 = disconnected} \quad [43]$$

Finally, the information of the IVHM tool should be beneficial, not only for the operation of the aircraft, but also for the maintenance. The health assessment and health indicators should be transferred to the CAMO, which normally is the airline or the MRO organization. And the decision of launching a repair work order can be triggered.

5.2 Metal-metal contact under aircraft operational conditions

IVHM has additional benefits in addition to the maintenance cost reduction for diagnostics and higher availability of the vehicle for prognostics. The outcomes of the IVHM can help during the design stage, this is particularly relevant for PbMs due to the synergies between PbM applied for IVHM and those used during the design [18]. The understanding of the physics of failure due to the PbM, initially developed for IVHM can be used to mitigate or totally avoid the failure mode in future designs of the system if the failure phenomena is better understood.

This section evaluates the results of the PbM under the aircraft operational conditions and discusses the impact of the main parameters (speed, load and inlet lubricant temperature). It should be noted that the comparison with experimental results has been conducted under lower operational conditions. The aim of this section is to understand the relevance of each parameter, in particular load and lubricant temperature.

The PbM described in chapter 4, implemented for the hydrodynamic bearing of the planetary transmission of the IDG, is evaluated for different aircraft operational conditions: speeds from 10 to 6000 rpm under different loading conditions (40 and 80 Nm) and inlet lubricant temperatures (20, 40, 80, 100 and 140 °C). The impact of lubricant temperature and load in the severity of metal-metal contact is analysed.

5.2.1 Description

The IDG normally operates at high speeds (>3000 rpm) and metal-metal contact is a failure mode that normally occurs at low speed. However, the range of loading conditions is wide and the lubricant can reach high temperatures due to the heating in the hydraulic unit that regulates the speed, leading to metal-metal contact at nominal conditions.

The load is directly related to the electrical demand of the aircraft. The friction and heat dissipation in the lubrication system of the IDG do not significantly affect the oil temperature as to provoking a failure. However, the same lubricant is used by the hydraulic unit to regulate the speed of the aircraft and this unit can significantly heat the oil that will later be used to lubricate the IDG.

The PbM experimental validation is conducted with lower load and ambient lubricant temperature to provoke the failure at low speeds and avoid stalling and total failure during the tests. However, under higher loads and lubricant temperatures metal-metal contact can occur at higher speed as shown in the background section as shown in section 1.1. These effects are discussed in this section.

5.2.2 Load and inlet lubricant temperature impact

In this subsection the numerical results of friction and percentage of load transmitted through metal-metal contact under the wide range of operational conditions of the IDG are presented.

The load transmitted through the hydrodynamic bearing is directly related to the input torque of the IDG, that is, the torque of the carrier shaft, as shown in Eq. [44]; where $L_{bearing}$ is the load transmitted through each hydrodynamic bearing, P_{input} is the input torque to the IDG, and R_{pitch} is the planetary gear pitch radius. The impact of the load is assessed by comparing the friction and metal-metal contact for P_{input} 40, 80 and 296 Nm.

$$L_{bearing} = \frac{P_{input}}{2R_{pitch}} \quad [44]$$

The hydrodynamic pressure increases at higher loads unless severe metal-metal contact occurs. In order to increase the hydrodynamic pressure to compensate the load the eccentricity increases and the minimum film thickness is reduced. Thus, high loads produce a smaller film thickness and can lead to metal-metal contact.

Metal-metal contact occurs because the lubricant cannot support all the load transmitted through the bearing and the film thickness is at the same order of magnitude as the roughness of the bearing surface. Some of the asperities get in contact and load is transmitted through them, with the subsequent higher friction, degradation and risk of stalling.

The capacity of the lubricant to generate a fully lubricated film also depends on the lubricant viscosity. More viscous lubricants can generate higher hydrodynamic pressure with the same eccentricity; thus, carry higher loads. Under fully lubricated conditions excessive viscosity would lead to excessive film thickness and unnecessary mechanical losses. However, high viscosity reduces the risk of metal-metal contact because higher loads can be transmitted with less eccentricity and thicker film thickness than lubricant with low viscosity.

The lubricant viscosity is strongly dependent on the temperature; e.g. the kinematic viscosity of the IDG's lubricant is 27.6 cSt at 40°C and 5.1 cSt at 100°C. Therefore, high inlet lubricant temperatures can significantly affect the risk of metal-metal contact due to the reduced viscosity of the lubricant.

In the following the friction and percentage of load transmitted through metal-metal contact as a function of the rotating speed will be presented for different loading conditions and inlet lubricant temperatures.

Under 40Nm and ambient lubricant temperature metal-metal contact occurs at very low speeds, as shown in Figure 24 and Figure 25. Mixed lubrication occurs at higher speeds if the lubricant temperature increases. However, in order to have metal-metal contact under the nominal range of speeds of the IDG, which is above 3000 rpm, lubricant temperatures should be above 100 °C, which is not probable to occur.

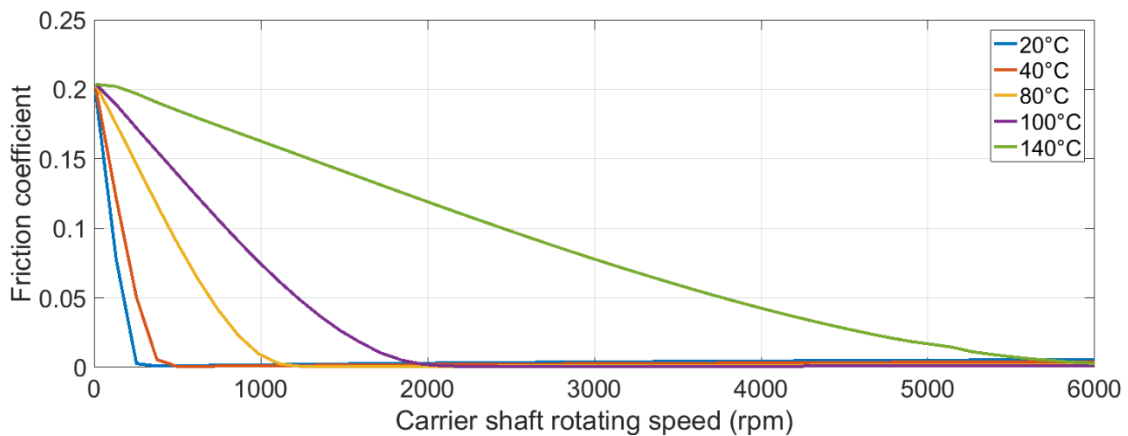


Figure 24 Estimated friction coefficient by the PbM in the hydrodynamic bearing of the IDG – Generator torque 40 Nm

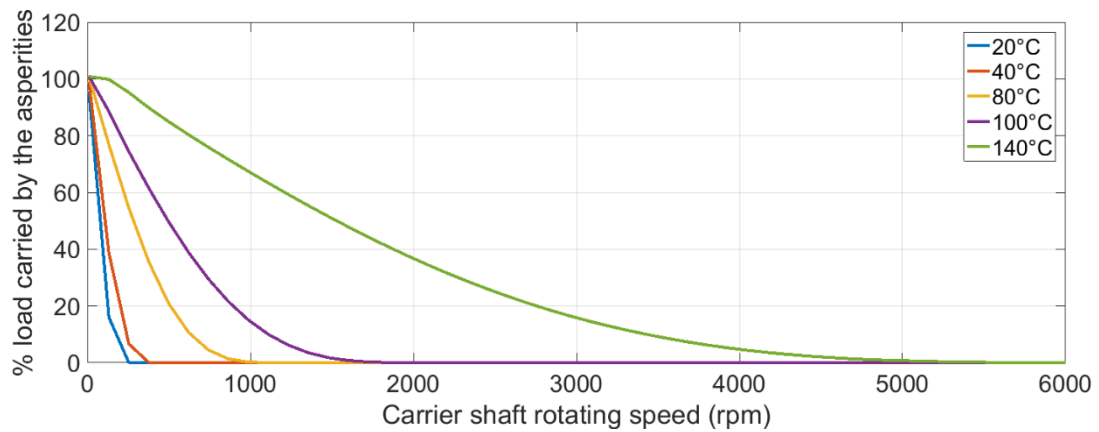


Figure 25 Estimated percentage of load transmitted through the asperities by the PbM in the hydrodynamic bearing of the IDG – Generator torque 40 Nm

Under medium load conditions (80 Nm) mixed lubrication is expected to occur at higher speeds. As shown in Figure 26 and Figure 27, partial metal-metal contact may occur under the range of nominal speeds if the lubricant temperature is 100 °C.

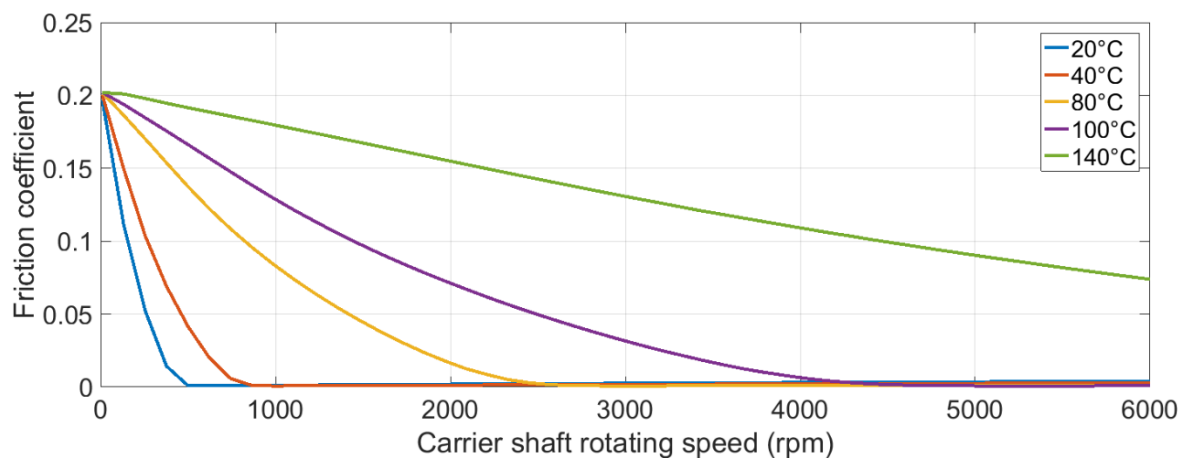


Figure 26 Estimated friction coefficient by the PbM in the hydrodynamic bearing of the IDG – Generator torque 80 Nm

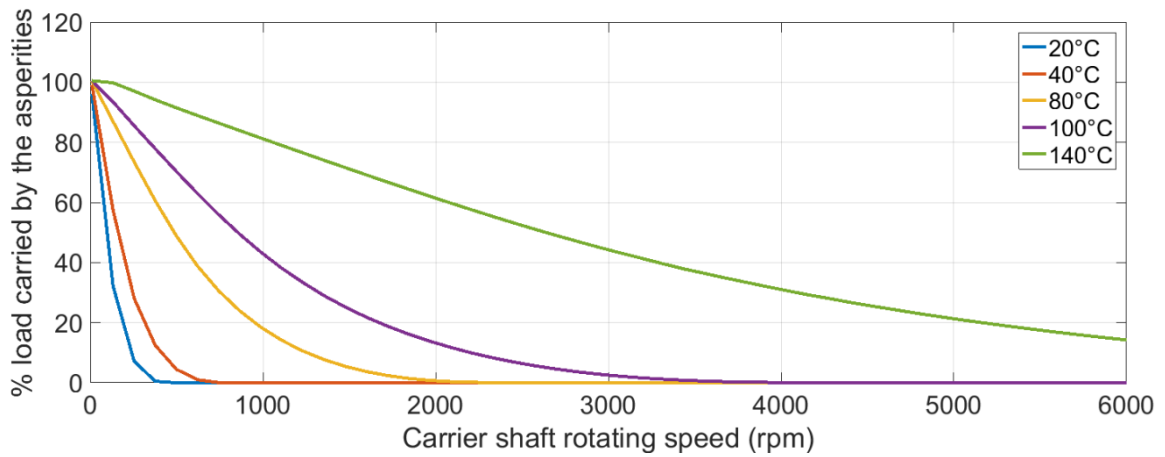


Figure 27 Estimated percentage of load transmitted through the asperities by the PbM in the hydrodynamic bearing of the IDG – Generator torque 80 Nm

For excessive load conditions (296 Nm), uncommon under normal operation, metal-metal contact is estimated in the speed range of the IDG even if the lubricant is at ambient temperature, as shown in Figure 28 and Figure 29. Under higher temperatures severe metal-metal occurs.

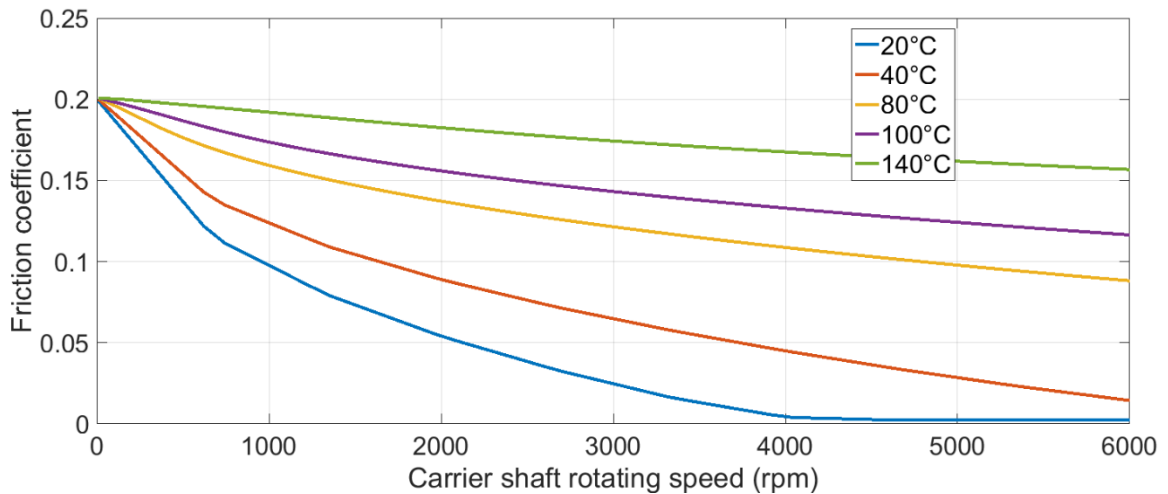


Figure 28 Estimated friction of load transmitted through the asperities by the PbM in the hydrodynamic bearing of the IDG – Generator torque 296 Nm

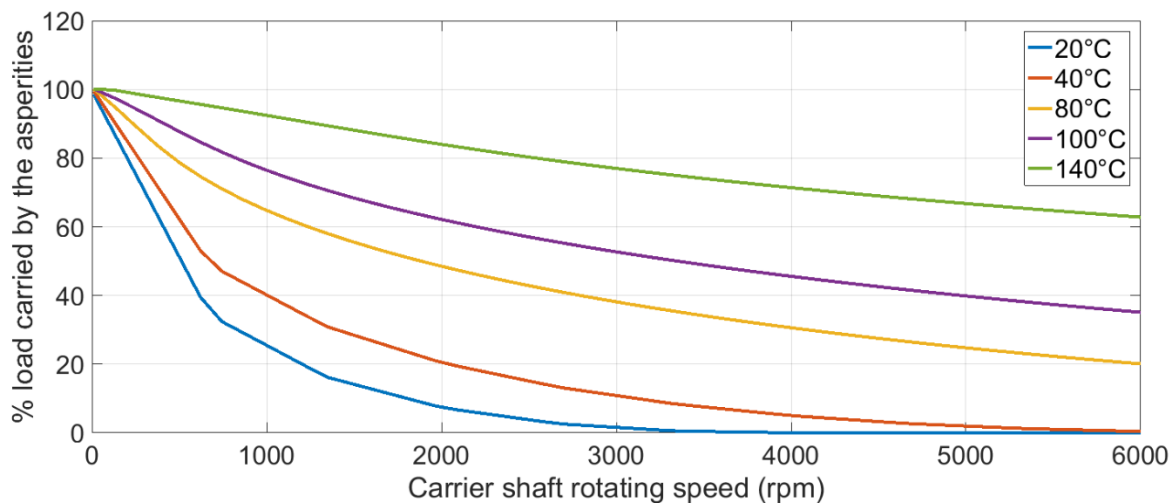


Figure 29 Estimated percentage of load transmitted through the asperities by the PbM in the hydrodynamic bearing of the IDG – Generator torque 296 Nm

From the numerical results of the PbM under different loads and temperatures the following conclusions can be obtained:

- Under low load conditions (40 Nm) mixed lubrication under the nominal range of speeds of the IDG only occurs at excessively high lubricant temperatures above 100 °C.
- Under medium load conditions (80 Nm) mixed lubrication can occur in the range of speeds of the IDG at lubricant temperatures above 80 °C.
- Under maximum load conditions (296 Nm) mixed lubrication can occur in the range of speeds of the IDG even if the lubricant is at ambient temperature. At higher temperatures the predicted metal-metal contact is severe.
- The lubricant temperature is a critical factor in the failure mode and external heat sources, e.g. the hydraulic unit responsible of regulating the speed of the planetary transmission, can cause the failure due to metal-metal contact in the hydrodynamic bearing.

5.3 Summary

Along this chapter the application of the PbM for the health condition monitoring system capable of detecting metal-metal contact in the hydrodynamic bearing of the planetary transmission has been described and discussed.

In conjunction with the novel PbM presented in chapter 4, this chapter covers one of the main novelties of this thesis:

- *The development of a novel technique to detect metal-metal contact in the hydrodynamic bearing of a planetary transmission of an aircraft's IDG using a PbM approach without installing additional sensors in the aircraft.*

The development of a novel PbM technique to detect metal-metal contact covers one of the relevant gaps in the knowledge identified in chapter 2:

- *Physics-based Models have not been used for the detection of metal-metal contact in hydrodynamic bearings.*

The novelty of this approach relies on the representation of the degradation phenomena, which was covered in chapter 4. However, the integration of the PbM in an IVHM system requires the calculation of the health indicators in real-time, the health assessment and the management of the predictions provided by the PbM for the operation of the aircraft and the maintenance. All these aspects are covered in this chapter.

In order to represent the capabilities and functionalities of the proposed technique, a proof of concept of the IVHM tool has been developed in Matlab using a GUI that replicates the interaction between the aircraft, the IVHM system and the pilot. This IVHM tool accesses the simulated results of the PbM from a database, calculates the health indicators, provides a health assessment, provides recommendations to the pilot and is in agreement with the safety requirements of the IDG disconnection if a failure occurs.

The IDG can operate in a wide range of operational conditions. The speed can vary from 3000 up to 6000 rpm, the load in the system depends on the electrical demand and the lubricant temperature can increase due to the hydraulic unit that regulates the speed. The load and lubricant temperature can significantly affect the speed at which metal-metal contact occurs. The numerical results provided by the PbM have been presented to analyse the impact of both factors.

Based on numerical results, under low load condition (40 Nm) metal-metal contact occurs at relatively low speeds. Under the nominal range of speed of the IDG partial metal-metal contact only occurs at very high lubricant temperatures above 100 °C. However, under a medium load (80 Nm) partial metal-metal contact can occur at the nominal range of speed of the IDG for lubricant temperatures above 80 °C. At maximum load conditions (296 Nm) metal-metal contact is expected to occur at the nominal range of speeds even at ambient lubricant temperature, and increases its severity at higher temperatures. Therefore, the lubricant temperature is a critical factor that should be considered, particularly under high load conditions, as it can be significantly increased by the hydraulic unit responsible for regulating the output speed of the planetary transmission.

6 Design of experiments

The technique to detect metal-metal contact in the IDG of an aircraft proposed in this thesis should be compared to experimental results. Historical data is not available; therefore, experiments in a test rig are required to evaluate the effectiveness of the technique. The PbM is compared to experiments of metal-metal contact of a plain journal bearing from the literature [82] along with tests of a replica of the planetary transmission at low speeds.

The aim of the experiments is to test the effectiveness of the PbM and to evaluate other potential health indicators as outlet oil temperatures or lubrication parameters.

In these experiments, metal-metal contact is provoked by modifying the speed and load of the system and controlling whether metal-metal contact occurs due to the additional sensors installed in the test rig. The effectiveness of the PbM approach is evaluated by comparing the operational conditions at which metal-metal contact is expected to occur by the PbM and the operational conditions at which it occurs during the experiments.

The chapter is divided in both sets of experiments, the plain journal bearing and the replica of the planetary transmission of the IDG. The PbM is compared to the experimental data of a plain journal bearing, previously studied by Lu et al. [82] to provide evidence of its effectiveness detecting metal-metal contact. The implementation of the PbM for this bearing was described in subsection 4.2.2. The friction coefficient is measured directly during the experiments; thus providing a direct comparison of the PbM output with experimental results and allowing the comparison of the metal-metal contact severity. The design of experiments of the plain journal bearing is described in section 6.1.

In order to provide additional evidence of the effectiveness of the PbM in the planetary transmission in particular a different experimental set-up is needed. The replica of the transmission is tested under different speeds and loads but the friction coefficient cannot be measured directly in the planetary transmission. Instead, metal-metal contact is detected by monitoring the mechanical losses in the transmission. A comprehensive description of the test rig, experiments and data analysis is provided in subsection 6.2.

Several experiments are needed under different conditions; therefore, total failure should be avoided in the planetary transmission. The experiments are conducted at ambient temperature and 20-40 Nm in order to provoke the failure at low speeds and minimize the risk of total failure. It should be noted that higher loads and temperatures can occur in the aircraft, leading to the risk of metal-metal contact at higher speeds, as shown in section 5.2.

6.1 Plain journal bearing experimental set-up

The experimental set-up for a plain journal bearing is based on the work of Lu et al. [82]; where experimental line contact of a plain journal bearing is compared to theoretical predictions. The advantage of these experiments is that the friction coefficient can be measured in the test rig, allowing a direct comparison of the PbM output under any operational conditions, and not only the conditions at which metal-metal contact occurs.

The experimental set-up, consists in a Lewis LRI-8H machine to measure the friction coefficient in a journal bearing as shown in the simplified diagram of Figure 30. The hydrodynamic bearing (4,3) is driven by a motor that can reach up to 3300rpm and the load is applied using a dead weight. The transversal load applied in the bearing, caused by friction, is supported by a linkage bar (2) and a load cell (1); thus, providing a direct measurement of the friction in the journal bearing. The dead weight is applied using a hanger device (5) with a scale 1:10. The lubricant temperature, flow and pressure are also monitored.

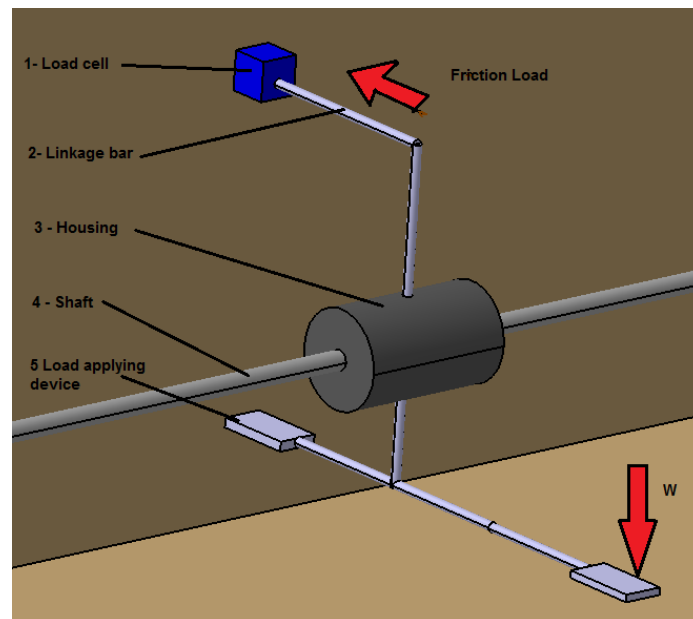


Figure 30 Schematic of the Lewis LRI-8H machine

The main advantage of this solution is that the main parameters: lubricant temperature, speed and load are fully controlled and the experimental friction coefficient μ_{exp} can be measured directly as shown in Eq. [45]. Where W is the bearing radial load, produced by a dead weight, and the friction load, F_{shear} , is the shear force measured by the load cell.

$$\mu_{exp} = \frac{F_{shear}}{W} \quad [45]$$

The properties of the bearing and lubricant, already provided in the implementation of the PbM in subsection 4.2.2, are also shown in Table 15 and Table 16. The plain journal bearing is made of hardened AISI 1021 steel and the exterior brushing is made of SAE 660 alloy bronze.

Table 15 Plain journal bearing properties [82]

Length (mm)	Shaft diameter (mm)	Bushing inner diameter (mm)	Yung's modulus (GPa)		Poisson's ratio		Surface roughness R_a (μm)	
			Shaft	Bushing	Shaft	Bushing	Shaft	Bushing
25.4	24.54	24.71	209	100	0.29	0.33	0.05	0.2

Table 16 Plain journal bearing lubricant – SAE 30 oil properties

Viscosity (cSt)		Density at 15 °C (gr/cm^3)	Viscosity index
40 °C	100 °C		
93	10.8	0.89	100

The experiments require an initial procedure to avoid sources of error. The system is balanced before any measurement is taken to ensure that no friction is registered under static conditions. In addition, the lubrication system is run for 2 hours at 100rpm to reach stationary conditions. Then for a given load different speeds are tested for a period of 4 minutes.

Two radial loads, 667 N and 1112 N, are tested for a range of speeds from 2 to 500 rpm. With a lubricant inlet temperature of 40 °C. The experimental results will be discussed and compared to the PbM in the following chapter 7.

The friction coefficient is obtained from the experimental set-up as shown in Eq. [45]. Thus, no further post-processing is required. These results are obtained from [82].

6.2 IDG journal bearing experimental set-up

The previous experiments used a machine capable of measuring the friction coefficient in a plain journal bearing. By doing so, the effectiveness of the PbM prediction of the friction coefficient could be assessed. However, it does not represent the particularities of the hydrodynamic bearing of the IDG; e.g. the inlet oil groove, the hollow shaft or the complexity of a planetary transmission. An additional experimental set-up, representative of the complexity of the IDG, is advisable.

However, historical data is not available and a test rig is needed. This section covers the design of the test rig and a replica of the planetary transmission along with a detailed description of the experimental procedure. The experimental results from the hydrodynamic bearing of the IDG are a contribution of this thesis. The purpose of this section is to provide a technical description of the test rig set-up (subsection 6.2.1) and a comprehensive description of the experimental procedure (subsection 6.2.2).

6.2.1 Test rig Design

A test rig has been devised in order to evaluate metal-metal contact health monitoring technique in a representative environment of the planetary transmission of the IDG. The design, construction and operation of the test rig are part of this project.

In order to evaluate metal-metal contact faulty conditions have to be provoked and certified IDGs cannot be used for the validation of the proposed technique. Instead, a replica of the planetary transmission has been re-designed and manufactured. As opposed to the certified IDG, the hydraulic unit that regulates the speed is not needed to test metal-metal contact, simplifying the design. The transmission is connected to a motor that replicates the turbine on one side, and the generator that supplies the AC power on the other. The test rig allows for multiple sensors not available in the aircraft in order to provide additional evidence of metal-metal contact for the comparison with the results of the PbM.

Transmission

The replica of the planetary transmission of the IDG should be representative of the failure mode as it occurs in the aircraft. The dimensions and geometry of the adjacent components to the hydrodynamic bearings are identical, as shown in Figure 31. However, other subsystems of the IDG that are not essential to test the failure mode can be substituted to simplify the design. That is the case of the hydraulic unit that regulates the speed; instead of regulating the speed of the hydrodynamic bearings with such a system, the speed is regulated by using a Variable Speed Drive (VSD) that controls the speed of the motor.



Figure 31 Redesigned replica of the planetary transmission of the IDG

The planetary gears, hydrodynamic bearings and carrier shaft surrounding the hydrodynamic bearings remain unmodified, whereas the crown gear and the carrier shaft couplings are modified to adapt the transmission to the test rig as shown in Figure 32.

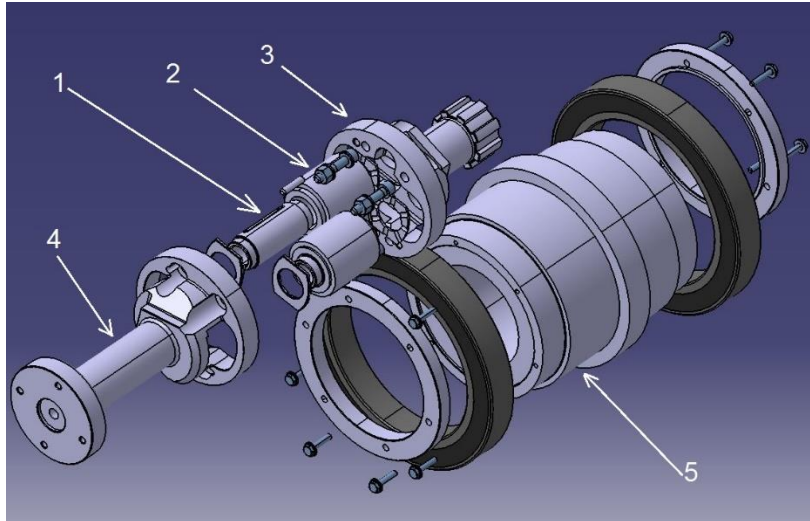


Figure 32 3D Replica of the planetary transmission. 1 – Hydrodynamic bearing, 2 – Planetary gear, 3 and 4 – Carrier shaft (input), 5 – Crown gear (output)

As shown in Figure 32 and Figure 33, the power is transmitted through the carrier shaft (3, 4) to the planetary gears (2), which are geared between each other and rotating in opposite direction. One of them is geared to the hydraulic pump (6), a fixed gear in the test rig, and the other planetary gear transmits the power to the crown gear (5), which rotates at double the speed of the carrier shaft and transmits the power to the generator (7). The hydrodynamic bearing and planetary gear are made of steel BS 080M40, with dimensions and mechanical properties as shown in Table 17.

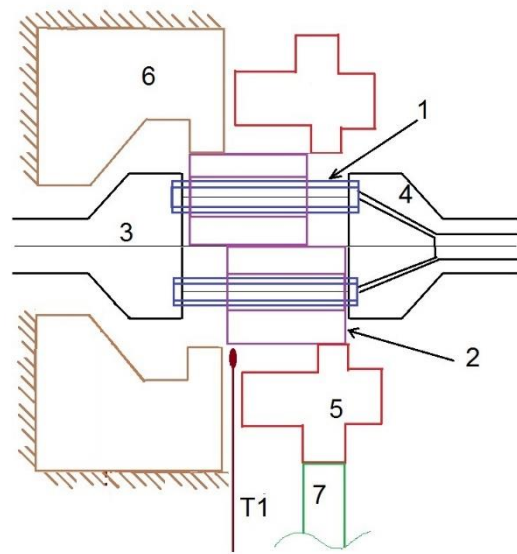


Figure 33 Layout of replica of planetary transmission. 1 – Hydrodynamic bearing, 2 – Planetary gear, 3 and 4 – Carrier shaft (input), 5 – Crown gear (output), 6 – External gear, T1 – thermocouple close to bearing

Table 17 Properties of the hydrodynamic bearing of the IDG replica

Parameter	Value
Clearance	0.1018 mm
Surface roughness R_a	0.0002 mm
Radius	12.11 mm
Length	48.34 mm
Young's modulus	209 GPa

Mechanical design

The transmission described above, which replicates the planetary transmission of the IDG, is connected to an electrical motor through the carrier shaft, replicating the power coming from the turbine. The output of the transmission is connected to a generator that replicates the load demanded by the aircraft.

The replica of the planetary transmission effectively increases the speed by 2:1; however, it is later reduced by 1:2 again due to the speed limitations of the test rig generator, as shown in Figure 34.

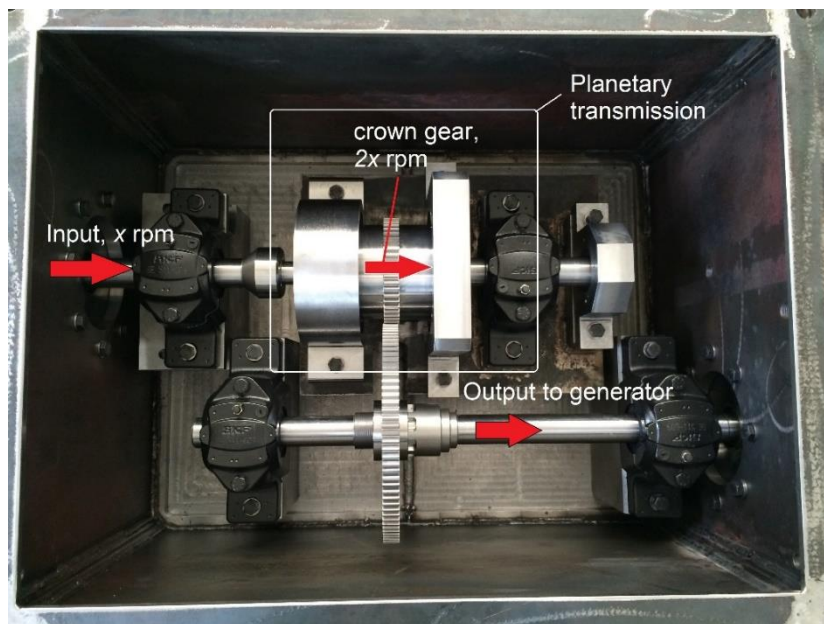


Figure 34 Test rig housing

The motors are capable of reaching up to 288 Nm input torque. The input rotating speed of the carrier shaft is limited to 3000 rpm. Both, motor and generator, are identical 95kW electrical motors connected back-to-back as shown in Figure 35, i.e. the power generated by the generator is used by the input motor using a DC link between the VSDs of each motor.

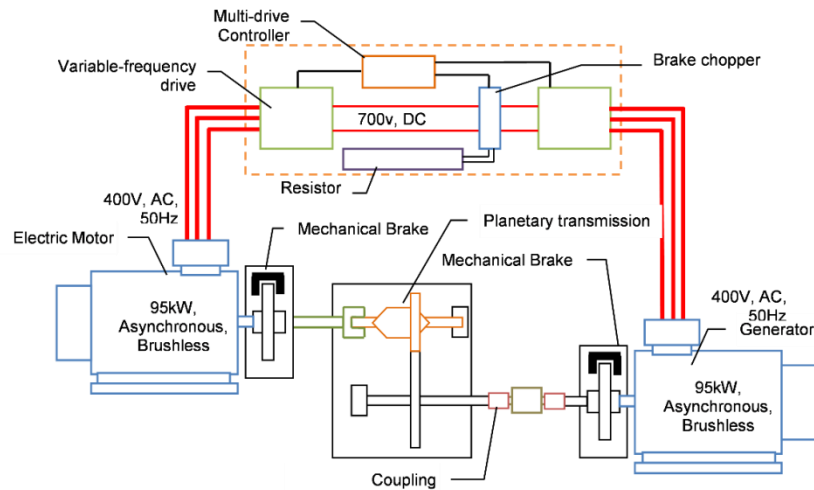


Figure 35 Test rig layout – Electrical set-up

The input motor is controlled by determining the input speed through the corresponding VSD, as it would occur in the aircraft, where the speed is determined by the turbine thrush. The torque demanded by the generator is determined by its VSD as well, replicating the electrical load of the aircraft.

The lubrication system of the test rig provides a continuous supply of oil to all rotating components of the transmission (see Figure 36). The oil circulates through lubrication channels drilled into the rotating components and drips out of hydrodynamic bearings into the sump. A pump recirculates the oil, which filtered before it enters the transmission again

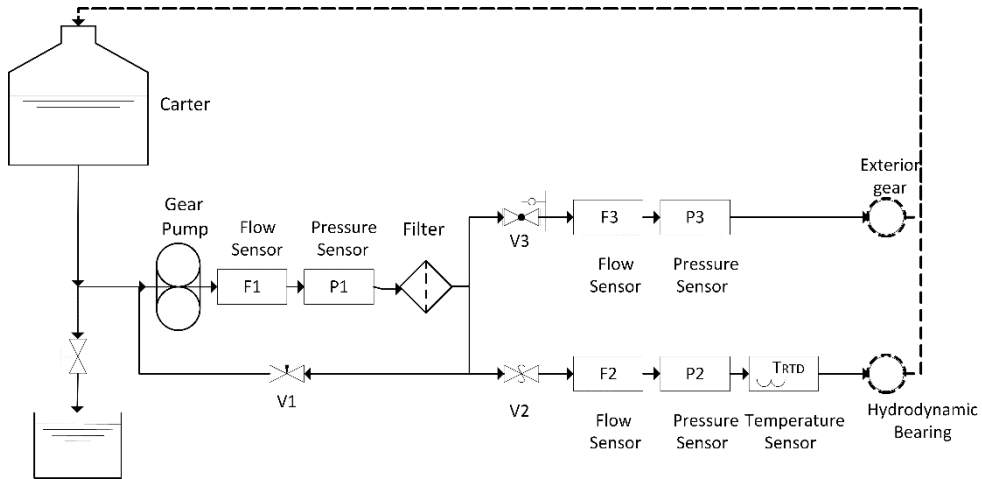


Figure 36 Lubrication system layout

In order to identify if metal-metal contact can affect the lubrication system of the IDG, the lubrication system of the test rig has been designed to conduct tests in which the flow and pressure of lubricant can be monitored. The characteristics of the lubrication system are shown in Table 18.

Table 18 Main characteristics of the lubrication system

Parameter	Value
Max. Pressure	20bar
Max. Flow	2.5l/min
Sensors	1 Temperature sensor 3 Pressure sensors 3 Flow sensors
Lubricant	Mobil jet oil II

Sensors and Data acquisition

The sensor capabilities of the IDG are limited. The aim of the thesis is to develop a health condition monitoring algorithm that only requires sensors already available in the aircraft. However, additional sensors are installed in the test rig for comparison with the PbM and research purposes.

The control and data acquisition (DAQ) system consist in independent units, both developed using Labview. The first one controls the motors and lubrication systems, and records motor's parameters with a sample rate of 0.667 Hz. Whereas the DAQ unit records the critical sensors at sample rates above 50 Hz (temperatures, torque and lubricant parameters), as shown in Figure 37.

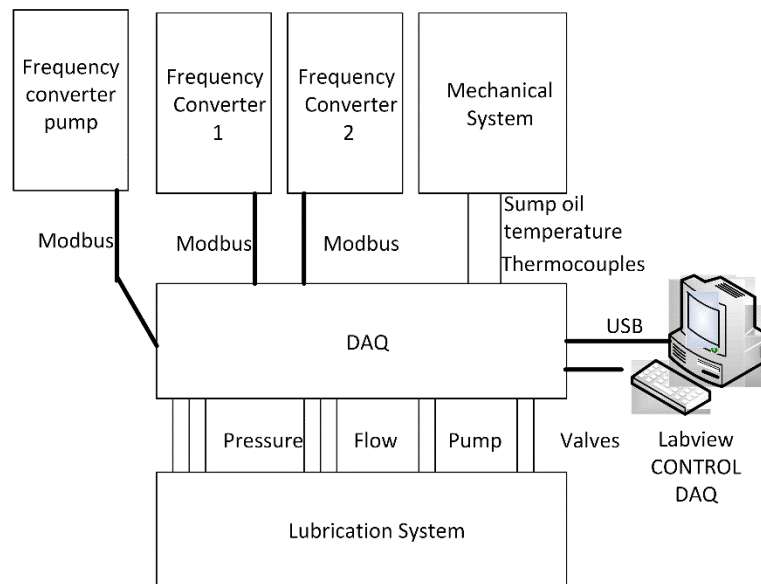


Figure 37 IDG rig Control and DAQ systems

The data available in the aircraft is limited. The information from the generator is available, including the output torque of the IDG and other electrical parameters. However, the input torque is not available and the mechanical losses cannot be monitored in the aircraft. However, the mechanical losses can be monitored in the test rig, allowing the detection of metal-metal contact during the experiments.

In the IDG there is only one temperature sensor at the sump, controlling the inlet oil temperature. However, there are not additional sensors controlling the outlet oil temperature from the lubrication system before it is mixed again with the oil from the hydraulic pump that regulates the speed of the IDG. The test rig also monitors the outlet oil temperature with a thermocouple, as shown in Figure 33, along with the ambient temperature.

In the IDG the pressure in the lubrication system is regulated but the flow is not monitored. The test rig monitors flow and pressure along the lubrication system before the hydrodynamic bearing. The potential of these lubrication parameters and temperature measurements for the detection of metal-metal contact is also analysed in this thesis. The sensors available in the test rig and in the IDG are summarized in Table 19.

It should be noted that the input torque is not available in the IDG and is not used by the PbM technique either. It is only used for validation in the test rig.

Table 19 IDG and test rig sensors

Sensor	Description	Units	Location
T_{RTD}	Inlet temperature to hydrodynamic bearing	°C	IDG and test rig
T_1	Outlet temperature after planetary bearing	°C	Test rig
Torque _{motor}	Torque generated by the motor	Nm	Test rig
Torque _{gen}	Torque produced by the generator (<i>all torque references in the thesis refer to generator torque</i>)	Nm	IDG and test rig
Flow	Inlet flow to hydrodynamic bearing	lpm	Test rig
Pressure	Inlet pressure to hydrodynamic bearing	Bar	Test rig and IDG
Speed	Motor speed (all speed references in the paper refer to motor speed)	rpm	Test rig and IDG

6.2.2 Experiments

In order to test metal-metal contact in the hydrodynamic bearing of the IDG a similar experimental procedure to the previous one of the plain journal bearing is used. The experiments are conducted for a given load at different speeds after stationary conditions are reached. However, the friction coefficient cannot be measured directly, instead, the additional sensors are monitored, e.g. outlet temperature T_1 or mechanical losses.

All the experiments are tested with a lubricant flow of 0.23 lpm. For each experiment the rig is run initially for 3 hours at 40 rpm and for 40 minutes at each speed to reach stationary conditions. The data presented in this thesis for comparison with the PbM refers to the last 5 minutes of each experiment. Each experiment includes 4 repetitions and 7 speeds are tested at low (20Nm) and medium load (40Nm) as shown in Table 20; thus, 56 experiments are conducted in total.

Table 20 IDG experimental procedure – range of operational conditions

Range of speed (rpm)	40, 80, 130, 180, 230, 280, 500
Range of generator torque (Nm)	20, 40

The lubricant is identical to the one used in the IDG, Mobil Jet Oil II [132]. The main characteristics of the lubricant can be shown in Table 21. The lubricant temperature is monitored and varies in the range of 20-30 °C; however, higher temperatures can be reached in the aircraft due to the hydraulic pump.

Table 21 Jet oil II properties [132]

Parameter	Value
Kinematic viscosity at 40 °C	27.6 cSt
Kinematic viscosity at 100 °C	5.1 cSt
Density at 15 °C	1.0035 kg/l
Flash point °C	270 °C
Fire point °C	285

6.3 Summary

This chapter provides an understanding of the experimental procedure required to test and validate the PbM and the metal-metal contact detection technique proposed in this thesis.

This failure mode does not occur under normal operation, as opposed to failure modes driven by a regular degradation mechanism e.g. fatigue or creep; where the component is degraded regularly and the RUL can be estimated. Therefore, accelerated aging testing is not the ideal approach; another common experimental procedure for IVHM, seeded faults, is difficult to apply because the damage is caused by the additional friction rather than the damage in the bearing. Provoking the failure has been the experimental approach selected to test metal-metal contact.

Provoking the failure, as opposed to seeded faults, has the advantage of replicating the actual failure mode; rather than the consequences of it. However, replacing the component may be unaffordable for expensive equipment if the failure leads to degradation or total failure and several experiments are required. This is the case of this case study, it is not affordable to replace several transmissions if total failure occurs. However, it is possible to provoke the same degradation mechanism, metal-metal contact, at lower speeds than those of the aircraft and reproduce metal-metal contact without provoking total failure. The IDG transmission and plain journal bearing are tested at low load conditions and lubricant temperatures below 40 °C; thus, provoking metal-metal contact at relatively low speeds and reducing the risk of stalling the hydrodynamic bearing and provoking a total failure.

7 Experimental and PbM results

As shown in the methodology, the development of a novel technique to detect metal-metal contact in a hydrodynamic bearing requires the following: a component selection and failure analysis (chapter 1), model development (chapter 4 and 5), test rig design and experiments (chapter 6) and finally, validation of the model by comparing the results with the experiments. The latter is introduced in this chapter.

Two cases studies are used. Experimental results of a plain journal bearing from the literature is used to compare the results of the PbM in section 7.1. The replica of the planetary transmission of the IDG has been tested and compared to the results of the PbM in section 7.2 to provide additional evidence of the effectiveness of the metal-metal detection technique proposed in this.

The first case study, the plain journal bearing, is used because the friction coefficient, which is the output of the model, can be measured directly during the experiments. The second case study, the replica of the planetary transmission, is more representative of the IDG failure phenomena but the friction coefficient cannot be measured during the experiments. Instead, the mechanical losses caused by metal-metal contact are monitored and compared to the results of the PbM.

Additional results of the PbM that can help to understand the failure phenomena are also discussed. Information not available in the aircraft is monitored and its potential to detect metal-metal contact is also discussed in this section.

7.1 Results of plain journal bearing

The comparison between the experimental results of a plain journal bearing and the PbM proposed in this thesis is presented in this section. The same conditions of the experiments are simulated by the PbM and the output of the model and experiments, the friction coefficient, is compared in order to validate the PbM. The comparison is done under different speeds and loads by representing the Stribeck curves obtained from both, PbM and experiments. The results provided in this section are based on the work published by the author of this thesis in the journal *Tribology Transactions* (Taylor and Francis) [111], see appendix B for further details.

The numerical results of the PbM are also used to analyse the failure phenomena, considering for instance the relevance of the solid deformation or a comparison between the order of magnitude of the hydrodynamic and contact pressure distributions.

A PbM of a plain journal bearing identical to the bearing tested by Lu et al. [111] has been simulated under the same operational conditions. More details about the PbM and its implementation are provided in subsection 4.2.2. The experiments are conducted for an inlet oil temperature of 40 °C under high load (1112 N), and low load (667 N) and the rotating speed range goes from 2 to 500 rpm, 300 data points are simulated for each load condition. A more detailed description of the experiments is provided in section 6.1.

7.1.1 Results

This section covers several aspects of the PbM, from the influence of considering solid deformations to the evolution of mixed lubrication in terms of forces and contact area. However, the most important results of this section are those that compare the friction coefficient estimated by the PbM with the experimental results.

Curves representing the friction coefficient under different conditions are normally referred as Stribeck curves. The Stribeck curves obtained by the PbM have been compared to the experimental results for the plain journal bearing as shown in Figure 38 and the model proposed by Lu et al. [82].

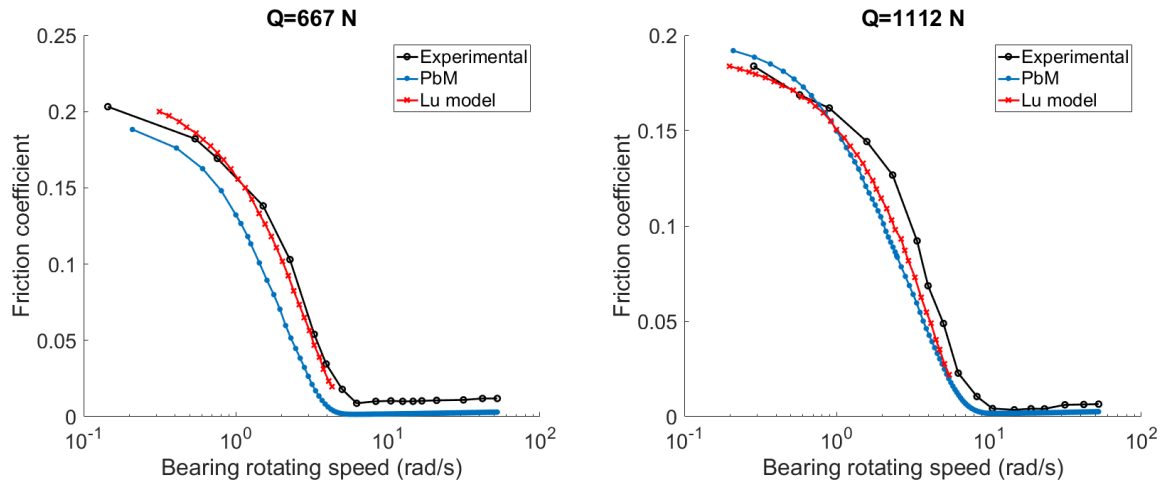


Figure 38 PbM, Lu et al. [82] model and experimental comparison of Stribeck curve for (left) 667 N and (right) 1112 N loads

A good agreement with the experimental results is obtained under low and high loaded conditions, as shown in Figure 38. At low load, the friction coefficient increases at speeds below 5 rad/s whereas the model predicts an increase in friction at 5.62 rad/s. Under higher a higher load the experiments show increased a friction coefficient at speeds below 10.53 rad/s and the model predicts them at speeds below 9.98 rad/s. The errors, as defined in Eq. [46], are 0.123 under 667N and 0.0525 under 1112N.

$$PbM_{error} = \frac{|\omega_{contact,PbM} - \omega_{contact,exp}|}{\omega_{contact,exp}} \quad [46]$$

Not only the speed at which metal-metal contact occurs corresponds to the PbM prediction, which is the most important aspect from a health condition monitoring point of view, but the prediction of the friction coefficient as metal-metal contact becomes more severe is also in accordance with the experimental results.

The aim of the PbM is to correctly estimate the friction coefficient in the hydrodynamic bearing under normal operation and when metal-metal contact occurs. The PbM accurately estimates the friction coefficient under both regimens for the plain journal bearing, as shown in Figure 38.

The good agreement between the PbM and the experiments is promising and can justify the use of the PbM in other hydrodynamic bearing, e.g. the hydrodynamic bearing of the IDG. However, the PbM should be implemented for each specific case study and additional experimental results representative of each case study are advisable. The additional experimental results for the planetary transmission are presented in the following section 7.2.

In addition to the comparison of the PbM and experimental friction coefficient, the numerical results of the PbM can be discussed to better understand the physics of failure of metal-metal contact in hydrodynamic bearings.

The CFD/FEA PbM considers that the hydrodynamic phenomena and the solid deformations are coupled for any condition. However, the relevance of the solid deformations is not the same under all operational conditions, as shown in Figure 39. The effect of the deformations in the film thickness δ is not significant under high speeds. At low speeds the influence of the solid deformations in the film thickness become significant and cannot be neglected. The impact of the deformations is more significant under high load conditions. Moreover, the estimated film thickness would be negative if deformations are not considered under high load conditions, which is physically impossible.

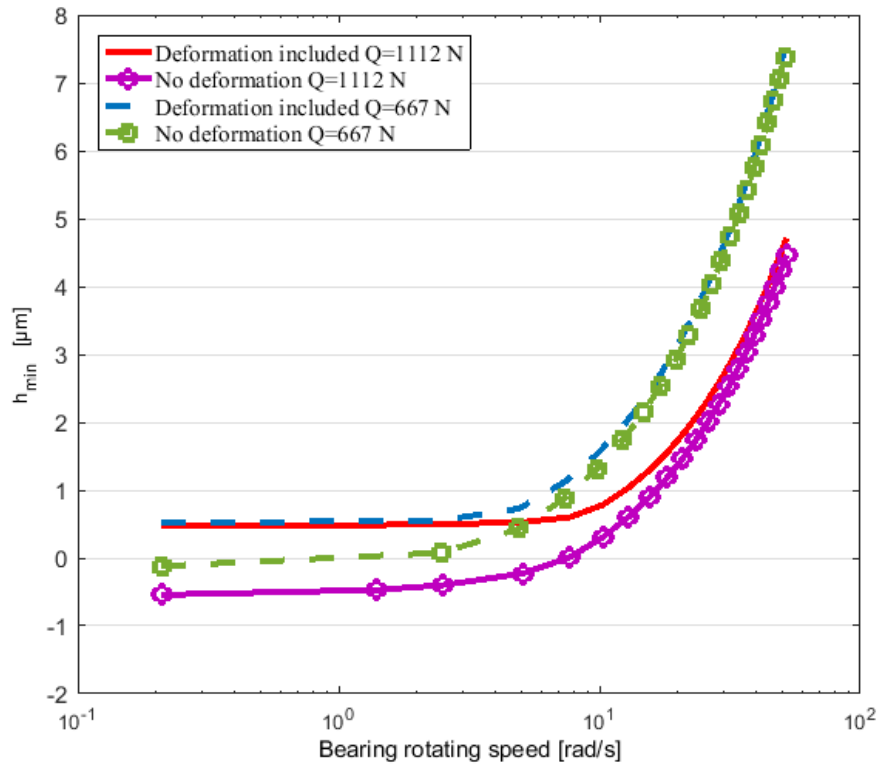


Figure 39 Comparison of minimum film thickness considering the deformations of the bearing or the hydrodynamic phenomena only, for high and low loaded conditions

The influence of the deformations is relevant, but so is the phenomena directly related to metal-metal contact. A significant portion of load is transmitted through the asperities if metal-metal contact occurs. The effect can be represented by comparing the maximum hydrodynamic and asperity contact pressure, as shown in Figure 40.

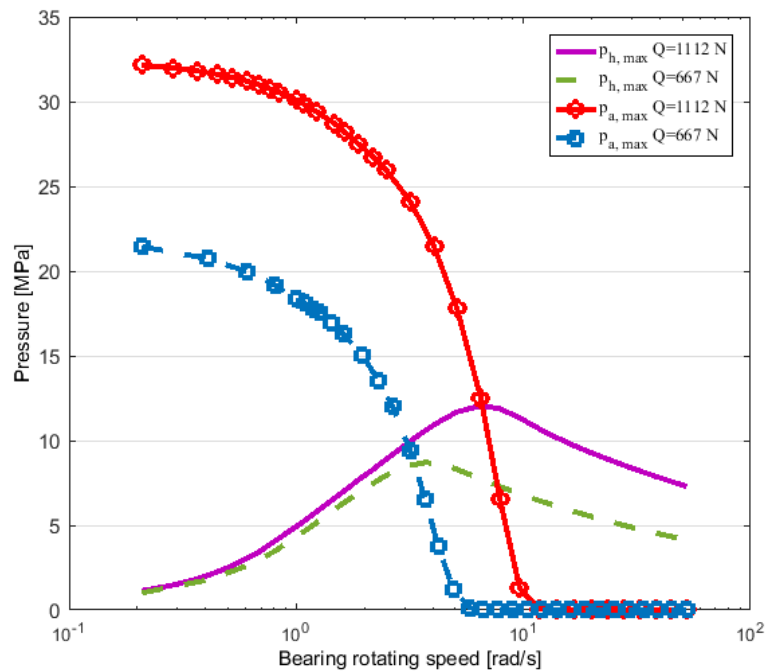


Figure 40 Comparison of maximum hydrodynamic pressure ($p_{h,max}$) and maximum asperity contact pressure ($p_{a,max}$) for high and low load in the plain journal bearing

The maximum contact pressure increases as the speed reduces when metal-metal contact occurs because a bigger proportion of the load is transmitted through the asperities, as shown in Figure 40. However, the maximum hydrodynamic pressure does not reduce immediately when metal-metal contact initiates, it only reduces if there is significant metal-metal contact. The reason is that, even if some load is transmitted through the asperities as the speed is reduced, the film thickness is reduced as well, leading to higher pressure distributions in addition to the contact pressure.

As shown in Figure 41, the contact area is inexistent under the hydrodynamic region and raises up to a maximum of 4-5% of the total lubricated area as metal-metal contact occurs.

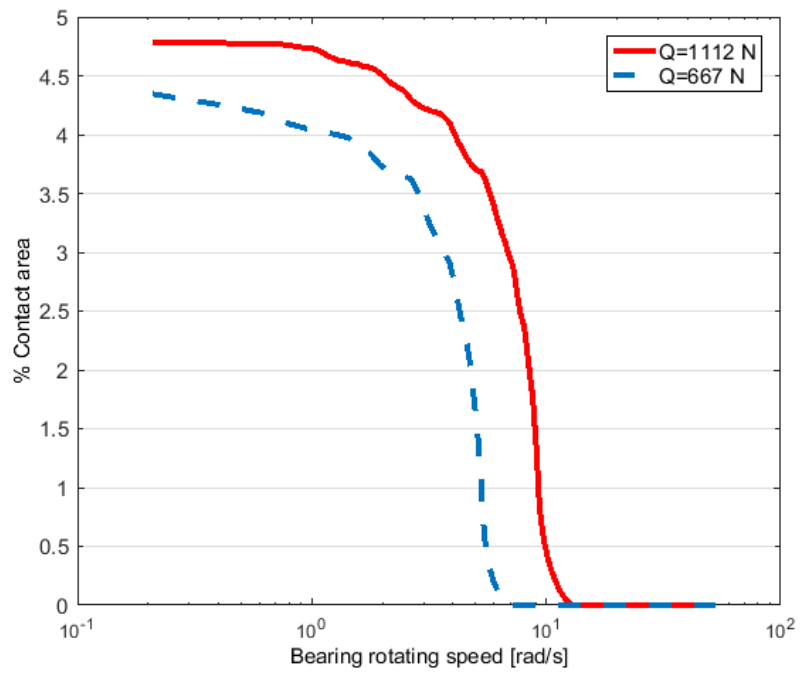


Figure 41 Comparison of the percentage of contact area for high and low load in the plain journal bearing

7.1.2 Conclusions of results of plain journal bearing

Along this section the proposed PbM has been compared to experimental results for the plain journal bearing. The main output of the PbM, the friction coefficient in the hydrodynamic bearing, is measured by the experimental set-up; thus, allowing a direct comparison of the model and experiments. In addition, the assumptions of the model and failure phenomena have been analysed based on the numerical results.

A good agreement between the experimental results and the PbM is obtained for high and low load conditions, as shown in Figure 38. The prediction of metal-metal contact and the evolution of the friction coefficient as mixed lubrication becomes more severe is in good agreement with the experiments as well.

The analysis of the PbM for the plain journal bearing has shown that, under EHL and partial metal-metal contact condition, solid deformations are required and an asperity contact model is needed to take into account both, contact and hydrodynamic pressure distributions. At higher speeds in fully lubricated regimes the asperity contact component is not required and the deformations do not significantly affect the hydrodynamic phenomena. The following conclusions have been drawn from the numerical results:

- Film thickness is significantly affected by the deformation of the solid for high eccentricities and cannot be neglected under mixed lubrication
- Metal-metal contact area is higher under heavily loaded conditions
- The maximum asperity pressures under mixed lubrication are significantly higher than the maximum hydrodynamic pressures
- The hydrodynamic pressure does not immediately reduce if metal-metal contact occurs. The reason is that the film thickness still can be reduced under the initial stages of partial metal-metal contact

7.2 Results of the hydrodynamic bearings of the IDG's planetary transmission

In addition to the results provided in the previous section 7.1, it is advisable to have additional evidence of the validity of the PbM for the hydrodynamic bearing of the IDG under more representative conditions.

The previous section compared the results of the PbM for a plain journal bearing because the friction coefficient could be measured. Allowing for a direct comparison between the PbM output, the friction coefficient, and the experimental results under all the range of operational conditions.

This section evaluates the PbM implemented for the hydrodynamic bearing of the planetary transmission and compares the results to experimental data of a replica of the transmission. However, the planetary transmission of the IDG does not allow for a direct measurement of the friction coefficient. Instead, the mechanical losses can be monitored due to the additional signals available in the test rig. It should be noted that the mechanical losses cannot be monitored in the aircraft directly because the input torque is not monitored. For more details regarding the implementation of the PbM see subsection 4.2.1 and for more details about the experimental set-up see section 6.2.

Under lubricated conditions the friction and mechanical losses are expected to decrease as the speed is reduced. However, when metal-metal contact occurs the friction in the hydrodynamic bearing increases; hence the mechanical losses can indicate metal-metal contact. The experiments are conducted at relatively low loads and ambient lubricant temperature compared to the nominal conditions in the aircraft in order to provoke metal-metal contact at low speeds and avoid total failure during the experiments.

This section has two aims; on the one hand, to demonstrate that metal-metal contact occurs in the planetary transmission of the IDG and that the PbM can identify metal-metal contact; and on the other, the experiments will serve to analyse additional signals that could alternatively be used for detecting metal-metal contact.

It should be noted that some alternative techniques that cannot be easily implemented in the aircraft for online monitoring have not been considered, e.g. debris analysis, vibration analysis or AEs. In addition to this limitation, all the components of the original planetary transmission are rotating, including both crown gears, complicating the installation of an accelerometers or microphones close to the source of damage.

The experimental and PbM results are obtained for the same operational conditions; that is, for torques of 20 and 40 Nm with the lubricant, Mobile Jet Oil II at ambient temperature and speeds from 40 to 500 rpm. Each experiment includes four repetitions.

7.2.1 Comparison between PbM and experiments

A variety of aspects are covered in this section. The PbM results include not only the friction coefficient, represented by the Stribeck curve, but also the development of the contact area as metal-metal contact increases.

The aim of representing the friction coefficient estimated by the PbM and the experimental results of the mechanical losses in the transmission, is to compare the speeds at which metal-metal contact occurs under low and medium load conditions.

As it occurred in the previous section, the most relevant result from the PbM is the friction coefficient estimation, shown in Figure 42. Metal-metal contact is estimated at speeds below 120 rpm for a torque of 20 Nm; whereas for a higher torque of 40 Nm metal-metal contact is predicted at speeds below 230 rpm.

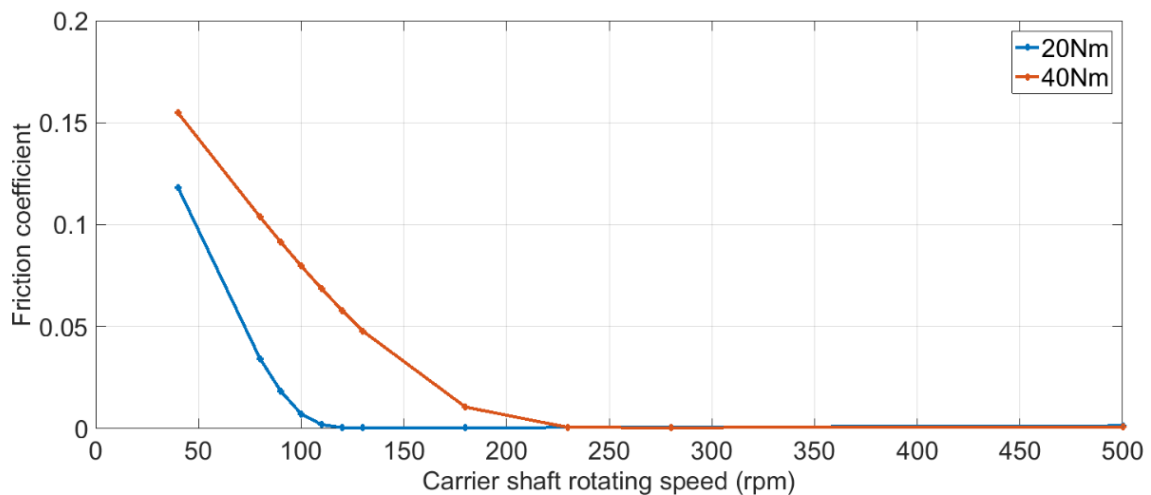


Figure 42 PbM predicted Stribeck curve for a generator torque of 20 and 40 Nm

The equivalent experiments for both, high load (40 Nm) and low load (20 Nm), under the same range of speeds have been conducted using 4 repetitions. The results are shown in Figure 43 for 20 Nm and Figure 44 for 40 Nm.

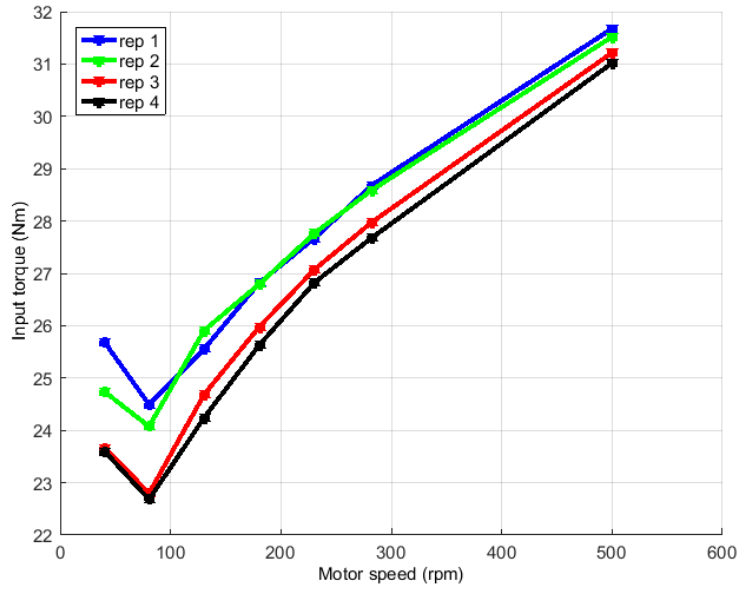


Figure 43 Planetary transmission experimental results of input torque for a constant generator torque of 20 Nm with lubricant at ambient temperature

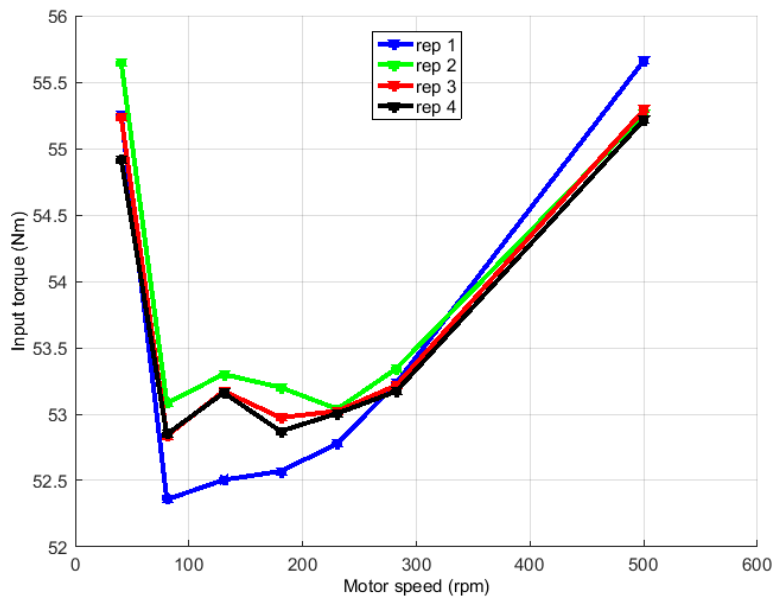


Figure 44 Planetary transmission experimental results of input torque for a constant generator torque of 40 Nm with lubricant at ambient temperature

It can be shown in Figure 43 and Figure 44 that, under a constant generator torque of 20 Nm, the input torque increases for speeds below 80 rpm; thus, indicating higher mechanical losses. A similar effect occurs for a higher generator torque of 40 Nm, where metal-metal contact initiates at higher speeds, 250 rpm, and the increased mechanical losses are more gradual as the speed reduces, in agreement with the PbM results, where the friction coefficient also increases more gradually for a generator torque of 40 Nm (see Figure 42).

The speed at which metal-metal contact stops decreasing in the PbM is compared to the speed at which the mechanical losses stop decreasing in order to compare the effectiveness of the PbM in detecting metal-metal contact. At low torque the experiments show metal-metal contact at speeds below 80 rpm whereas the PbM predicts metal-metal contact at 120. At high torque the experiments show that the mechanical losses stop decreasing at 250 rpm, whereas the PbM predicts metal-metal contact at 230. Thus, there is a speed deviation of 40 and 20 rpm respectively. The error of the PbM can also be calculated following Eq. [46], showing an error of 0.5 and 0.08 respectively for low and high load.

There is a good agreement between the speeds at which metal-metal contact is predicted by the PbM and the experimental results for the hydrodynamic bearing of the IDG, with a deviation of 20 rpm under low load conditions and no significant deviation under 40 Nm. Thus, providing further evidence of the potential of the proposed PbM technique to detect metal-metal contact in addition to the good agreement obtained between the PbM and the experiments for the plain journal bearing in the previous section 7.1. The model errors are summarized in Table 22.

Table 22: comparison of experimental and PbM on the detection of metal-metal contact

Model/Experiment	Speed deviation of metal-metal contact (rpm)	PbM_{error}
Plain bearing/low load	5.92	0.123
Plan bearing/high load	5.73	0.0525
IDG bearing/low load	40	0.5
IDG bearing/high load	20	0.08

7.2.2 Additional results

There are additional findings from the experimental and numerical results for the transmission of the IDG. The PbM can help to better understand the failure phenomena and mitigate or avoid the failure mode in future designs, which is one of the advantages of PbM as opposed to DDM approaches. The analysis of additional signals from the test rig serves to compare the PbM proposed in this thesis with alternative methods based on temperature measurements or lubrication parameters.

Most mixed lubrication models available in the literature calculate the total friction in the hydrodynamic bearing, but do not apply the complete model locally along the lubricated surface. The advantage of the PbM proposed in this thesis is that the areas where metal-metal contact is predicted are provided by the PbM. Thus, providing a better understanding of the failure phenomena.

Development of metal-metal contact

Mixed lubrication occurs in the highly loaded area of the bearing, but it is mitigated due to the solid deformations that allow sufficient film thickness to avoid metal-metal contact. This mitigation effect is less effective near the journal supports, where deformation is more limited, than in the middle of the bearing; thus, metal-metal contact initially starts in the corner of the journal in the highly loaded region as shown in Figure 45. These results may differ if there is significant misalignment.

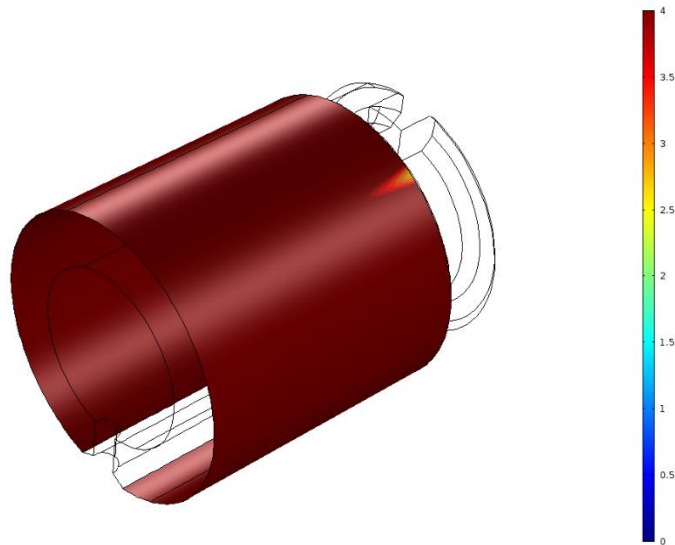


Figure 45 Lambda (λ) representing mixed lubrication at 250 rpm, 40 Nm, 20 °C (metal-metal contact if $\lambda < 4$)

As metal-metal contact becomes more severe the contact area extends to the middle of the bearing regardless of the journal deformations (see Figure 46), until most of the highly loaded region is in contact, as shown in Figure 47.

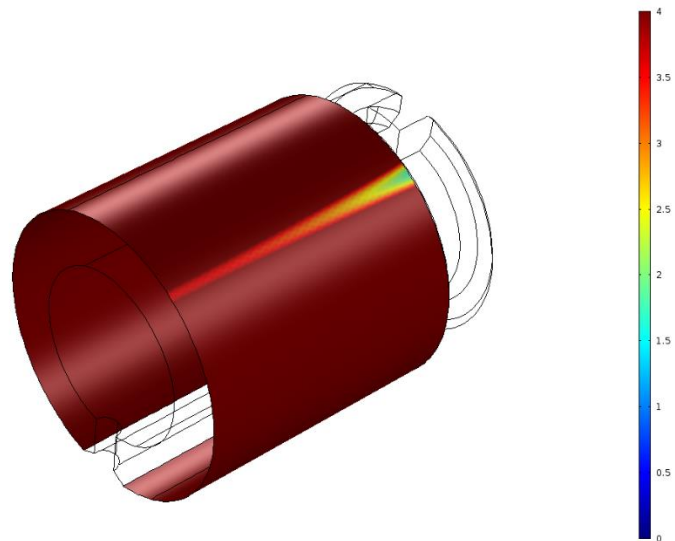


Figure 46 Lambda (λ) representing mixed lubrication at 132 rpm, 40 Nm, 20 °C (metal-metal contact if $\lambda < 4$)

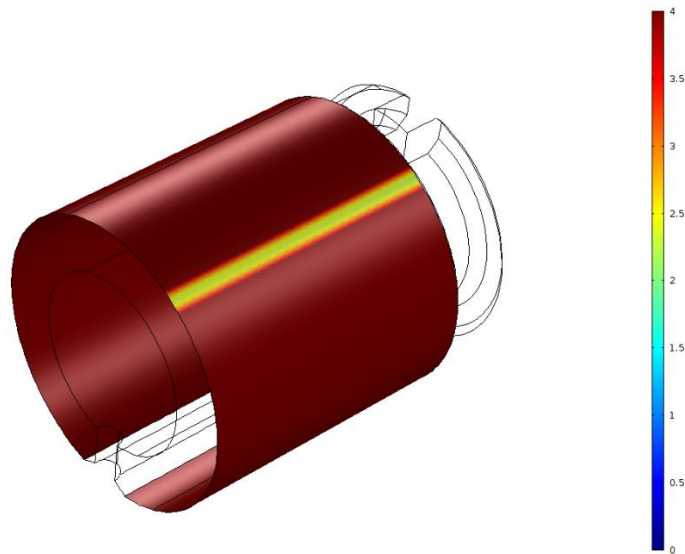


Figure 47 Lambda (λ) representing mixed lubrication at 10 rpm, 40 Nm, 20 °C (metal-metal contact if $\lambda < 4$)

Temperature and lubrication parameters

The experimental results include the analysis of the mechanical losses, necessary to detect metal-metal contact during the experiments, but also the analysis of additional data that could potentially be used for health condition monitoring. In particular, outlet and inlet lubricant temperatures and lubrication parameters: inlet lubricant pressure and flow.

As shown in section 6.2, the experimental set-up ensures stationary conditions for all the experiments. Before any test is started the rig is run for 2 and a half hours to ensure constant temperatures and each data point is tested for 40 minutes to ensure constant temperature for all the experiments. Thus, allowing the analysis of the inlet and outlet lubricant temperatures under stationary conditions and its potential to detect metal-metal contact.

The main function of the hydrodynamic bearing of the IDG is to support the rotating machinery with minimum friction rather than heat dissipation. Therefore, the main heat source is the friction inside the bearing. Under hydrodynamic conditions the friction is lower than under mixed lubrication; thus, an increased friction due to metal-metal contact can lead to a higher lubricant temperature gradient ΔT . However, the heat generated due to friction is minimal and additional factors like the ambient temperature, additional heat sources and heat dissipation in the transmission can overcome this effect.

In order to detect an increased heat due to metal-metal contact the outlet lubricant temperature T_1 can potentially be used for health monitoring. The transmission installed in the test rig can monitor T_1 and the inlet lubricant temperature T_{RTD} . However, the IDG does not monitor T_1 . First, the evolution of T_1 is presented in Figure 48 and Figure 49 for high and low load respectively. No significant changes in temperature can be found due to metal-metal contact.

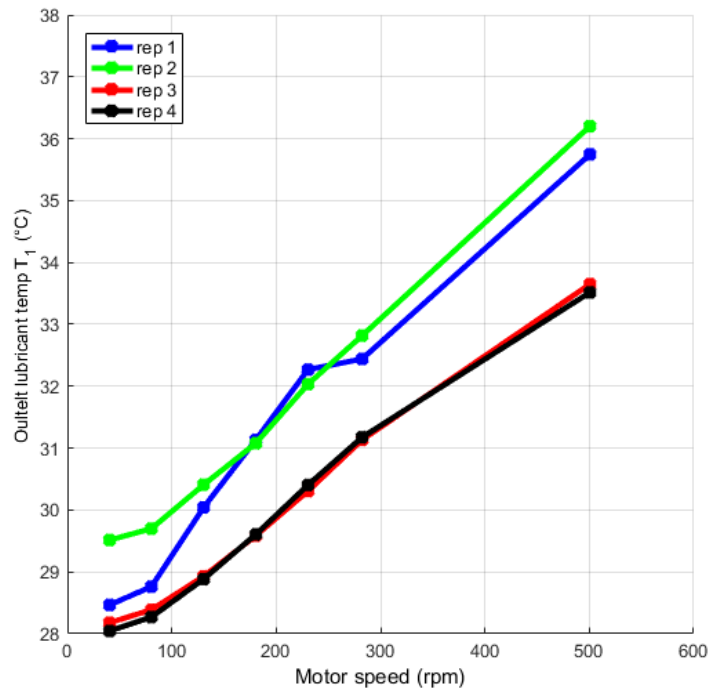


Figure 48 Experimental absolute outlet lubricant temperature T_1 for a generator torque of 20 Nm

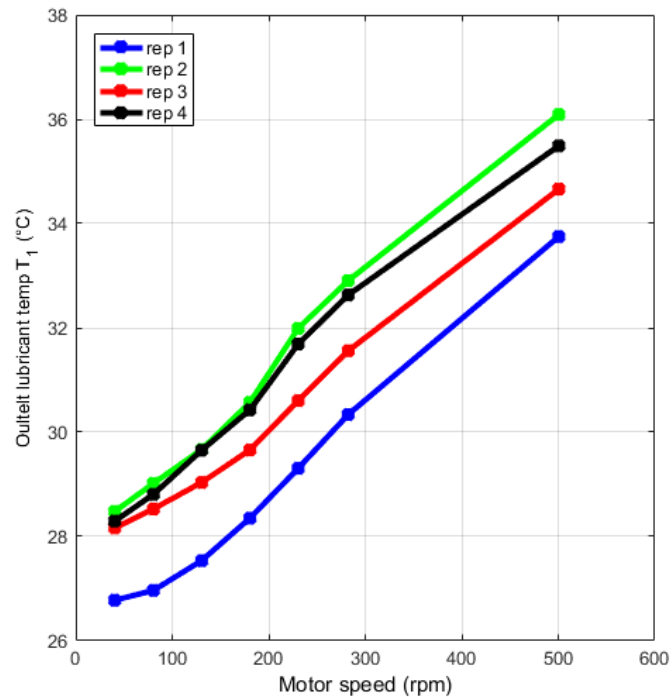


Figure 49 Experimental absolute outlet lubricant temperature T_1 for a generator torque of 40 Nm

An increased friction can lead to an increased heat in the bearing with the subsequent temperature gradient ΔT . However, in order to monitor ΔT the inlet lubricant temperature T_{RTD} and the outlet lubricant temperature T_{outlet} must be monitored to obtain $\Delta T = T_{outlet} - T_{RTD}$. It should be noted that the heat generated due to friction is minimal and the temperature gradient ΔT can be overcome by changes in the ambient temperature and heat dissipation. The experimental results of ΔT are shown in Figure 50 and Figure 51. An increased gradient cannot be detected for all the experiments but a change in the ΔT trend can be found. However, in order to use ΔT as a health indicator stationary conditions would be required.

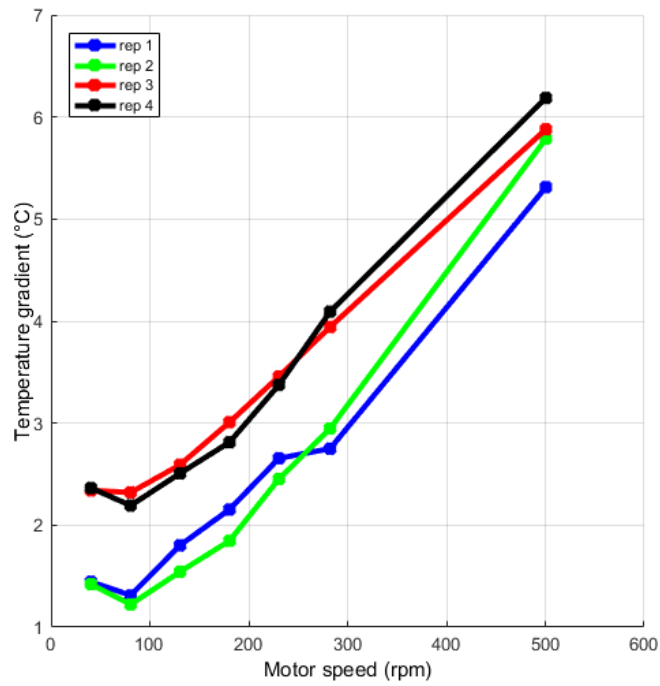


Figure 50 Experimental temperature gradient $\Delta T = T_1 - T_{RTD}$ for a generator torque of 20 Nm

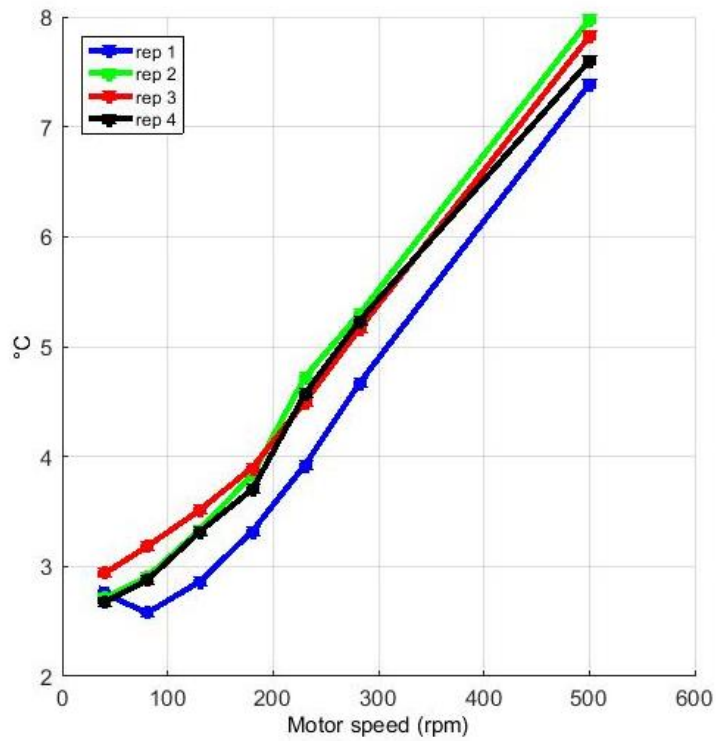


Figure 51 Experimental temperature gradient $\Delta T = T_1 - T_{RTD}$ for a generator torque of 40 Nm

In addition to the temperature, the main lubrication parameters inlet pressure and flow are analysed. Under hydrodynamic lubrication the lubricant resistance in the hydrodynamic bearing is reduced as the speed increases. This phenomenon can be observed in the experiments, as shown in Figure 52 and Figure 53. However, no significant changes are observed when metal-metal contact.

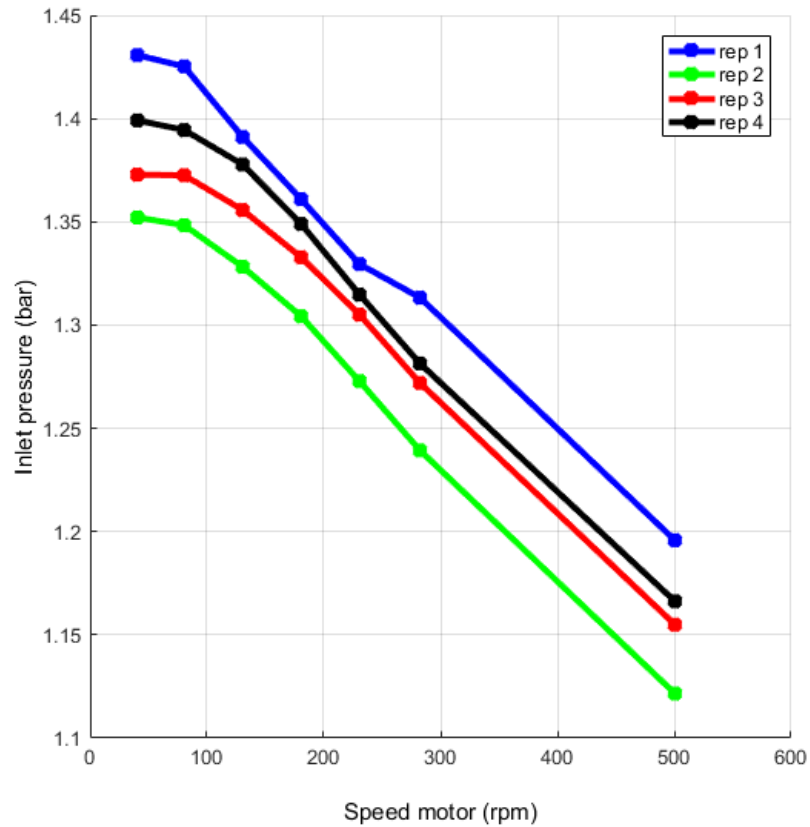


Figure 52 Experimental inlet pressure for a generator torque of 20 Nm

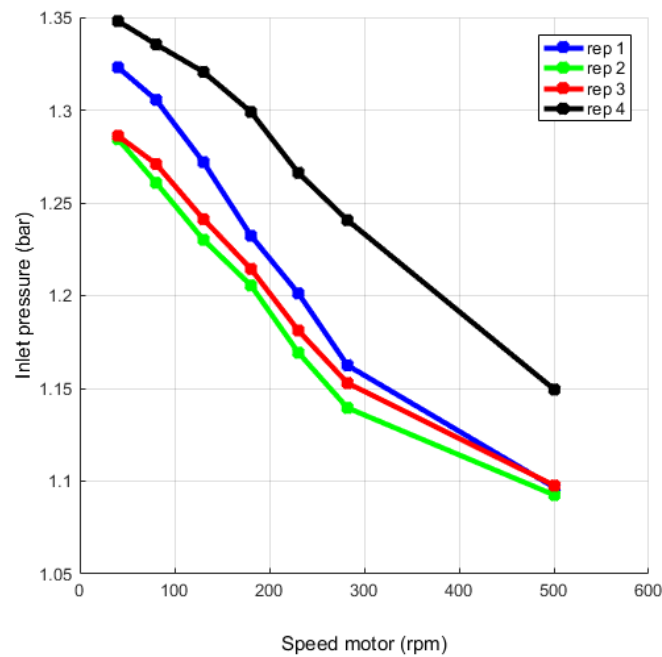


Figure 53 Experimental inlet pressure for a generator torque of 40 Nm

The results regarding the lubrication parameters should not be extrapolated to other lubrication systems. The lubrication system of the test rig is controlled through a gear pump at constant speed for which the flow does not significantly changes. Therefore, significant flow changes depending on the operational conditions are not expected, which is in accordance with the experimental results as shown in Figure 54 and Figure 55 for low and high load respectively. Summarizing, inlet pressure and flow do not show significant changes due to metal-metal contact.

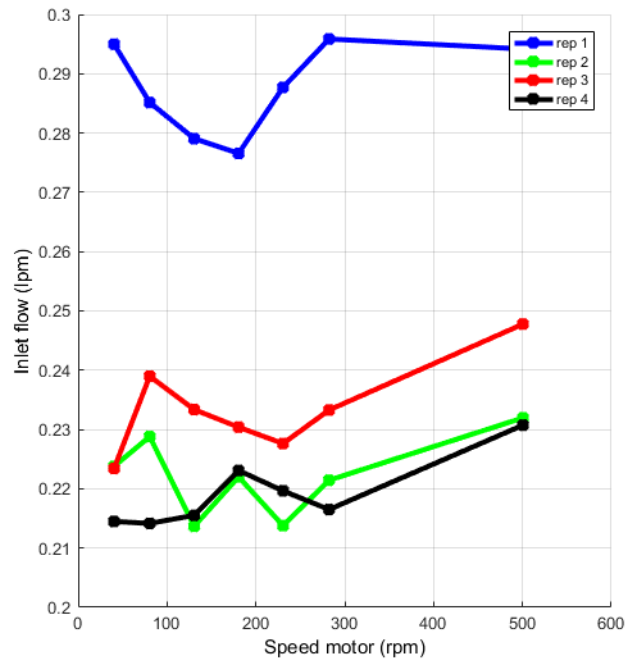


Figure 54 Experimental inlet flow for a generator torque of 20 Nm

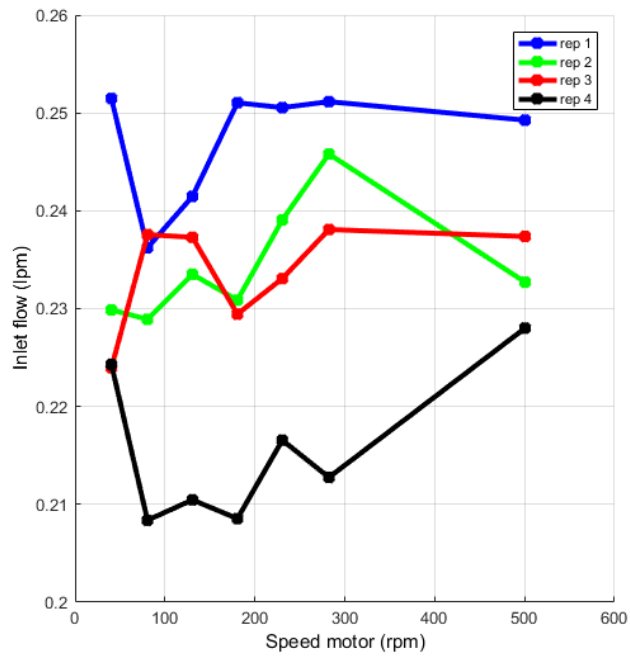


Figure 55 Experimental inlet flow for a generator torque of 40 Nm

7.2.3 Conclusions of results of hydrodynamic bearing of the IDG's planetary transmission

The previous section 7.1 provided the comparison of the PbM with experimental data by using a plain journal bearing where the friction coefficient was measured directly and a good agreement between the PbM and the experimental results was obtained. However, further evidence of the PbM effectiveness in the planetary transmission of the IDG is advisable.

The results presented in this section provide additional evidence of the potential of the PbM technique to detect metal-metal contact phenomena. However, in the planetary transmission the friction coefficient cannot be measured directly; instead, the mechanical losses of the system are monitored to detect when metal-metal occurs under low and high loaded conditions.

It has been shown that, in addition to the good agreement between the PbM and the experimental results for the plain journal bearing, there is an agreement between the speeds at which metal-metal contact is predicted by the PbM and measured in the experiments.

As opposed to most mixed lubrication models available in the literature. The model proposed in this thesis is evaluated locally along the lubricated surface; thus, providing not only results of the whole bearing, but also about the local effects. The results of the PbM can be used to better understand the failure mode and mitigate or avoid it in future designs. For instance, the area where metal-metal contact initiates and how it develops can be obtained from the numerical results. It has been shown that, if there is not any misalignment, metal-metal contact initiates in the sides of the bearing, where deformations are more limited, and extends to the middle of the bearing as metal-metal contact becomes more severe.

Temperature measurements can potentially be used to detect metal-metal contact by monitoring the temperature gradient in the bearing. However, steady conditions are required and external heat sources and ambient temperature can affect the measurements. In addition, an extra temperature sensor that monitors the outlet lubricant temperature should be installed and stationary conditions may not be reached in the aircraft.

The lubrication parameters have been analysed as well. Inlet pressure varies as a function of the rotating speed. However, it does not provide a clear indication of metal-metal contact. The inlet lubricant flow is independent of the operational conditions. These results depend on the configuration of lubrication system; however, neither lubricant flow nor pressure have proven good indicators of metal-metal contact in the replica of the planetary transmission.

7.3 Summary

Along this chapter all the experimental results with the corresponding PbM predictions of metal-metal contact have been presented in order to validate the proposed PbM technique using both, the plain journal bearing and the planetary transmission of the IDG. In addition, the numerical results of the PbM have been used to better understand the failure phenomena and the potential of alternative sensors to detect metal-metal contact has been studied.

This chapter addresses the third contribution, presented in chapter 3:

- The validation of the PbM with experimental results (chapter 7) provides the necessary data for a critical analysis of different potential health indicators of metal-metal contact.

The two main novelties of this thesis have been covered in chapter 4 and 5. However, the results provided in this chapter are needed to show the good agreement between the PbM and the experimental results for a plain journal bearing and the planetary transmission of the IDG.

For the plain journal bearing the friction coefficient is measured directly in the experiments. Whereas for the planetary transmission the mechanical losses are monitored to detect metal-metal contact instead because the friction coefficient in the bearing cannot be measured.

A good agreement between the experimental results and the PbM for the plain journal bearing is obtained for high and low load conditions. The prediction of metal-metal contact and the evolution of the friction coefficient as mixed lubrication becomes more severe is in good agreement with the experiments as well. In addition, there is an agreement between the speeds at which metal-metal contact is measured in the experiments and predicted by the PbM for the replica of the planetary transmission.

Regarding the understanding of the failure phenomena the following conclusions can be obtained from the numerical results of the plain journal bearing:

- Film thickness is significantly affected by the deformation of the solid for high eccentricities and cannot be neglected under mixed lubrication
- The maximum asperity pressures under mixed lubrication are significantly higher than the maximum hydrodynamic pressures
- The hydrodynamic pressure does not immediately reduce if metal-metal contact occurs. The reason is that the film thickness still can be reduced under the first stages of partial metal-metal contact
- The hydrodynamic pressure does not immediately reduce if metal-metal contact occurs. The reason is that the film thickness still can be reduced under the initial stages of metal-metal contact.

It has been shown that in the planetary transmission of the IDG, if there is not any misalignment, metal-metal contact initiates in the sides of the bearing, where deformations are more limited, and extends to the middle of the bearing as metal-metal contact becomes more severe.

All the inputs of the PbM are available in the IDG; thus, no additional sensors are needed. Alternative methods based on temperature measurements or lubrication parameters do not show clear indications of metal-metal contact. Vibration, AEs or debris analysis are not covered by this thesis but would require additional sensors as well, complicating the certification of such techniques.

As a final remark, it should be noted that, from a health condition monitoring point of view, metal-metal contact main challenges are the lack of reliable failure indicators and the limitations in terms of sensors available. Under metal-metal contact conditions, the heat generated is minimal and cannot easily be detected, the lubrication system is barely affected, the speed is not affected unless total failure occurs and the mechanical losses can only be detected if the input torque is monitored. The technique presented in this thesis is particularly relevant due to these challenges. No additional sensor are needed and alternative techniques based on temperature or lubrication parameters seem challenging due to the lack of robust indicators. Other techniques studied in the literature like vibration analysis, AEs or debris analysis would require additional sensors in the IDG and are not part of the scope of this thesis.

8 Discussion

The contributions of each chapter are not independent from each other and a comprehensive discussion of the thesis is needed. The main novelties of the thesis, based on the gaps in the knowledge identified in the literature review (chapter 2) were presented in chapter 3 as follows:

First novelty

The development of a PbM able to represent mixed lubrication through an asperity contact approach locally along the lubricated surface of the bearing using a CFD/FEA novel approach.

Second novelty

The development of a novel technique to detect metal-metal contact in the hydrodynamic bearing of a planetary transmission of an aircraft's IDG using a PbM approach without installing additional sensors in the aircraft.

The first novelty is discussed in section 8.1 whereas the second one is discussed in section 8.2

8.1 Mixed lubrication Physics-based Model

Based on the literature review of mixed lubrication models in the field of tribology, there are models available, which either modify the Reynolds equation, or include an asperity contact component that divides the problem in dry and fully lubricated contact. The last approach is well accepted, but has only been applied to the whole bearing, which lead to the first gap in the knowledge, stated as follows:

- *Mixed lubrication models based on asperity contact dividing the phenomena into dry and fully lubricated contact have not been applied locally along the lubricated surface in hydrodynamic bearings.*

There are potential advantages for integrating the asperity contact in a CFD/FEA model that computes metal-metal contact locally. The real geometry of the bearing can be taken into account instead of assuming a standard hydrodynamic bearing. The case study of the transmission of the IDG is an example of these advantages: the slot that distributes the lubricant, the deformation of the hollow shaft and the more realistic boundary conditions could all be taken into account by the PbM. In addition, by analysing metal-metal contact locally, the failure phenomena is better understood, being able to predict where metal-metal contact starts in the early stages of the failure and how the hydrodynamic and contact pressure distributions evolve as metal-metal contact develops; thus, providing useful inputs for the design as well.

This thesis covers this gap in the knowledge by presenting a CFD/FEA model that integrates the asperity contact component locally along the lubricated surface with the corresponding comparison with experimental data for a plain journal bearing. A good agreement between the predicted friction of the PbM and the experimental results presented by Lu et al. [82] has been obtained for high and low loads for a plain journal bearing. In addition, the following findings were obtained:

- Film thickness is significantly affected by the deformation of the solid for high eccentricities and cannot be neglected under mixed lubrication
- The maximum asperity pressures under mixed lubrication are significantly higher than the maximum hydrodynamic pressures
- The hydrodynamic pressure does not immediately reduce if metal-metal contact occurs. The reason is that the film thickness still can be reduced under the initial stages of partial metal-metal contact

The presented PbM and its contribution to the field of tribology has been published in Tribology transactions (Taylor and Francis) along with the comparison with experimental results of a plain journal bearing [111].

The PbM has been implemented for a plain journal bearing and the hydrodynamic bearing of the IDG. However, it can be applied to other hydrodynamic bearings by modifying the boundary conditions, materials and lubricant properties.

Regarding the limitations of the PbM, the model considers the lubricant temperature constant along the lubricated surface. This assumption is acceptable if the main function of the bearing is not to dissipate heat. However, it should be noted that changes in the viscosity due to variations of the lubricant temperature along the bearing are not considered. In addition, multi-physics software capable of handling CFD and FEA and significant computational power and memory may be required to execute the model, as opposed to models of the whole bearing based on analytical equations that can be executed with fewer resources.

8.2 Novel technique to predict metal-metal contact in the hydrodynamic bearing of the IDG

One of the main contributions of the thesis is the novel physics-based approach to detect metal-metal contact in the hydrodynamic bearing of a IDG's planetary transmission without using additional sensors. As opposed to DDM techniques, in which the health indicators do not directly represent the failure phenomena, the proposed PbM approach provides a health indicator that is a direct measure of the severity of metal-metal contact, that is, the percentage of load transmitted through metal-metal contact. Therefore, the health assessment can be as simple as a threshold as the main contribution of the proposed technique relies on the novel PbM.

The research on health condition monitoring of hydrodynamic bearings, and metal-metal contact in particular, is limited. Most techniques rely on DDM using vibration analysis or acoustic emissions. However, they have proven successful when the sensor could be installed directly in the hydrodynamic bearing. Thus requiring a short path between the source of damage and receiver. This is not the case in the hydrodynamic bearing of a planetary transmission. All the components of the bearing are rotating and the closest location for a sensor would have a path that includes gears and additional.

An additional limitation, particularly for the aerospace sector, is the restrictive regulation regarding design modifications of legacy aircraft. The sensors and information available about the planetary transmission are limited and do not include debris analysis, vibration analysis or acoustic emissions. Whereas the proposed PbM technique does not require any additional sensor.

A mixed lubrication PbM approach has never been used for health condition monitoring of hydrodynamic bearings; thus, covering the second main gap in the knowledge targeted in this thesis. However, there are models in the literature capable of representing the hydrodynamic and mixed lubrication phenomena in the field of tribology. Thus, there is potential for a technique based on these tribology models to detect metal-metal contact in hydrodynamic bearings.

The mixed lubrication models based on an asperity contact component in the literature assume a simple plain bearing and do not analyse the lubricated surface locally. The hydrodynamic bearing of the planetary transmission has many features that affect the mixed and hydrodynamic lubrication phenomena. The PbM proposed in this thesis addresses these limitations. See previous section 8.1 for a more detailed discussion on this topic.

The proposed PbM health monitoring technique to detect metal-metal contact in the hydrodynamic bearing of the IDG only requires 3 variables: rotating speed, generator torque and lubricant temperature. A significant advantage of this method is that all these signals are available in the aircraft and no additional sensors have to be installed. Moreover, all the CFD/FEA simulations are computed on the ground, leaving relatively simple tasks to be completed in the aircraft and avoiding significant changes in the design, which is critical in legacy aircraft.

Most benefits of having an IVHM system are maintenance cost and time reduction, along with the potential for higher availability. The health status predicted by the IVHM tool can be used by the CAMO to launch a maintenance work order before the plane is on the ground. In addition, fault identification and localization times along with secondary damage can be reduced.

The proposed IVHM tool can also prove beneficial for the operation of the aircraft. The IVHM tool could provide recommendations to the pilot if an alarm is triggered to avoid the failure and the subsequent maintenance operations. In addition, it includes the necessary logic to ensure the safety of the aircraft if the IDG is disconnected.

In order to compare the results of this technique to detect metal-metal contact two experimental data sets have been used. On the one hand, experimental data of a plain journal bearing [82] has shown a good agreement between the friction coefficient predicted by the PbM and measured during the experiments. On the other, a replica of the IDG's planetary transmission has been tested and the prediction of metal-metal contact by the PbM is in agreement with the experiments as well.

The experiments of the planetary transmission were conducted at low temperature and torque to provoke metal-metal contact at low speeds without risk of stalling. It should be noted that in the aircraft there may be higher loads and lubricant temperatures than in the experiments. The load is produced by the electrical demand of the aircraft systems and can reach up to 296 Nm and the lubricant temperature can increase due to the operation of the hydraulic unit that regulates the speed; leading to metal-metal contact in the range of operation of the IDG as shown in section 5.2 using numerical results.

The input torque, used during the experiments to calculate the mechanical losses and validate the PbM, is not required by the proposed health condition monitoring technique. In fact, in the IDG the output torque is known, which is the input of the PbM along with the speed and lubricant temperature, also available in the aircraft.

The benefits of the proposed technique to detect metal-metal contact have been discussed. However, there are some limitations that should be considered. The IVHM tool consists in a proof of concept and there are several challenges to be addressed before it can be implemented. The aircraft operational conditions have been analysed in chapter 5, but the experiments have been conducted under low load and low lubricant temperature to avoid total damage and the actual operational conditions during flight have not been tested. The definition of the thresholds is not within the scope of this thesis and further research would be needed to define failure criteria.

9 Conclusions and contributions

Throughout this thesis, research has focused on modelling mixed and hydrodynamic lubrication, in the field of tribology, and the application of the mixed lubrication model for the detection of metal-metal contact in hydrodynamic bearings for health condition monitoring, in the bearing of the planetary transmission of an aircraft's IDG in particular. The following gaps in the knowledge have been identified:

- 1. Mixed lubrication models based on asperity contact dividing the phenomena in dry and fully lubricated contact have not been applied locally along the lubricated surface in hydrodynamic bearings.*
- 2. Physics-based Models have not been used for the detection of metal-metal contact in hydrodynamic bearings.*

In order to address these gaps in the knowledge; first, a PbM that studies metal-metal contact locally along the lubricated surface has been devised with good agreement between the estimated friction coefficient and the experiments for a plain journal bearing. Secondly, the model has been used for the development of a novel PbM technique to detect metal-metal contact in the hydrodynamic bearings of the IDG without requiring additional sensors with good agreement between the speeds at which metal-metal contact is predicted by the PbM and measured in the experiments as well.

The contributions to knowledge of this thesis can be summarized in the following main novelties:

First novelty

A CFD/FEA model that integrates the asperity contact component locally along the lubricated surface has been presented in this thesis. The actual bearing geometry can be considered instead of assuming plain shaft, allowing more complex hydrodynamic bearings models. In addition, the study of metal-metal contact locally can provide a better understanding of how metal-metal contact develops.

A good agreement has been obtained between the friction coefficient predicted by the PbM and the friction measured during the experiments for a plain journal bearing, as shown in Figure 38. The PbM accurately estimates the speed at which metal-metal contact initiates under low and high load. The estimated rate at which the friction increases is also in accordance with the experiments.

Second novelty

The mixed lubrication model, which is the first novelty of the thesis, is applied to the detection of metal-metal contact. The PbM has been implemented into a novel PbM technique to detect metal-metal contact in the hydrodynamic bearings of a planetary transmission of an aircraft's IDG without requiring additional sensors. A rig has been devised to test the transmission under metal-metal contact conditions. A good agreement is obtained between the speeds at which metal-metal contact is predicted by the PbM and measured in the experiments for the plain journal bearing (Figure 38) and also for the replica of the transmission (Figure 42-44).

The proposed technique computes the PbM on the ground, the results are accessible by the IVHM tool installed in the aircraft; which provides a health assessment and recommendation for the pilot to avoid additional damage, ensuring a safe disconnection of the IDG if a critical failure occurs. In addition, the health assessment can be used for maintenance purposes as well.

10 Future work

Throughout this thesis a comprehensive description of a novel PbM to detect metal-metal contact and its application for health condition monitoring have been presented.

Regarding the field of tribology, the PbM takes into account solid deformations, cavitation and metal-metal contact interaction. However, changes in lubricant temperature along the bearing and the effect in the lubricant viscosity are not taken into account. For hydrodynamic bearings that dissipate significant amounts of heat this effect may have to be considered.

The proposed PbM for health condition monitoring in hydrodynamic bearings has been applied to the planetary transmission of the IDG. However, the PbM and a similar IVHM tool can be used in other systems.

The failure mode of the planetary transmission of the IDG cannot be detected before total failure occurs in the current system configuration. The proposed health condition monitoring technique can potentially detect metal-metal contact before total failure occurs. The technique presented in this thesis is a proof of concept in a rig with ambient lubricant temperature and low loading conditions. Further testing under more severe conditions and comparison with historic data would increase the technology readiness level of this technique.

References

- [1] A. Cubillo, S. Perinpanayagam, and M. Esperon-Miguez, "A review of physics-based models in prognostics: Application to gears and bearings of rotating machinery," *Adv. Mech. Eng.*, vol. 8, no. 8, doi: doi:10.1177/1687814016664660, Aug. 2016.
- [2] R. Kothamasu, S. H. Huang, and W. H. Verduin, "System health monitoring and prognostics - A review of current paradigms and practices," *Int. J. Adv. Manuf. Technol.*, vol. 28, no. 9, pp. 1012–1024, 2006.
- [3] I. K. Jennions, *Integrated vehicle health management :perspectives on an emerging field*. Warrendale, Pa.: SAE International, 2011, ISBN: 978-0768064322.
- [4] J. E. Land, "HUMS-the benefits-past, present and future," in *Aerospace Conference, 2001, IEEE Proceedings.*, 2001, vol. 6, pp. 3083–3094 vol.6.
- [5] M. Esperon-Miguez, P. John, and I. K. Jennions, "Uncertainty of performance requirements for IVHM tools according to business targets" *Eur. Conf. Progn. Heal. Manag. Soc.*, vol. 3, pp. 1-11, 2012.
- [6] J. H. MacConnell, "ISHM & Design: A review of the benefits of the ideal ISHM system," in *2007 IEEE Aerospace Conference*, 2007, pp. 1–18.
- [7] E. Baroth, W. T. Powers, J. Fox, B. Prosser, J. Pallix, K. Schweikard, and J. Zakrajsek, "IVHM (Integrated Vehicle Health Management) techniques for future space vehicles," in *37th Joint Propulsion Conference and Exhibit 2001*, 2001, pp. 1–10.

- [8] O. Benedettini, T. S. Baines, H. W. Lightfoot, and R. M. Greenough, "State-of-the-art in integrated vehicle health management," *Proc. Inst. Mech. Eng. Part G J. Aerosp. Eng.*, vol. 223, no. 2, pp. 157–170, 2009.
- [9] E. Bechhoefer and A. P. F. Bernhard, "Setting HUMS condition indicator thresholds by modeling aircraft and torque band variance," in *Aerospace Conference, 2004. Proceedings. 2004 IEEE*, 2004, vol. 6, p. 3590–3595 Vol.6.
- [10] P. J. Dempsey, "Threshold Assessment of Gear Diagnostic Tools on Flight and Test Rig Data," *NASA/TM-2003-212220*, 2003.
- [11] O. Niculita, P. Irving, and I. K. Jennions, "Use of COTS Functional Analysis Software as an IVHM Design Tool for Detection and Isolation of UAV Fuel System Faults," in *Annual Conference of the Prognostics and Health Management Society 2012*, 2012, vol. 3, pp. 22–27.
- [12] M. Esperon-Miguez, P. John, and I. K. Jennions, "A review of Integrated Vehicle Health Management tools for legacy platforms: Challenges and opportunities," *Prog. Aerosp. Sci.*, vol. 56, pp. 19–34, 2013.
- [13] J. Z. Sikorska, M. Hodkiewicz, and L. Ma, "Prognostic modelling options for remaining useful life estimation by industry," *Mech. Syst. Signal Process.*, vol. 25, no. 5, pp. 1803–1836, 2011.
- [14] J. Lee, F. Wu, W. Zhao, M. Ghaffari, L. Liao, and D. Siegel, "Prognostics and health management design for rotary machinery systems—Reviews, methodology and applications," *Mech. Syst. Signal Process.*, vol. 42, no. 1–2, pp. 314–334, 2014.
- [15] S. J. Engel, B. J. Gilmartin, K. Bongort, and A. Hess, "Prognostics, the real issues involved with predicting life remaining," in *IEEE Aerospace Conference Proceedings*, 2000, vol. 6, pp. 457–470.
- [16] O. F. Eker, F. Camci, and I. K. Jennions, "Major Challenges in Prognostics: Study on Benchmarking Prognostics Datasets," *Proc. of PHM*, vol. 3, pp. 1–8, 2012.

- [17] A. Heng, S. Zhang, A. C. C. Tan, and J. Mathew, "Rotating machinery prognostics: State of the art, challenges and opportunities," *Mech. Syst. Signal Process.*, vol. 23, no. 3, pp. 724–739, 2009.
- [18] J. Luo, M. Namburu, K. Pattipati, L. Qiao, M. Kawamoto, and S. Chigusa, "Model-based prognostic techniques [maintenance applications]," in *AUTOTESTCON 2003. IEEE Systems Readiness Technology Conference. Proceedings*, 2003, pp. 330–340.
- [19] C. Li and M. Liang, "Time–frequency signal analysis for gearbox fault diagnosis using a generalized synchrosqueezing transform," *Mech. Syst. Signal Process.*, vol. 26, pp. 205–217, 2012.
- [20] X. Mu-jun and X. Shi-Yong, "Fault diagnosis of air compressor based on RBF neural network," in *Mechatronic Science, Electric Engineering and Computer (MEC), 2011 International Conference on*, 2011, pp. 887–890.
- [21] S. Ferreiro, A. Arnaiz, B. Sierra, and I. Irigoien, "Application of Bayesian networks in prognostics for a new Integrated Vehicle Health Management concept," *Expert Syst. Appl.*, vol. 39, no. 7, pp. 6402–6418, Jan. 2012.
- [22] E. Zio and F. Di Maio, "Fatigue crack growth estimation by relevance vector machine," *Expert Syst. Appl.*, vol. 39, no. 12, pp. 10681–10692, 2012.
- [23] N. G. Pantelelis, A. E. Kanarachos, and N. Gotzias, "Neural networks and simple models for the fault diagnosis of naval turbochargers," *Math. Comput. Simul.*, vol. 51, no. 3–4, pp. 387–397, 2000.
- [24] A. Saxena and A. Saad, "Evolving an artificial neural network classifier for condition monitoring of rotating mechanical systems," *Appl. Soft Comput.*, vol. 7, no. 1, pp. 441–454, 2007.
- [25] H. Su and K.-T. Chong, "Induction Machine Condition Monitoring Using Neural Network Modeling," *Ind. Electron. IEEE Trans.*, vol. 54, no. 1, pp. 241–249, 2007.
- [26] M. M. Reda Taha and J. Lucero, "Damage identification for structural health

- monitoring using fuzzy pattern recognition,” *SEMC 2004 Struct. Heal. Monit. Damage Detect. Long-Term Perform. Second Int. Conf. Struct. Eng. Mech. Comput.*, vol. 27, no. 12, pp. 1774–1783, 2005.
- [27] P. Baraldi, F. Mangili, and E. Zio, “A Kalman Filter-Based Ensemble Approach With Application to Turbine Creep Prognostics,” *Reliab. IEEE Trans.*, vol. 61, no. 4, pp. 966–977, 2012.
- [28] R. Polikar, “Ensemble based systems in decision making,” *Circuits Syst. Mag. IEEE*, vol. 6, no. 3, pp. 21–45, 2006.
- [29] A. K. S. Jardine, D. Lin, and D. Banjevic, “A review on machinery diagnostics and prognostics implementing condition-based maintenance,” *Mech. Syst. Signal Process.*, vol. 20, no. 7, pp. 1483–1510, 2006.
- [30] Y. Lei, J. Lin, Z. He, and M. J. Zuo, “A review on empirical mode decomposition in fault diagnosis of rotating machinery,” *Mech. Syst. Signal Process.*, vol. 35, no. 1–2, pp. 108–126, 2013.
- [31] A. S. Sait and Y. I. Sharaf-Eldeen, “A review of gearbox condition monitoring based on vibration analysis techniques diagnostics and prognostics,” in *Conference Proceedings of the Society for Experimental Mechanics Series*, 2011, vol. 5, pp. 307–324.
- [32] C. 77, “Engine Bearing Failure & Analysis Guide,” Form # CL77-3-402. Dana Corporation. USA, 2002.
- [33] F. Y. Zeidan and B. S. Herbage, “Fluid film bearing fundamentals and failure analysis,” in *Proceedings of the 20th Turbomachinery Symposium*, 1991, pp. 161–186.
- [34] Q. Wang, “Seizure failure of journal-bearing conformal contacts,” *Wear*, vol. 210, no. 1–2, pp. 8–16, 1997.
- [35] Q. HUANG, J. WANG, L. MA, and C.-J. ZHAO, “Fatigue Damage

- Mechanism of Oil Film Bearing Sleeve,” *J. Iron Steel Res. Int.*, vol. 14, no. 1, pp. 60–68, 2007.
- [36] A. Vencel and A. Rac, “Diesel engine crankshaft journal bearings failures: Case study,” *Eng. Fail. Anal.*, vol. 44, pp. 217–228, 2014.
- [37] K. Okamoto, H. Shiihara, Y. Nagayama, and T. Kurosawa, “Effective Condition Monitoring Methods for Diesel Main Bearing-High Frequency Vibration Measurement and Wear Particle Detection,” *JIME*, vol. 42, no. 4, pp. 560–565, 2007.
- [38] A. Moosavian, H. Ahmadi, A. Tabatabaeefar, and M. Khazaei, “Comparison of two classifiers; K-nearest neighbor and artificial neural network, for fault diagnosis on a main engine journal-bearing,” *Shock Vib.*, vol. 20, no. 2, pp. 263–272, 2013.
- [39] S. A. Mirhadizadeh and D. Mba, “Observations of acoustic emission in a hydrodynamic bearing,” *J. Qual. Maint. Eng.*, vol. 15, no. 2, pp. 193–201, 2009.
- [40] D. An, N. H. Kim, and J. H. Choi, “Options for prognostics Methods: A review of data-driven and physics-based prognostics,” in *54th AIAA/ASME/ASCE/AHS/ASC Structures, Structural Dynamics, and Materials Conference*, 2013.
- [41] J. Luo, A. Bixby, K. Pattipati, L. Qiao, M. Kawamoto, and S. Chigusa, “An interacting multiple model approach to model-based prognostics,” in *Systems, Man and Cybernetics, 2003. IEEE International Conference on*, 2003, vol. 1, pp. 189–194, 2003.
- [42] B. Li, M.-Y. Chow, Y. Tipsuwan, and J. C. Hung, “Neural-network-based motor rolling bearing fault diagnosis,” *Ind. Electron. IEEE Trans.*, vol. 47, no. 5, pp. 1060–1069, 2000.
- [43] P. C. Paris, M. P. Gomez, and W. E. Anderson, “A rational analytic theory of fatigue,” *trend Eng.*, vol. 13, no. 1, pp. 9–14, 1961.

- [44] M. Corbetta, C. Sbarufatti, A. Manes, and M. Giglio, "Sequential Monte Carlo sampling for crack growth prediction providing for several uncertainties," in *Proceedings of the 2nd European conference of the prognostics and health management society*, vol. 5, pp. 1-13, 2014.
- [45] A. Ray and S. Tangirala, "Stochastic modeling of fatigue crack dynamics for on-line failure prognostics," *Control Syst. Technol. IEEE Trans.*, vol. 4, no. 4, pp. 443–451, 1996.
- [46] M. Orchard, G. Kacprzynski, K. Goebel, B. Saha, and G. Vachtsevanos, "Advances in uncertainty representation and management for particle filtering applied to prognostics," in *Prognostics and Health Management, 2008. PHM 2008. International Conference on*, 2008, pp. 1–6.
- [47] C. H. Oppenheimer and K. A. Loparo, "Physically based diagnosis and prognosis of cracked rotor shafts," in *Components and Systems Diagnostics, Prognostics, and Health Management II*, 2002, vol. 4733, pp. 122–132.
- [48] C. J. Li and H. Lee, "Gear fatigue crack prognosis using embedded model, gear dynamic model and fracture mechanics," *Mech. Syst. Signal Process.*, vol. 19, no. 4, pp. 836–846, 2005.
- [49] A. Coppe, M. J. Pais, N.-H. Kim, and R. T. Haftka, "Identification of equivalent damage growth parameters for general crack geometry," in *Annual Conference of the Prognostics and Health Management Society*, 2010.
- [50] L. C. Jaw and W. Wang, "Mathematical formulation of model-based methods for diagnostics and prognostics," in *2006 ASME 51st Turbo Expo*, 2006, vol. 2, pp. 691–697.
- [51] T. Tinga, *Principles of Loads and Failure Mechanisms: Applications in Maintenance, Reliability and Design*. Springer Science & Business Media, 2013, ISBN: 978-1-4471-4917-0.

- [52] A. Wöhler, “Versuche über die Festigkeit der Eisenbahnwagenachsen,” *Zeitschrift für Bauwes.*, vol. 10, pp. 160–161, 1860.
- [53] B. Standard, “Guide to Fatigue Design and Assessment of Steel Products,” BSI Standards Publication, 2014.
- [54] O. H. Basquin, “The exponential law of endurance tests,” vol. 10 (II), no. Proceedings of ASTM, pp. 625–630, 1910.
- [55] S. Manson and L. F. Coffin, “Behaviour of materials under conditions of thermal stress,” no. NACA TN 2933. National Advisory Committee for Aeronautics, Cleveland, OH, 1954.
- [56] L. Coffin, “Apparatus for study of effects of cyclic thermal stresses on ductile metals,” vol. 76, no. Transactions ASME, pp. 931–950, 1954.
- [57] M. P. Singh, B. K. Thakur, and W. E. Sullivan, “Assessing useful life of turbomachinery components,” in *Proceedings of the 34th turbomachinery symposium*, 2005, pp. 177–192.
- [58] G. J. Kacprzynski, G. J. Roemer, G. Modgil, A. Palladino, and K. Maynard, “Enhancement of physics-of-failure prognostic models with system level features,” in *2002 IEEE Aerospace Conference*, 2002, vol. 6, pp. 2919–2925.
- [59] M. A. Miner, “Cumulative damage in fatigue,” vol. 12, no. J. Appl. Mech, pp. 159–164, 1945.
- [60] J. Qiu, B. B. Seth, S. Y. Liang, and C. Zhang, “Damage Mechanics Approach Fof Bearing Lifetime Prognostics,” *Mech. Syst. Signal Process.*, vol. 16, no. 5, pp. 817–829, 2002.
- [61] M. R. Hoeprich, “Rolling element bearing fatigue damage propagation,” *J. Tribol.*, vol. 114, no. 2, pp. 328–333, 1992.
- [62] Y. Li, S. Billington, C. Zhang, T. Kurfess, S. Danyluk, and S. Liang, “Dynamic prognostic prediction of defect Propagation on rolling element bearings,” *Tribol. Trans.*, vol. 42, no. 2, pp. 385–392, 1999.

- [63] M. N. Kotzalas and T. A. Harris, "Fatigue failure progression in ball bearings," *J. Tribol.*, vol. 123, no. 2, pp. 238–242, 2001.
- [64] F. Sadeghi, B. Jalalahmadi, T. S. Slack, N. Raje, and N. K. Arakere, "A review of rolling contact fatigue," *J. Tribol.*, vol. 131, no. 4, pp. 1–15, 2009.
- [65] M. J. Pais and N. H. Kim, "Predicting fatigue crack growth under variable amplitude loadings with usage monitoring data," *Adv. Mech. Eng.*, vol. 7, no. 12, Dec. 2015.
- [66] R. F. Orsagh, J. Sheldon, and C. J. Klenke, "Prognostics/diagnostics for gas turbine engine bearings," in *Aerospace Conference, 2003. Proceedings. 2003 IEEE*, 2003, vol. 7, pp. 3095–3103.
- [67] Y. Li, T. R. Kurfess, and S. Y. Liang, "Stochastic prognostics for rolling element bearings," *Mech. Syst. Signal Process.*, vol. 14, no. 5, pp. 747–762, 2000.
- [68] Y. Li, S. Billington, C. Zhang, T. Kurfess, S. Danyluk, and S. Liang, "Adaptive prognostics for rolling element bearing condition," *Mech. Syst. Signal Process.*, vol. 13, no. 1, pp. 103–113, 1999.
- [69] T. Slack and F. Sadeghi, "Explicit finite element modeling of subsurface initiated spalling in rolling contacts," *Tribol. Int.*, vol. 43, no. 9, pp. 1693–1702, 2010.
- [70] S. Fu and Y. Gao, "Fan blade crack diagnosis method study," *Adv. Mech. Eng.*, vol. 8, no. 5, May 2016.
- [71] S. M. Quraishi, M. M. Khonsari, and D. K. Baek, "A thermodynamic approach for predicting fretting fatigue life," *Tribol. Lett.*, vol. 19, no. 3, pp. 169–175, 2005.
- [72] M. Amiri and M. M. Khonsari, "On the thermodynamics of friction and wear—a review," *Entropy*, vol. 12, no. 5, pp. 1021–1049, 2010.
- [73] A. Dasgupta and M. Pecht, "Material failure mechanisms and damage

- models,” *Reliab. IEEE Trans.*, vol. 40, no. 5, pp. 531–536, 1991.
- [74] M. Watson, C. Byington, D. Edwards, and S. Amin, “Dynamic modeling and wear-based remaining useful life prediction of high power clutch systems,” *Tribol. Trans.*, vol. 48, no. 2, pp. 208–217, 2005.
- [75] A. Ghosh, N. Paulson, and F. Sadeghi, “A fracture mechanics approach to simulate sub-surface initiated fretting wear,” *Int. J. Solids Struct.*, vol. 58, pp. 335–352, 2015.
- [76] C. A. Coulomb, “Theorie des Machines Simples, en Ayant egard au frottement de leurs parties et a la roideur des cordages,” no. Mémoires de Mathématique et de Physique de l’Académie Royale des Sciences: X, pp. 161–342, 1785.
- [77] J. Choi, S. S. Kim, S. S. Rhim, and J. H. Choi, “Numerical modeling of journal bearing considering both elastohydrodynamic lubrication and multi-flexible-body dynamics,” *Int. J. Automot. Technol.*, vol. 13, no. 2, pp. 255–261, 2012.
- [78] F. Stefani and A. Reborá, “Steadily loaded journal bearings: Quasi-3D mass–energy-conserving analysis,” *Tribol. Int.*, vol. 42, no. 3, pp. 448–460, 2009.
- [79] H. Jin and W. Zuo, “Simulation and Heat Transfer Calculation on A Journal Bearing With A Center Circumferential Groove in Load Zone,” *IJACT Int. J. Adv. Comput. Technol.*, vol. 5, no. 1, pp. 54–61, 2013.
- [80] E. R. M. Gelinck and D. J. Schipper, “Calculation of Stribeck curves for line contacts,” *Tribol. Int.*, vol. 33, no. 3–4, pp. 175–181, 2000.
- [81] Q. Liu, “Friction in Mixed and Elastohydrodynamic Lubricated Contacts Including Thermal Effects,” PhD thesis, Universiteit Twente, 2002.
- [82] X. Lu, M. M. Khonsari, and E. R. M. Gelinck, “The Stribeck curve:

- Experimental results and theoretical prediction,” *J. Tribol.*, vol. 128, no. 4, pp. 789–794, 2006.
- [83] I. C. Faraon, “Mixed lubrication of line contacts,” PhD thesis, Universiteit Twente, 2005.
- [84] I. C. Faraon and D. J. Schipper, “Stribeck curve for starved line contacts,” *J. Tribol.*, vol. 129, no. 1, pp. 181–187, 2007.
- [85] D. Y. Hua, L. Qiu, and H. S. Cheng, “Modeling of lubrication in micro contact,” *Tribol. Lett.*, vol. 3, no. 1, pp. 81–86, 1997.
- [86] J. Castro and J. Seabra, “Global and local analysis of gear scuffing tests using a mixed film lubrication model,” *Tribol. Int.*, vol. 41, no. 4, pp. 244–255, 2008.
- [87] Y. Wang, C. Zhang, Q. J. Wang, and C. Lin, “A mixed-TEHD analysis and experiment of journal bearings under severe operating conditions,” *Tribol. Int.*, vol. 35, no. 6, pp. 395–407, 2002.
- [88] C. Zhang, H. S. Cheng, and Q. J. Wang, “Scuffing Behavior of Piston-Pin/Bore Bearing in Mixed Lubrication—Part II: Scuffing Mechanism and Failure Criterion,” *Tribol. Trans.*, vol. 47, no. 1, pp. 149–156, 2004.
- [89] S. Li and A. Kahraman, “A fatigue model for contacts under mixed elastohydrodynamic lubrication condition,” *Int. J. Fatigue*, vol. 33, no. 3, pp. 427–436, 2011.
- [90] S. Li and A. Kahraman, “A physics-based model to predict micro-pitting lives of lubricated point contacts,” *Int. J. Fatigue*, vol. 47, pp. 205–215, 2013.
- [91] S. Li, A. Kahraman, N. Anderson, and L. D. Wedeven, “A model to predict scuffing failures of a ball-on-disk contact,” *Tribol. Int.*, vol. 60, pp. 233–245, 2013.
- [92] S. Marble and B. P. Morton, “Predicting the remaining life of propulsion

- system bearings,” in *IEEE Aerospace Conference Proceedings*, Big Sky, MT, 2006.
- [93] B. Avitzur, “Modeling the effect of lubrication on friction behavior,” *Wear*, vol. 126, no. 3, pp. 227–249, 1988.
- [94] B. Avitzur, “Boundary and hydrodynamic lubrication,” *Wear*, vol. 139, no. 1, pp. 49–76, 1990.
- [95] A. Meldahl, “Contribution to the Theory of the Lubrication of Gears and of the Stressing of the Lubricated Flanks of Gear Teeth,” *Brown Boveri Rev*, vol. 28, no. 11, pp. 374–382, 1941.
- [96] A. N. Grubin, I. E. Vinogradova, and K. F. Ketova, *Investigation of the Contact of Machine Components*. Central Scientific Research Institute for Technology and Mechanical Engineering, 1949.
- [97] X. Jiang, H. S. Cheng, and D. Y. Hua, “A Theoretical Analysis of Mixed Lubrication by Macro Micro Approach: Part I—Results in a Gear Surface Contact,” *Tribol. Trans.*, vol. 43, no. 4, pp. 689–699, 2000.
- [98] L. Chang and Y.-R. Jeng, “A Mathematical Model for the Mixed Lubrication of Non-Conformable Contacts With Asperity Friction, Plastic Deformation, Flash Temperature, and Tribo-Chemistry,” *J. Tribol.*, vol. 136, no. 2, p. 22301, Feb. 2014.
- [99] L. Chang and Y.-R. Jeng, “Parametric Analyses of the Mixed-Lubrication Performance of Rolling/Sliding Contacts in High-Load and High-Speed Conditions,” *Tribol. Trans.*, vol. 57, no. 5, pp. 879–889, 2014.
- [100] S. Xiong*, Q. J. Wang, W. K. A. M. Liu, Q. Yang, K. Vaidyanathan, D. Zhu, and C. Lin, “Approaching Mixed Elastohydrodynamic Lubrication of Smooth Journal-Bearing Systems with Low Rotating Speed,” *Tribol. Trans.*, vol. 49, no. 4, pp. 598–610, 2006.
- [101] N. Patir and H. S. Cheng, “An average flow model for determining effects

- of three-dimensional roughness on partial hydrodynamic lubrication.,” *TRANS. ASME SER. F, J. LUBR. TECHNOL.*, vol. 100, no. 1, Jan. 1978. pp. 12–17, 1978.
- [102] A. Fatu, D. Bonneau, and R. Fatu, “Computing hydrodynamic pressure in mixed lubrication by modified Reynolds equation,” *Proc. Inst. Mech. Eng. Part J J. Eng. Tribol.*, vol. 226, no. 12, pp. 1074–1094, Dec. 2012.
- [103] A. Mihailidis, K. Agouridas, and K. Panagiotidis, “Non-Newtonian Starved Thermal-Elastohydrodynamic Lubrication of Finite Line Contacts,” *Tribol. Trans.*, vol. 56, no. 1, pp. 88–100, 2013.
- [104] D. Zhu, “Effect of Surface Roughness on Mixed EHD Lubrication Characteristics,” *Tribol. Trans.*, vol. 46, no. 1, pp. 44–48, 2003.
- [105] O. Reynolds, “On the Theory of Lubrication and Its Application to Mr. Beauchamp Tower’s Experiments, Including an Experimental Determination of the Viscosity of Olive Oil.,” *Proc. R. Soc. London*, vol. 40, no. 242–245, pp. 191–203, 1886.
- [106] B. S. Shenoy, R. S. Pai, D. S. Rao, and R. Pai, “Elasto-hydrodynamic lubrication analysis of full 360° journal bearing using CFD and FSI techniques,” *World J. Model. Simul.*, vol. 5, no. 4, pp. 315–320, 2009.
- [107] D. Bonneau, A. Fatu, and D. Souchet, *Thermo-hydrodynamic lubrication in hydrodynamic bearings*. John Wiley & Sons, 2014, ISBN: 9781119005001.
- [108] Z. S. Zhang, Y. M. Yang, X. D. Dai, and Y. B. Xie, “Effects of Thermal Boundary Conditions on Plain Journal Bearing Thermohydrodynamic Lubrication,” *Tribol. Trans.*, vol. 56, no. 5, pp. 759–770, Sep. 2013.
- [109] C. A. Laukiavich, M. J. Braun, and A. J. Chandy, “An Investigation into the Thermal Effects on a Hydrodynamic Bearing’s Clearance,” *Tribol. Trans.*, vol. 58, no. 6, pp. 980–1001, Nov. 2015.
- [110] K. Keller, W. Majkowski, and K. Swearingen, “Integrating health management into legacy platforms,” in *Aerospace conference, 2009 IEEE*,

2009, pp. 1–8.

- [111] A. Cubillo, A. Uriondo, and S. Perinpanayagam, “Computational Mixed-TEHL model and Stribeck curve of a journal bearing,” *Tribol. Trans*, doi: 10.1080/10402004.2016.1245456, Oct. 2016.
- [112] Dmitri Kopeliovich, “Hydrodynamic journal bearing.” [Online]. Available: http://www.substech.com/dokuwiki/doku.php?id=hydrodynamic_journal_bearing.
- [113] J. Frêne, D. Nicolas, B. Degueurce, D. Berthe, and M. Godet, *Hydrodynamic lubrication: bearings and thrust bearings*, vol. 33, Elsevier, 1997, ISBN: 9780080534312.
- [114] N. Lorenz, G. Offner, and O. Knaus, “Fast thermo-elasto-hydrodynamic modeling approach for mixed lubricated journal bearings in internal combustion engines,” *Proc. Inst. Mech. Eng. Part J J. Eng. Tribol.*, vol. 229, no. 8, pp. 962-976, Mar. 2015.
- [115] M. J. Braun and W. M. Hannon, “Cavitation formation and modelling for fluid film bearings: A review,” *Proc. Inst. Mech. Eng. Part J J. Eng. Tribol.*, vol. 224, no. 9, pp. 839–863, 2010.
- [116] H. G. Elrod and Ml. Adams, “A computer program for cavitation and starvation problems,” *Cavitation Relat. Phenom. Lubr.*, pp. 37–41, 1974.
- [117] H. G. Elrod, “A Cavitation Algorithm,” *J. Lubr. Technol.*, vol. 103, no. 3, pp. 350–354, Jul. 1981.
- [118] N. Patir and H. S. Cheng, “Application Of Average Flow Model To Lubrication Between Rough Sliding Surfaces.,” *J Lubr Technol Trans ASME*, vol. 101, no. 2. pp. 220–230, 1979.
- [119] C. Barus, “Isothermals, isopiestic and isometrics relative to viscosity,” *Am. J. Sci.*, no. 266, pp. 87–96, 1893.
- [120] C. J. A. Roelands, “Correlational aspects of the viscosity-temperature-pressure relationship of lubricating oils.” PhD thesis, TU Delft, Delft

University of Technology, 1966.

- [121] D. Bonneau, A. Fatu, and D. Souchet, *Mixed Lubrication in Hydrodynamic Bearings*. Hoboken, NJ, USA: John Wiley & Sons, Inc., 2014, ISBN: 978-1-119-00805-7.
- [122] C. J. Seeton, "Viscosity--temperature correlation for liquids," *Tribol. Lett.*, vol. 22, no. 1, pp. 67–78, 2006.
- [123] R. Larsson, P. O. Larsson, E. Eriksson, M. Sjöberg, and E. Höglund, "Lubricant properties for input to hydrodynamic and elastohydrodynamic lubrication analyses," *Proc. Inst. Mech. Eng. Part J J. Eng. Tribol.*, vol. 214, no. 1, pp. 17–27, Jan. 2000.
- [124] J. A. Greenwood and J. B. P. Williamson, "Contact of nominally flat surfaces," *Proc. R. Soc. London. Series A. Mathematical Phys. Sci.*, vol. 295, no. 1442, pp. 300–319, 1966.
- [125] D. J. Whitehouse and J. F. Archard, "The properties of random surfaces of significance in their contact," in *Proceedings of the Royal Society of London A: Mathematical, Physical and Engineering Sciences*, 1970, vol. 316, no. 1524, pp. 97–121.
- [126] Georgie E. Totten, *Handbook of Lubrication and Tribology: Volume I Application and Maintenance*, 1st edition. CRS PRes, 2006, ISBN: 9781420003840.
- [127] J. A. Greenwood and J. H. Tripp, "The contact of two nominally flat rough surfaces," *Proc. Inst. Mech. Eng.*, vol. 185, no. 1, pp. 625–633, 1970.
- [128] G. Offner, "Modelling of condensed flexible bodies considering non-linear inertia effects resulting from gross motions," *Proc. Inst. Mech. Eng. Part K J. Multi-body Dyn.*, vol. 225, no. 3, pp. 204–219, Sep. 2011.
- [129] G. Offner, "Friction Power Loss Simulation of Internal Combustion Engines Considering Mixed Lubricated Radial Slider, Axial Slider and Piston to Liner

Contacts,” *Tribol. Trans.*, vol. 56, no. 3, pp. 503–515, Jan. 2013.

- [130] L. Chen, X. Song, D. Xue, and Z. Ming, “Elastohydrodynamic Lubrication and Asperity Contact Simulation of Engine Main Bearing with Flexible Rotating Crankshaft and Flexible Engine Block,” in *Advanced Tribology SE - 327*, J. Luo, Y. Meng, T. Shao, and Q. Zhao, Eds. Springer Berlin Heidelberg, 2010, pp. 967–972.
- [131] S. Akbarzadeh and M. M. Khonsari, “Effect of surface pattern on Stribeck curve,” *Tribol. Lett.*, vol. 37, no. 2, pp. 477–486, 2010.
- [132] ExxonMobil, “Mobil Jet Oil II characteristics.” [Online]. Available: <http://www.exxonmobil.com/english-US/Aviation/pds/GLXXMobil-Jet-Oil-II>.

Appendices

Appendix A

Cubillo, A., Perinpanayagaman, S., Esperon-Miguez, M. "A review of physics-based models in prognostics: Application to gears and bearings of rotating machinery", *Advances in Mechanical Engineering*, SAGE publications, July 2016 vol. 8 (8), pp. 1-21, DOI: 10.1177/1687814016664660.

Article attached at the end of the thesis

Appendix B

Cubillo, A., Uriondo, A., Perinpanayagaman, S. "Computational Mixed-TEHL model and Stribeck curve of a journal bearing", Tribology Transactions, Taylor & Francis, October 2016, DOI: 10.1080/10402004.2016.1245456.

Article attached at the end of the thesis

